THE EFFECT OF ADDITIONAL SURFACE COATING ON THE PERFORMANCE OF ADDITIVELY MANUFACTURED FIBER REINFORCED COMPOSITE MOLD

A Dissertation

Submitted to the Faculty

of

Purdue University

by

Garam Kim

In Partial Fulfillment of the

Requirements for the Degree

of

Doctor of Philosophy

August 2020

Purdue University

West Lafayette, Indiana

THE PURDUE UNIVERSITY GRADUATE SCHOOL
STATEMENT OF COMMITTEE APPROVAL

Dr. Ronald Sterkenburg, Chair

School of Aviation and Transportation Technology

Dr. Sergey Dubikovsky

School of Aviation and Transportation Technology

Dr. Peng Hao Wang

School of Aviation and Transportation Technology

Dr. Waterloo Tsutsui

School of Aeronautics and Astronautics

Approved by:

Dr. Kathryne A. Newton

Associate Dean for Graduate Programs

To my beloved family

ACKNOWLEDGMENTS

First of all, I would like to express my sincere appreciation to my advisor Dr. Ronald Sterkenburg. I had such a great experience working with him since I was in undergraduate program. He was my mentor, guardian, and a good friend who always took great care of me. He always believed me and provided unconditional support to me all the time. I will not forget all the good times I had with him. Also, I would also like to extend my gratitude to Tyler Futch and Yuwei He for their great support and being the best partner all the time.

I would like to thank to my committee members; Dr. Sergey Dubikovsky, Dr. Peng Hao Wang, and Dr. Waterloo Tsutsui for their support during this project. They always encouraged me and provided useful advice. This project could not have reached its goal without their support.

Also, I am grateful to Dr. R. Byron Pipes and Dr. Eduardo Barocio for their unwavering support and guidance. Their insightful suggestion and mentorship had always inspired me, and this work would not have been possible without their input.

I would like to extend my sincere thanks to people in the Composite Manufacturing and Simulation Center (CMSC). I had the great pleasure of working with them and learned so much valuable knowledge and experience from them. Special thanks to Jorge Ramirez and Sushrut Karmarkar for helping me to manufacture test specimens for this project using CAMRI.

Finally, I would like to express my biggest thanks to my beloved parents, Yong Sun Kim and Suk Hee Choi, and my sister, Eun Bi Kim and my relatives for supporting me during my academic years. Nothing has been possible without their unconditional support and prayers.

Thank you all!

TABLE OF CONTENTS

LIST OF TABLES

LIST OF FIGURES

Figure Page

Figure Page

ABSTRACT

Kim, Garam Ph.D., Purdue University, August 2020. The Effect of Additional Surface Coating on the Performance of Additively Manufactured Fiber Reinforced Composite Mold. Major Professor: Ronald Sterkenburg.

A composite part manufacturing mold was considered one of the most important factors that affected a successful composite part manufacturing process for this research. A highly durable surface was required for the mold to prevent surface damages and increase mold life. A high surface finish quality of the mold improved the surface quality of the composite part and lowered the demolding force. However, the surface of additively manufactured fiber reinforced composite molds usually had lower durability and surface finish quality compared to traditional metal molds. To solve these issues, the author applied an additional coating on top of the additively manufactured fiber reinforced composite mold surface. A thermal analysis of the additively manufactured fiber reinforced composite material and the coating material were performed to select an applicable coating technique and coating material. The thermoset polymer coating with ceramic particles that was applied with a liquid spray coating technique was selected as a coating material. Various surface property tests were performed to evaluate the coated surface compared to the non-coated surface. The additively manufactured fiber reinforced composite test specimen manufacturing process and the coating application process were demonstrated in this study. The surface durability of the test specimens was tested using a surface hardness test and an abrasion resistance test. The surface performance of the test specimens was measured using a surface roughness test and a demolding test. The sustainability of the coating material on the additively manufactured fiber reinforced composite was tested using coefficient of thermal

expansion (CTE) test, coating adhesion test, and mold life experiment. In the mold life experiment, the non-coated and coated molds were used for multiple composite part manufacturing processes to investigate how the coating affected the life of the mold. The test results showed that the coated surface had a significantly improve surface abrasion resistance and demolding performance. However, the coating did not significantly improved surface hardness and roughness. The adhesion strength of the coating was not degraded even there was a coefficient of thermal expansion (CTE) mismatch between the additively manufactured fiber reinforced composite and the coating material. The coated additively manufactured fiber reinforced composite mold was able to be used for multiple autoclave composite part manufacturing cycles. The coating covered most of the small voids on the mold surface and provided a more homogeneous surface compared to the non-coated mold, but the voids which could not be covered with the coating caused a chipped coating issue. Once the chipped coating occurred, the size of chipped coating got larger each time the tool was used for a composite part manufacturing cycle. Although the additional coating provided some improvements for the surface properties, the coating applied in this research could not be an ultimate solution to meet all the surface property requirements for composite part manufacturing mold.

CHAPTER 1. INTRODUCTION

The author introduced an overview, background, and significance of the proposed research in this chapter. The research questions demonstrated the purpose of the research, and the scope of the research was defined in assumptions, limitations, and delimitations sections. The definition section provided the definition of the terms used in this research.

1.1 Background

The use of fiber reinforced composite materials in industries, such as aerospace, automobile, maritime, and sporting goods had increased rapidly due to the favorable physical and mechanical properties of the material (Mallick, 2007). Fiber reinforced composite parts were manufactured in a unique way. The fiber reinforced composite material was laid up on a composite part manufacturing mold. Then, pressure and heat were applied to consolidate the material into the shape of the mold while the material was cured (Sterkenburg & Wang, 2014). After the part was cured, it was demolded from the mold and trimmed to the required dimensions. (Sterkenburg & Wang, 2014). Composite part manufacturing molds played a significant role in the composite part manufacturing process. Since the composite material was directly laid up on the surface of the mold, the surface properties, such as surface roughness and texture, of the mold influenced the composite part surface quality (Mohammadi, Ghani, Komeili, Crawford, & Milani, 2017). If there was a defect on the mold surface, it was inevitable to have that defect transferred to the part surface. The high demolding force could damage the mold or part during the part demolding process. Also, high surface durability was required for the mold to maximize the number of production runs before the mold failed (Campbell Jr,

2003). Composite part manufacturing molds were often made from aluminum, steel, tooling board, or composite materials (Sterkenburg & Wang, 2014). Among these options, composite molds had high strength, low-weight, and could withstand relatively high temperatures and pressures. The coefficient of thermal expansion (CTE) of the carbon fiber reinforced composite was small, like that of the molded material. Therefore, carbon fiber reinforced composite molds had good dimensional stability at elevated temperatures (Stewart, 2009). However, the composite mold manufacturing process was a complicated and labor-intensive process. Recently, rapidly developing additive manufacturing technology allowed 3D printing of fiber reinforced composite materials. Additive manufacturing composite material was a promising technology for mold manufacturing because it reduced cost, time, and labor to make a composite mold (Sudbury, Springfield, Kunc, & Duty, 2017). Surface quality requirements still demanded machining of the near-net-shape additively manufactured molds. Even with a machining process, due to heterogeneous nature of extruded fiber reinforced composite material, the machined surface of the additively manufactured fiber reinforced composite mold was generally rougher than conventional metal molds. Also, the air voids trapped inside or in-between the printed bead during the additive manufacturing process caused surface porosity of the mold surface. Further, the surface was prone to have damages, such as fiber breakage, fiber pull-out, matrix cracking, and melted polymer during the machining process (Chardon, Chanal, Duc, & Garnier, 2017). Often, the additively manufactured fiber reinforced composite mold had a high surface roughness which increased the demolding force in the composite part manufacturing process. The surface of the additively manufactured fiber reinforced composite mold was not as durable as a traditional metal mold (Stewart, 2009). Therefore, it was more prone to have a damaged surface, such as scratches, nicks, and dents during the composite part manufacturing process (Stewart, 2009). To overcome these issues, the author suggested applying an additional coating on the additively manufactured fiber reinforced composite mold. However, only a limited

number of research studies have been conducted on coating technologies for additive manufactured fiber reinforced composite mold. Hence, the objective of this work was to investigate the effects of a coating on the surface properties of the additively manufactured composite mold. Durability, performance, and sustainability of the coated mold for the composite manufacturing process were characterized in this study.

1.2 Significance

The newly emerged additively manufactured fiber reinforced composite molds for composite part manufacturing had limitations to achieve a high-performance mold surface. The surface of the mold was prone to have a high roughness level which could result in degradation of the surface quality of the part and relatively high required demolding force (Duty & Springfield, 2015). Also, the mold could be easily damaged due to the low durability of the surface that could result in a big economic loss (Campbell Jr, 2003). In this study, the author investigated additional coating on the additively manufactured fiber reinforced composite mold. The author identified and implemented a cost-effective coating technology for additively manufactured fiber reinforced composite mold. The author demonstrated the systematic approach of testing applicability of coating material using thermal analysis of the substrate and coating material. The author developed a protocol for testing coatings applied to additively manufactured fiber reinforced composite. The author introduced multiple surface property tests to assess the durability, performance, and sustainability of the surface of the mold. Thus, the differences in durability, performance, and sustainability between coated and non-coated surfaces of printed mold could be evaluated. This study provided a guideline for coating selection and its application for additively manufactured fiber reinforced composite mold, and how to evaluate the performance of the coating in the composite part manufacturing process.

1.3 Research Question

How did additional surface coating affect the surface properties of the additively manufactured fiber reinforced composite mold for a composite part manufacturing process?

1.3.1 Sub-questions

1. Did additional coating improve the surface durability of the additively manufactured fiber reinforced composite mold?
2. Did additional coating improve the performance of the additively manufactured fiber reinforced composite mold for the composite part manufacturing process?
3. Did additional coating improve the sustainability of the additively manufactured fiber reinforced composite mold for the composite part manufacturing process?

1.4 Assumptions

This research was conducted under the following assumptions:

- The surface properties of the additively manufactured fiber reinforced composite mold needed to be improved due to its low durability, high surface roughness, and low sustainability.
- All additively manufactured fiber reinforced composite test specimens were manufactured and prepared in the same way and the surface properties of all test specimens were equivalent (similar).
- The methodology of this study was appropriate to evaluate surface properties of the coated and non-coated surface of an additively manufactured fiber reinforced composite.

1.5 Limitations

This research was conducted under the following limitations:

- The maximum size of the additively manufactured fiber reinforced composite mold was limited to 0.5 m x 0.5 m x 0.38 m due to the capacity of the composite additive manufacturing research instrument (CAMRI) (Barocio, 2020).
- The fiber reinforced composite material that was used to build test specimens was printed with extrusion deposition additive manufacturing (EDAM) process of CAMRI.
- The coating technique and coating material for this study were sourced from those that were commercially available.

1.6 Delimitations

This research was conducted under the following delimitations:

- This study only focused on coatings for additively manufactured fiber reinforced composite molds.
- This study only focused on a composite part manufacturing mold that could be used for a high-temperature cure (between 121°C and 180°C).
- The composite part manufacturing mold in this study was only used for a one-sided prepreg hand layup.
- The aesthetic quality of the coating was not considered in this study.

1.7 Challenges

- The author performed various surface property tests in this study. However, not all test equipment was accessible immediately. The author was able to use the equipment in a limited amount of time.
- Some test equipment could not be found in any of the Purdue facilities. Therefore, the author designed and built a customized test fixture and used it for the test.

1.8 Definitions

This research includes the following definitions:

Composite material: A material made from two or more constituent materials with significantly different physical or chemical properties that, when combined, produced a material with characteristics different from the individual components (Campbell Jr, 2003; Sheikh-Ahmad, 2009).

Advanced composite material: (commonly: *fiber reinforced polymer composite*) Composite material that consisted of high-performance fiber reinforcement and polymer matrix.

Fiber reinforcement: A fibrous component in advanced composites.

Carbon fiber: The fiber which had a high content of carbon (90% or above) (Mahltig & Kyosev, 2018).

Matrix: A homogeneous material which bound the fiber reinforcement in advanced composites.

Polymer: A substance which had molecules made from chains of monomer.

Thermoset: A polymer which had molecules that are chemically joined through rigid 3-dimensional cross-linking to each other during the curing process, so it could not be reformed once it was cured (Campbell Jr, 2003; Mallick, 2007).

Thermoplastic: A polymer which had molecules that connected to each other with weak secondary bonding instead of chemical bonding during the curing process. Therefore, the secondary bonding could be broken at elevated temperatures, and it allowed the structure to be reformed (Campbell Jr, 2003; Mallick, 2007).

Crystallinity: The degree of how much polymer chain align with each other (Crawford, 2017).

Amorphous polymer: A polymer which had randomly arranged molecules.

Semi-crystalline polymer: A polymer which had a partially amorphous region and partially crystalline region.

Composite layup: The process of making composite part.

Prepreg: Prepreg referred to pre-impregnated reinforcements with resin while it was manufactured (Armstrong, Cole, & Bevan, 2005). The resin which impregnated the reinforcement was in B-stage which should have stored in a freezer to prevent self-curing during storing (Armstrong et al., 2005; Sterkenburg & Wang, 2014).

Resin: A natural or synthetic organic compound which got hardened under certain circumstances (ex: temperature and UV light).

Anisotropic: Having a different property in different directions.

Coefficient of thermal expansion (CTE): The quantified term for the dimensional change of the material in the variation of temperature. The CTE for the material could be defined in the following equation;

$$\alpha = \frac{1}{L_0}\frac{\triangle L}{\triangle T} \tag{1.1}$$

where α referred CTE of the material, L_0 was the original length of the material. $\triangle T$ was the difference in temperature. $\triangle L$ was the change in length of the material (Chun et al., 2018).

Sheet molding compound (SMC): Sheet form of high strength composite material consisted of thermoset resin, fiber reinforcement, catalyst, and fillers.

Vacuum bag: A vacuum bag process was wrapping the vacuum bag over the mold and sealed. Then air inside of the vacuum bag was evacuated from the bag through a vacuum port. Atmospheric pressure on the outside of the bag pressurized the part and the mold (Centea, Grunenfelder, & Nutt, 2015).

Filament winding: A composite part manufacturing process which winds impregnated thermoset or thermoplastic material on a mandrel (Armstrong et al., 2005).

Wet layup: A composite manufacturing technique which impregnates the dry fabric with a low viscosity resin and attached to the mold (Armstrong et al., 2005).

Resin transfer molding (RTM): One of the composite part manufacturing methods which impregnated a preformed fabric by transferring the resin through it (Armstrong et al., 2005).

Vacuum assisted resin transfer molding (VARTM): The RTM composite manufacturing process that only used vacuum pressure to transfer the resin through the reinforcement and consolidate the part.

Injection molding: Injection molding used a resin injection machine to inject the resin with high pressure into the mold. The high pressure injected resin transferred through the fabric and impregnated the fiber.

Automatic tape laying (ATL) & Automatic fiber placement (AFP): Both automated tape laying (ATL) and automatic fiber placement (AFP) were automatic material laying processes using a machine which had a robotic arm with multi-axis control head. The machine equipped material spools, winders, winder guides, a position sensor, a material cutter, a heating unit, and a compaction roller (Sterkenburg & Wang, 2014).

Press molding: Composite compression over molding using a press machine. The composite material was placed in between two compression molds, and a pressing machine pressed the mold assembly to form the material inside the mold (Sterkenburg & Wang, 2014).

Additive manufacturing: The process of bonding materials to make objects from 3D model data, usually, layer upon layer (ASTM International, 2010).

Thermal fatigue: A fatigue stress which occurs due to the repeated temperature variation.

Thermal shock: A part failure mechanism caused by thermal stress due to the different amount of local expansion of the part, which was caused by different thermal gradients of the part (Bhatnagar, 2016; Buschow et al., 2001).

Autoclave: An equipment which provided heat and pressure during the composite part curing process.

Delamination: A type of part failure due to fractures into the layers.

Fiber pullout: A fiber reinforced composite failure mechanism that the fiber was debonded from the matrix and pulled out.

Hardness: Material's resistance against local deformation of the surface, such as surface indentation or penetration of the material (Tabor, 1970).

Abrasion resistance: A surface property that measured the ability of the surface to resist abrasion.

Roughness: Surface roughness was the value which indicated the irregularity of the surface (Hashmi, 2016).

Arithmetic average height (R_a): One of the amplitude parameters in roughness test which was calculated using the following equation;

$$R_a = \frac{1}{n}\sum_{i=1}^{n}|y_i| \tag{1.2}$$

where n was number of samples and y_i was deviation from the sample mean line (Gadelmawla, Koura, Maksoud, Elewa, & Soliman, 2002).

Computer aided design (CAD): Use of computer technology for part design, modification, and analysis.

Computer numerical control (CNC): An automated computer-controlled system that controlled the movement of the machine. Generally, the CNC machine referred to tools which used the CNC system for cutting and shaping the material into the designed shape (Sterkenburg & Wang, 2014).

Computer aided manufacturing (CAM): The use of computer software and computer numerical control automatic machining tool in the part manufacturing process.

Master mold: A template mold that was used for fabricating composite part manufacturing mold.

American Society for Testing and Materials (ASTM): An international standards organization that developed standards for production and testing.

Extrusion deposition additive manufacturing (EDAM): Additive manufacturing technique which used extruder screw to transport the pelletized material for printing (Brenken, Barocio, Favaloro, Kunc, & Pipes, 2019).

Composite Additive Manufacturing Research Instrument (CAMRI): A composite additive manufacturing instrument developed by the additive manufacturing team in composite and manufacturing simulation center (CMSC) at Purdue University.

Big Area Additive Manufacturing (BAAM): A composite additive manufacturing instrument developed by Cincinnati incorporated, partnership with Oak Ridge National Laboratory.

Polyphenylene sulfide (PPS): A semi-crystalline aromatic polymer. Due to its good mechanical property, chemical resistance, stability in elevated temperature, and low material cost, PPS was a very competitive high-performance thermoplastic material. The melting temperature of PPS was about 280°C (Jiang, Hornsby, McCool, & Murphy, 2012).

Polyetheretherketone (PEEK): A highly aromatic semi-crystalline organic thermoplastic polymer. Due to its good mechanical properties and chemical resistance properties, PEEK was widely used for industrial applications. The melting temp of PEEK was about 343°C (Thomas & Visakh, 2011).

Glass transition temperature (T_g): A temperature where the polymer changed from a glassy state to a plastic state.

Tribological: The science which studied the adhesion, friction, wear, and lubrication of solids surface (Buckley, 1978).

Substrate: A workpiece that the coating was applied to.

Volatile organic compound (VOC): Organic chemicals that evaporated in room temperature due to its low boiling point.

Gelcoat: A coating material which was used for fiber reinforced composite material for high surface finish. Gelcoat was often made of thermal setting resin.

Physical vapor deposition (PVD): In the PVD process, the coating material was evaporated and transformed into the gas phase and deposited on the substrate without any chemical reaction (Bach, Laarmann, Wenz, & Nakhosteen, 2006; Graves, 2002).

Chemical vapor deposition (CVD): During the CVD process, the coating material was deposited by a chemical reaction (Asthana, Kumar, & Dahotre, 2006). The reactive gases were inserted into a chamber, and the chemical reaction occurred to deposit the coating material on the surface of the substrate.

Diamond-like-carbon (DLC): DLC was an amorphous carbon material which could be coated less than 1 μm thick on the substrate using either PVD or CVD (Grill, 1999).

Electroplating: A coating technique which deposited the metal ion on the substrate by making the substrate a cathode by flowing the current through the substrate. During the electroplating process, the metal ion was dissolved in the electrolyte from the anode electrolytically. The metal ion in the electrolyte was transported and deposited on the substrate (Bach et al., 2006).

Electroless plating: A coating material deposition technique which deposited the metal ion by making the standard electrode potential of the metal particle more positively charged than the substrate.

Thermal spray: A coating technique which deposited coating material by impacting high temperature molten coating material with high-velocity to the substrate (Bach et al., 2006).

Cold spray: A coating technique which deposited coating material by impacting soften and high-velocity coating material to the substrate (Raoelison et al., 2018).

Sol-gel coating technique: A coating technique which applied coating on the substrate by formatting an oxide network through hydrolysis and polycondensation of a molecular precursor in the liquid (Innocenzi, 2019).

Hot dipping coating: A coating technique that the substrate was coated by dipping into the molten metal bath.

Build-up soldered brazed coating: A coating technology which used liquid or pasty phase molten filler metal to coat the surface of the substrate.

Differential scanning calorimeter (DSC): DSC was a piece of equipment that measured the heat flux that comes in or out from the material as a function of time and temperature to investigate the thermal property of the material (Groenewoud, 2001).

Dynamic mechanical analysis (DMA): DMA measured the viscoelastic behavior of the material as a function of temperature and periodically changing stress or strain (ASTM International, 2015c).

Demolding: Removing the part from the mold after the part was made.

Digital image correlation (DIC): DIC was an image tracking technology which was used to measure material strain and displacement during the test.

1.9 Summary

This chapter provided a foundation of the study including the background and significance of the study. Research questions were introduced, and the scope of the study was defined in assumption, limitation, and delimitation sections. The

definition section explained the terms used in this study. The next chapter will provide a relevant literature review about fiber reinforced composite materials, composite molds, coating technologies, and coating materials.

CHAPTER 2. REVIEW OF RELEVANT LITERATURE

The author provided a review of information about composite materials, composite part manufacturing processes, and composite mold in this chapter. Coating technologies, including various coating techniques and coating materials, were presented. An overview of the methodology used in this study was laid out by summarizing previous research that was related to coatings used on a polymer substrate.

2.1 Composite materials

2.1.1 Introduction to composite materials

The term 'composite material' described a material made from two or more constituent materials with different physical or chemical properties that, when combined, produced a material with characteristics different from the individual components. The individual components remained separate and distinct within the finished structure, differentiating composites from mixtures and solid solutions (Campbell Jr, 2003; Sheikh-Ahmad, 2009). Among the various composite materials available, fiber reinforced composite material which was a combination of high-performance fiber reinforcement with a polymer matrix was often used in today's industry (Peters, 2013). Fiber reinforced composite was often called advanced composite (Peters, 2013). In fiber reinforced composite structures, the fiber reinforcement withstood most of the applied load for the composite structure. The fiber reinforcement provided longitudinal tensile and compression strength and modulus along the fiber direction (Campbell Jr, 2003; Mallick, 2007; Sterkenburg & Wang, 2014). It also provided stiffness of the structure and electrical conductivity

for some fibers. The commonly used fiber reinforcements in the advanced composite were carbon fiber, fiberglass, and Kevlar (Mallick, 2007; Peters, 2013; Sterkenburg & Wang, 2014). Carbon fiber was widely used in industries that required high performance parts. Carbon fiber had a high strength (25 - 820 GPa axial tensile modulus and 500 - 5000 MPa axial tensile strength), low density, low coefficient of thermal expansion (CTE), and high fatigue resistance (Asthana et al., 2006; Campbell Jr, 2003; Mallick, 2007). The matrix also played an important role in fiber reinforced composite structure. The matrix kept the fiber reinforcements in place and distributed and delivered applied load to the fibers (Campbell Jr, 2003). The matrix also provided fiber buckling resistance strength to the structure, and it covered the fiber reinforcements to protect them from the impact, abrasion, and environment, such as moisture ingression (Campbell Jr, 2003; Dutton, Kelly, & Baker, 2004; Mallick, 2007; Sterkenburg & Wang, 2014). In composite laminate, the matrix provided compressive strength, interlaminar shear, and in-plane shear strength (Campbell Jr, 2003). Figure 2.1 showed the schematic drawing of fiber reinforced composite material. The elastic modulus of continuous fiber reinforced composite along the longitudinal direction (fiber direction) was calculated using the general rule of the mixture equation as follows (Asthana et al., 2006);

$$E_c = V_f E_f + V_m E_m \tag{2.1}$$

where E_c, E_f, and E_m were elastic modulus of composite, fiber, and matrix respectively. V_f and V_m were volume fraction of reinforced fiber and the matrix in the composite. The elastic modulus of composite in the transverse direction (normal to the fiber direction) was calculated using the following equation (Asthana et al., 2006);

$$\frac{1}{E_{ct}} = \frac{V_f}{E_f} + \frac{V_m}{E_m} \tag{2.2}$$

where E_{ct} was the elastic modulus of composite in the transverse direction.

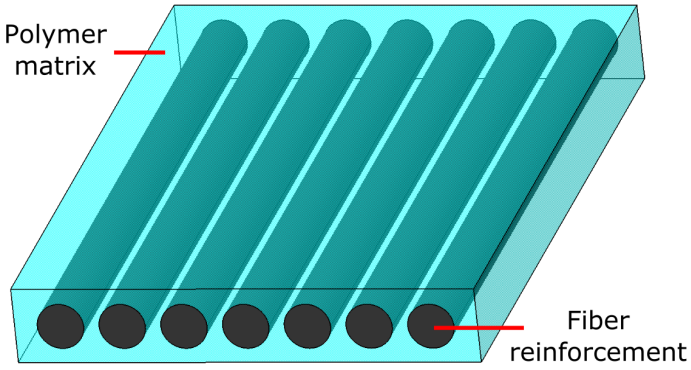

Figure 2.1. Schematic drawing of fiber reinforced composite material.

The polymer matrix could be divided into two categories; thermoset and thermoplastic (Campbell Jr, 2003; Mallick, 2007). Thermoset polymer molecules were chemically joined through rigid 3-dimensional cross-linking to each other during the curing process, so it could not be reformed once it was cured (Campbell Jr, 2003; Mallick, 2007). However, thermoplastic molecules connected to each other with weak secondary bonding instead of chemical bonding during the curing process. Therefore, the secondary bonding could be broken at elevated temperatures, and it allowed the structure to be reformed (Campbell Jr, 2003; Mallick, 2007). Generally, thermoplastic polymers had a higher damage tolerance and impact resistance than thermoset polymers (Campbell Jr, 2003; Mallick, 2007). During the part curing process, thermoplastic materials did not have a chemical reaction. Therefore, it was simpler and quicker than the thermoset polymer that took time before the molecules were crosslinked during the curing process (Campbell Jr, 2003; Mallick, 2007). However, thermoplastic polymers required a higher process temperature than thermoset polymers. Usually, thermoset materials cured around 180°C or lower, but thermoplastic materials needed to be heated up to 260°C - 430°C for the part manufacturing process (Campbell Jr, 2003). Also, the thermoset polymer had a higher thermal stability and higher fluid resistance that was less affected by solvent or paint stripper than thermoplastic (Campbell Jr, 2003; Mallick, 2007). Thermoplastic polymers could be categorized into two groups;

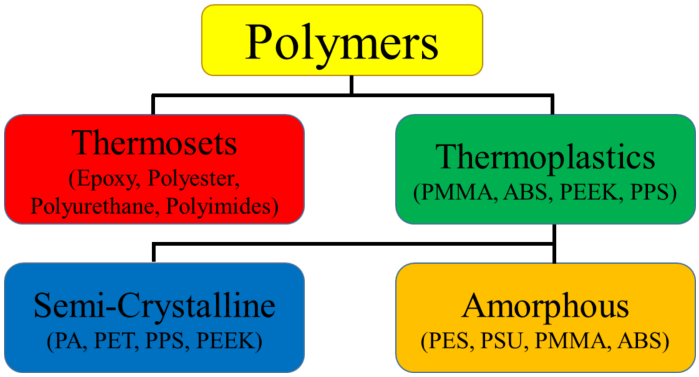

Figure 2.2. Families of polymers.

semi-crystalline polymer and amorphous polymer. The amorphous polymer had randomly arranged molecules and semi-crystalline polymer consisted of a partially crystalline region where the molecules were highly ordered and a partially amorphous region where the molecules were randomly ordered. Generally, the amorphous polymer had a higher impact resistance and dimensional stability than semi-crystalline polymer. The semi-crystalline polymer had a relatively sharp material transition and an amorphous polymer had a gradual material transition (Campbell Jr, 2003; Mallick, 2007). The high inter-molecule force of the crystallinity of the polymer made semi-crystalline polymer tougher than the amorphous polymer. The crystallinity of the polymer increased strength, stiffness, chemical resistance, and temperature resistance of the polymer (Campbell Jr, 2003; Mallick, 2007). Also, the crystallinity of the polymer was opaque. Therefore, transparent thermoplastic was an amorphous polymer (Campbell Jr, 2003). Figure 2.2 described families of polymers.

Different fiber reinforcements and different polymers had their unique characteristics. Depending on the application and desired characteristics of the composite structure, different fiber reinforcements and polymer matrix could be combined to built various composite materials (Mallick, 2007). Combining two or more different kinds of reinforcement fiber in one composite structure, as known as a hybrid composite, was newly developed to incorporate advantages of each fiber

(Dong & Davies, 2013; Sheikh-Ahmad, 2009). Different from metal structures, which were typically considered to have homogeneous properties through the entire structure, fiber reinforced composite structures had anisotropic properties (Hollaway, 1994). Fiber reinforcement in a composite structure had certain orientations which created different material properties depending on the ply or fiber axis directions (Hollaway, 1994; Sterkenburg & Wang, 2014).

2.1.2 Advantages of composite materials

A fiber reinforced composite structure had high strength and low density (Campbell Jr, 2003). Therefore, fiber reinforced composite usually had a higher strength-to-weight ratio than metal (Campbell Jr, 2003). For example, compared to 6061 aluminum alloy, unidirectional carbon fiber composites had five times higher tensile strength (carbon fiber composite: 1550 MPa and 6061-T6 aluminum alloy: 310 MPa) and two times higher modulus in fiber direction (carbon fiber composite: 137.8 GPa and 6061-T6 aluminum alloy: 68.9 GPa) with almost two times lighter weight (density of carbon fiber composite: 1.55 g/cm^3 and density of 6061-T6 aluminum alloy: 2.70 g/cm^3) (Mallick, 2007; Sterkenburg & Wang, 2014). Therefore, the industries which worked with weight critical products, such as aerospace, aviation, and automotive, used fiber reinforced composite materials. Composite materials also had a high fatigue resistance and tolerance, and it did not cause corrosion which was one of the biggest issues in metal structures (Campbell Jr, 2003; Mallick, 2007; Sterkenburg & Wang, 2014). Advanced composite material could have good design flexibility. Anisotropic property of the composite material allowed to create a unique design of the structure by positioning the fiber reinforcements toward the direction where the major stress was applied and high stiffness was required (Campbell Jr, 2003; Mallick, 2007). The advanced composite was also often used for sandwich structure with aluminum honeycomb, Nomex honeycomb, and foam core which provided another degree of design

flexibility (Kim, Sterkenburg, & Tsutsui, 2018; Mallick, 2007). The coefficient of thermal expansion (CTE) of fiber reinforced composite in fiber direction was relatively small. Carbon fiber reinforced composite had CTE between -1.8 μm/m-°C and 1.8 μm/m-°C in the fiber direction. Aluminum had CTE of 23.4 μm/m-°C and steel had CTE of 12.6 μm/m-°C (Mallick, 2007). Therefore, fiber reinforced composite material had higher dimensional stability in elevated temperature than the metal structure. Fiber reinforced composite material had good chemical resistance and less catastrophic failure mechanism than metal (Mallick, 2007).

2.1.3 Application of composite materials

The application of advanced composite materials was increasing (Campbell Jr, 2003). Especially, the aerospace, automotive, and sports good industries used composite material for their products to take advantage of its high strength, stiffness, and modulus to weight ratio (Campbell Jr, 2003; Mallick, 2007). Aerospace was the biggest market for advanced composite materials. One of the most important factors that needed to be considered while designing aircraft was to minimize the weight of the aircraft. By reducing weight, the aircraft could fly faster, carry more weight, and increase the fuel efficiency (Campbell Jr, 2003). However, at the same time, the aircraft structure should have had enough strength to resist pressure from the outside and impact during the flying operation (Dutton et al., 2004). Advanced composite materials were well suited as a material for aircraft structures because they satisfied both requirements; lightweight and high-strength. Therefore, metal aircraft parts which were used predominantly as an aircraft structural material in the past were now being replaced by composite materials (Mallick, 2007; Sterkenburg & Wang, 2014). The advanced composite material was used for both military aircraft and commercial aircraft (Mallick, 2007). Composite material was used for fuselage, wing, rudder, flap, aileron, and interior parts of aircraft (Deo, Starnes Jr, & Holzwarth, 2003; Mallick, 2007). The increased usage of

composites in the aerospace industry was apparent by the percentage usage of composite materials in modern aircraft. The composite material was used in 34% of the material by weight for the Lockheed Martin F-22 Raptor, 35% of the material by weight for the Lockheed Martin F-35 Lightning II, 53% of the material by weight for the Airbus A350 XWB, and more than 50% of the material by weight for the Boeing B787 Dreamliner (Bossi, 2006). Figure 2.3 showed the usage of composite material in the B787 aircraft structure. Carbon fiber reinforced composite was often used for space application due to its low coefficient of thermal expansion (CTE). Space applications, such as spacecraft, satellites, and space scopes, were exposed to high and low temperatures in space (between $-100°C$ to $100°C$) (Mallick, 2007). The carbon fiber reinforced composite structure provided dimensional stability in this temperature variable environment (Mallick, 2007).

The automobile industry had increased the use of composite materials in their vehicles to reduce weight and improve fuel efficiency (Golzar & Poorzeinolabedin, 2010). Advanced composite materials were often used to make external body parts of the automobile due to its high stiffness, dent resistance, and cosmetic purpose. Many automobile parts were manufactured by using compression molding with sheet molding compound (SMC) (Mallick, 2007). Figure 2.4 showed a SMC composite liftgate for an automobile. For some vehicles, not only the material for external body parts, but also materials for parts like leaf springs, driveshafts, and road wheels were replaced by composite materials (Mallick, 2007). Weight of sporting goods such as tennis rackets or golf clubs influenced the performance of the player critically. Therefore, materials for many sporting goods, such as wood or metal, had been replaced by composite materials for weight reduction. Composite materials were often used to make bicycle frames, golf shaft, Tennis racket, ski, fishing rod, and helmets (Mallick, 2007).

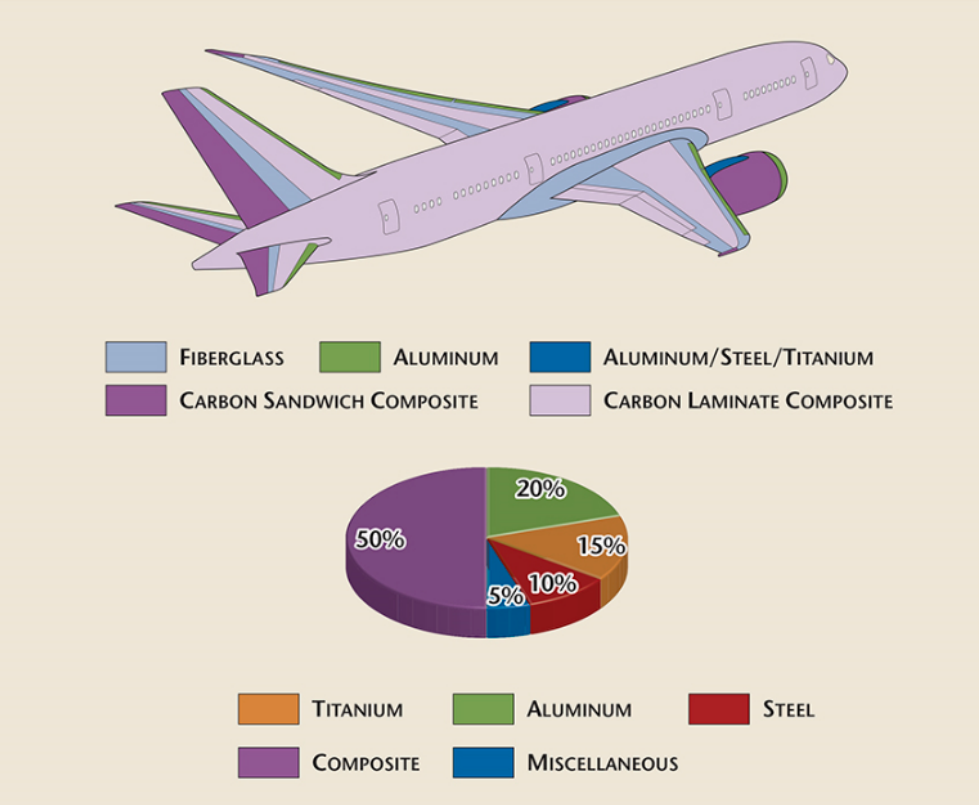

Figure 2.3. Composite materials used in a B787 aircraft structure. Adapted from "Structural Composites: Advanced Composites in Aviation," by R. Sterkenburg and P. H. Wang, 2014, p. 1-2. Copyright 2013 by Avotek Information Resources, LLC.

Figure 2.4. Sheet molding compound (SMC) composite liftgate for automobile.

2.1.4 Composite part manufacturing

In the traditional composite manufacturing process, the composite plies were laid up on the mold in specific fiber orientation, a vacuum bag was applied, and heat and pressure were applied to consolidate and cure the material as showed in Figure 2.5 (Asthana et al., 2006). After the curing process, the cured composite part was detached from the mold and it was trimmed and finished (Campbell Jr, 2003; Centea et al., 2015; Hollaway, 1994; Sterkenburg & Wang, 2014). There were many different kinds of composite part manufacturing techniques, such as filament winding, wet layup, prepreg layup, resin transfer molding (RTM), vacuum assisted resin transfer molding (VARTM), injection molding, automated tape laying, automatic fiber placement, press forming, and additive manufacturing (Hollaway, 1994). Except the additive manufacturing, other composite part manufacturing techniques required a mold to manufacture the part. However, composite additive manufacturing technology often used short fiber reinforcement which was not ideal for manufacturing the high strength structures (Parandoush & Lin, 2017). Therefore, composite additive manufacturing technology was often used to make a mold for composite part manufacturing instead of making the part directly. The mold played a very important role in the composite part manufacturing process. Since the composite material was directly contacted to the mold surface and consolidated, the surface of the mold was important to the composite part surface quality. Also, due to repeated temperature and pressure cycles applied to the mold during the composite part curing process, composite part manufacturing molds were required to have high durability, dimensional stability, thermal fatigue resistance, and thermal shock resistance (He, 2011; Kunc et al., 2016). An improperly prepared mold and its surfaces not only affected the quality of the composite part, but also had the possibility to damage the mold which could lead to a big economic loss. Therefore, the surface properties of the mold should have well understood and prepared before it was used.

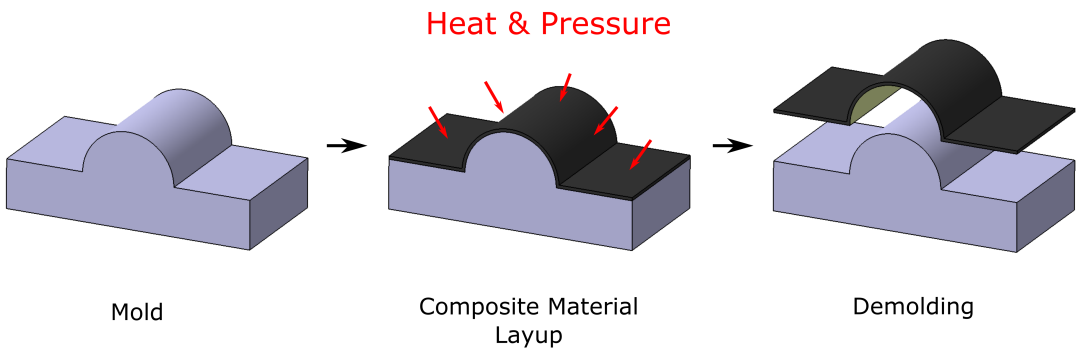

Figure 2.5. Schematic drawing of composite manufacturing process.

The vacuum bagged composite material on the mold, as showed in Figure 2.6, was often cured using either an oven or autoclave (Campbell Jr, 2003; Hassen, Lindahl, et al., 2016). An autoclave provided higher pressure than the vacuum pressure used in an oven to consolidate the composite material on the mold. Therefore, an autoclave was used to manufacture high performance composite parts which contained a very low void content (Hassen, Lindahl, et al., 2016; Kunc et al., 2016). An autoclave applied pressure to the part using pressurized gas. Therefore, the pressure could be applied regardless of the shape of the part if it could be vacuum bagged. However, the size of the part was limited by the size of the autoclave (Campbell Jr, 2003). The cured composite part often underwent post-machining to achieve the desired shape and dimensional accuracy. Machining composite material was different to metal machining (Sheikh-Ahmad, 2009). The heterogeneous nature of composite materials made the machining process more complicated. Improper machining process could cause part defects, such as delamination, matrix cracking, fiber pull-out, and matrix burning. The abrasive fiber in the composite material caused machining tool wear. Therefore, it was important to select the correct machining tool and machining parameters (Sheikh-Ahmad, 2009).

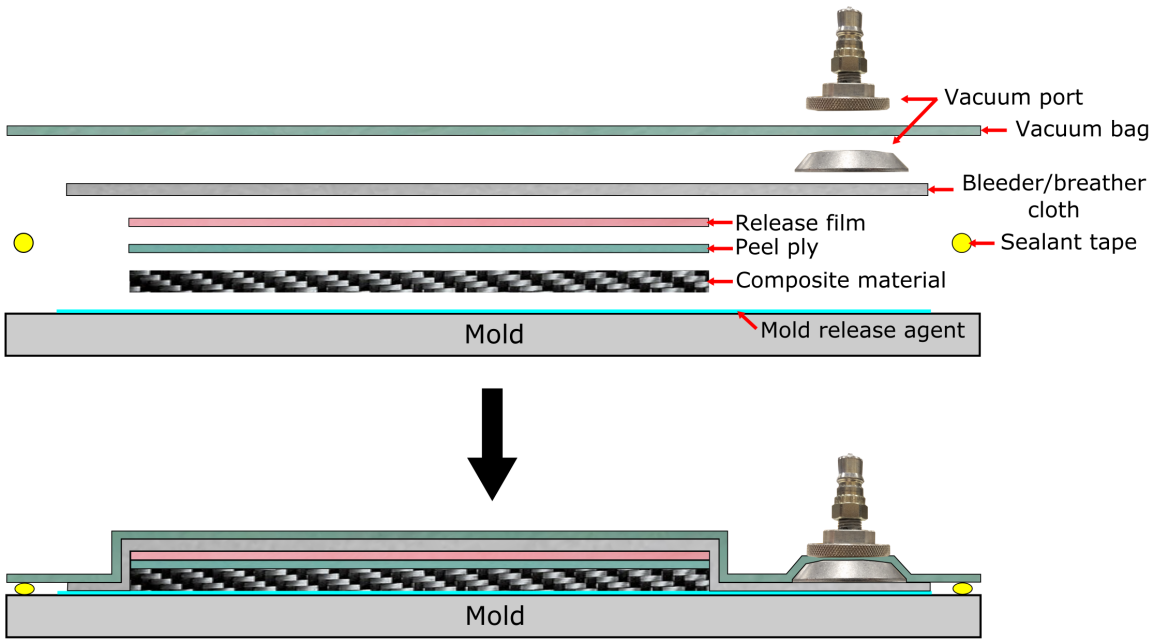

Figure 2.6. 2D Schematic drawing of vacuum bagging process.

2.2 Composite mold

The composite part manufacturing mold was an essential factor in the composite part manufacturing process. In the following section, the author discussed the surface properties of the mold and different materials used for mold manufacturing. The surface properties of the composite mold played an important role in the composite part manufacturing process. The author had listed surface properties that affected the performance of the mold. The definition of properties, how they affected mold performance, and how to measure them were described. Also, the author listed different materials used to make a mold, their characteristics, advantages, and disadvantages.

2.2.1 Surface properties of composite mold

Durability

The durability of the mold surface affected the life expectancy of the mold (Wen et al., 2018). A composite mold was often exposed to various types of damages, such as local impact, surface wear, cyclic load, and deformation (Jhavar, Paul, & Jain, 2013; Mohammadi et al., 2017; Wen et al., 2018). These stresses could lead to worn-out geometries, surface crack, dig, and scratch of the mold (Jhavar et al., 2013). In most cases, the failure of the mold was caused by the shape and dimension changes of the mold due to the deteriorations described above (Nunes, Silva, Andrade, Alexandre, & Baptista, 2017). During the part demolding process, pulling forces, friction, and shear stress between the composite part and the mold surface were applied. Since the fiber of the composite was abrasive, the composite part mold was prone to get wear and damage during the demolding process (He, 2011; Martínez-Mateo, Carrión-Vilches, Sanes, & Bermúdez, 2011). The composite part was often lifted using a scraping tool while it was demolded from the mold, and the excess resin on the surface of the mold was removed with a scraping tool. If the durability of the composite mold surface was low, the surface of the mold had a greater possibility to be scratched, nicked, and dented (Campbell Jr, 2003; Sterkenburg & Wang, 2014). A damaged mold surface led to degradation of the part quality. Therefore, high surface durability was required for composite part manufacturing molds. The durability of the mold surface should have considered when the composite part manufacturing mold was designed and manufactured (Campbell Jr, 2003; Wen et al., 2018). To increase the durability of the mold surface, including surface hardness and wear resistance, the additional coating was often applied on the surface of the mold (Nunes et al., 2017; Silva, Martinho, Alexandre, & Baptista, 2011).

The hardness of the material indicated material's resistance against local deformation, such as surface indentation or penetration of the material (Hashmi,

2016; Powers, Sakaguchi, Craig, et al., 2012; Tabor, 1970). The hardness level of the material surface was closely related to its abrasion resistance and scratching resistance (Siddique & Cachim, 2018). There were many ways to measure the hardness level of the surface; scratch hardness test, static indentation hardness test, and dynamic hardness test (Tabor, 2000). The scratch hardness test was conducted by scratching the material surface with a diamond stylus with a constant load (Tabor, 2000). The width and depth of the scratch were used to measure the hardness of the material. The Mohs hardness test was well known as the scratch hardness test (Powers et al., 2012; Tabor, 1970). The static indentation hardness test was conducted by applying a specific load to the material surface using a spherical, conical, or pyramidal shaped indenter which was made from very hard material (Hashmi, 2016; Neale, 2001; Tabor, 1970, 2000). The depth of the indent and the load applied were inferred to determine the hardness of the surface (Neale, 2001). Well known static indentation hardness tests were: Barcol, Brinell, Rockwell, and Vickers hardness tests (Tabor, 1970, 2000). The dynamic hardness test was conducted by crashing the indenter into the surface of the material (Tabor, 2000). The measured impact energy and the dimension of the indent were used to calculate the hardness of the material (Tabor, 2000).

Surface abrasion resistance represented the ability of the surface to resist from frictional wear. Surface abrasion resistance was often measured by weight loss of the test specimen during the cyclic abrasion effect on the surface. Taber abraser was commonly used for surface abrasion resistance test (Izdebska & Thomas, 2015). The test specimen was located on the turn table of the abraser, and two abrasive wheels were located on the test specimen with a specific load. The test specimen rotated with the turn table and the surface of the test specimen was abraded by two abrasive wheels (Izdebska & Thomas, 2015). The weight change of the test specimen was measured for every certain number of cycles to evaluate the surface abrasion resistance of the material.

Table 2.1. *Society of plastic industry (SPI) mold surface finish standard with typical surface roughness level (Silicon Semiconductor Magazine, 2019).*

Finish	SPI standard	Finishing Method	Surface Roughness (R_a)
Super High Glossy Finish	A-1	Grade #3, 6000 Grit Diamond Buff	0.012 to 0.025
High Glossy Finish	A-2	Grade #6, 3000 Grit Diamond Buff	0.025 to 0.05
Normal Glossy Finish	A-3	Grade #15, 1200 Grit Diamond Buff	0.05 to 0.1
Fine Semi-Glossy Finish	B-1	600 Grit Paper	0.05 to 0.1
Medium Semi-Glossy Finish	B-2	400 Grit Paper	0.1 to 0.15
Normal Semi-Glossy Finish	B-3	320 Grit Paper	0.28 to 0.32
Fine Matte Finish	C-1	600 Grit Stone	0.35 to 0.40
Medium Matte Finish	C-2	400 Grit Stone	0.45 to 0.55
Normal Matte Finish	C-3	320 Grit Stone	0.63 to 0.70
Satin Textured Finish	D-1	Dry Blast Glass Bead #11	0.80 to 1.0
Dull Textured Finish	D-2	Dry Blast #240 Oxide	1.0 to 2.8
Rough Textured Finish	D-3	Dry Blast #24 Oxide	3.2 to 18.0
As Machined	-	Finished to the machinist's discretion	3.2

Surface finish quality

Surface roughness was the value which indicated the irregularity of the surface (Hashmi, 2016). The surface roughness of the composite mold was an important factor that determined the performance of the mold. The surface quality of the composite part was influenced by the surface roughness of the mold (Martínez-Mateo et al., 2011; Mohammadi et al., 2017). The Society of Plastic Industry (SPI) classified the mold surface finish level A to D based on the surface roughness level of the mold (Mohammadi et al., 2017). The mold surface with a smaller surface roughness level was classified as a higher quality finished surface. Table 2.1 showed SPI mold surface finish standard with a typical surface roughness level.

Surface roughness was closely related to surface porosity and surface friction (Gadelmawla et al., 2002). Surface porosity was the measurement of how many pores there were on the material surface. Surface porosity increased surface roughness, and surface roughness increased the contacting area between the composite part and the mold. Surface friction was quantified by the force that occurred when the object moved on the surface. Surface friction was affected by many different factors, such as contact pressure, the mechanical property of

material, contact surface roughness (Y. Zhou et al., 2015). A high surface roughness led to a high coefficient of friction of the surface, and high surface friction increased the demolding force (Ivkovic, Djurdjanovic, & Stamenkovic, 2000). High demolding force not only caused local stress of the composite part, but also had the possibility to damage the mold. The high demolding force stressed the mold surface and it could cause cracking or chipping of the mold surface. Therefore, a mold surface that had a low demolding force was desirable for the composite part manufacturing process. The surface roughness also affected the volume of the mold cavity and the heat transfer between the mold surface and the part (Zhang, Ong, & Lam, 2007). Therefore, it affected temperature, viscosity, and shear rate of the resin on the mold surface. High roughness of the mold surface led to inaccuracies in simulating or predicting the part manufacturing process (Zhang et al., 2007). Mold makers often finished the mold surface by a hand finishing operation or applying an additional coating on the surface of the mold to lower the surface roughness and increase the releasability of the mold (Mellouli, Haddar, Köster, & Ayedi, 2014).
Martínez-Mateo et al. (2011) reported that a mold manufacturer spent 2/3 of the total mold cavity insert manufacturing cost in the machining and polishing process of the mold. However, an excessive polishing process deteriorated the dimensional tolerance of the mold (He, 2011). Therefore, it was ideal to achieve dimensional accuracy and a good surface roughness level with a minimum amount of polishing (Martínez-Mateo et al., 2011). The traditional method of measuring the surface roughness was scanning the surface using a fine stylus. The vertical movement of the stylus during the scanning was measured, and the surface roughness was calculated. Surface roughness measurement had many parameters, including amplitude parameter, spacing parameter, and hybrid parameter (Gadelmawla et al., 2002). The amplitude parameter was a key parameter which indicated the vertical characteristic of the surface deviation and it was often used to determine the quality of surface finish (Gadelmawla et al., 2002). There were arithmetic average height (R_a), ten-point height (R_z), and the maximum height of the profile (R_max) in the

amplitude parameters (Gadelmawla et al., 2002). The surface roughness also could be measured using a surface profiling technology with a laser scanning technique.

2.2.2 Materials for composite mold

A composite mold could be built using different kinds of material (Campbell Jr, 2003). Each material had different advantages and disadvantages as a material for composite part manufacturing molds. Therefore, the material for composite part manufacturing mold needed to be chosen carefully depending on the application and desired characteristic of the mold. In the following section, the different materials which were used for composite part manufacturing mold were introduced. Their characteristics, advantages, and disadvantages as a composite part manufacturing mold material were discussed.

Tooling board

Epoxy, polyurethane, or stereolithography resin-based tooling boards were often used to build a mold for composite part manufacturing (Sterkenburg & Wang, 2014; Stewart, 2009). Tooling board manufacturers offered a variety of choices of material types, hardness, density, and operable temperature range of tooling board to customers (Stewart, 2009). The tooling boards could be bonded to each other using an adhesive (Sterkenburg & Wang, 2014). Therefore, the size and shape of the mold stock could be customized as necessary. Tooling board was a cost-efficient material and easy to machine (Stewart, 2009). Recently, many tooling board manufacturers had developed tooling board which could be used for high temperature application with a relatively small CTE. A tooling board composite mold could be used to produce a limited number of composite parts. Therefore, it was often used for rapid prototyping or master tool type of mold making. Figure 2.7 showed tooling board composite part manufacturing mold.

Figure 2.7. Tooling board composite part manufacturing mold.

Aluminum

Metals had been popularly used for the manufacturing of composite part manufacturing molds for many years (Sterkenburg & Wang, 2014; Vangerko, 1988). Especially, aluminum molds were widely used in composite manufacturing processes. Aluminum was light (66% lighter than steel) and cost-efficient compared to other metals. Aluminum was a soft metal (Baranek, 2012). Therefore, it had good machinability and polishability, but at the same time, it could be easily scratched, nicked, and dented (Baranek, 2012; Campbell Jr, 2003; Sterkenburg & Wang, 2014). An aluminum mold could be heated up rapidly due to its high heat conductivity. Therefore, the composite part production cycle time could be shortened using an aluminum mold (Baranek, 2012). Aluminum had a high coefficient of thermal expansion (CTE) which was not a good characteristic for composite part manufacturing mold material (Campbell Jr, 2003). Therefore, a CTE analysis of the mold at the composite part curing temperature should have performed and used for compensating the shape of the mold for dimensional accuracy of the composite part (Sterkenburg & Wang, 2014). Figure 2.8 showed aluminum composite part manufacturing molds.

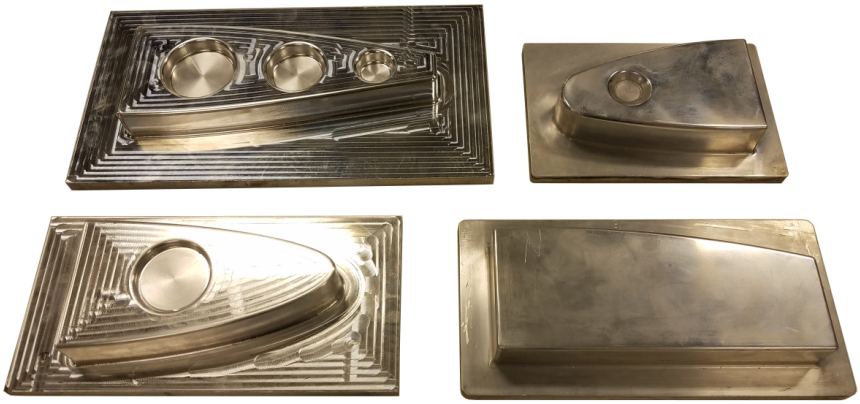

Figure 2.8. Aluminum composite part manufacturing mold.

Steel

Steel had been one of the most popular mold materials for the autoclave composite manufacturing process. It had a high durability with high surface hardness and wear resistance, and relatively low cost. Also, steel could be cast and welded which were helpful for manufacturing and repairing the mold (Campbell Jr, 2003). Steel molds for composite part manufacturing process had a long-life expectancy and high-volume production capability (more than 1500 autoclave cycle) (Campbell Jr, 2003). The commonly used steel for mold making was P-20 tool steel (40CrMnNiMo8-6-4) (Martínez-Mateo et al., 2011). Invar steel, a steel alloy with 36% nickel-steel, had a uniquely low CTE (Campbell Jr, 2003; Sterkenburg & Wang, 2014; Stewart, 2009). Due to these advantages, steel and Invar were widely used as a composite part manufacturing mold material. However, steel and invar were heavy, difficult to machine, and had a low heat conductivity (Baranek, 2012; Campbell Jr, 2003). Steel tended to corrode easily, and Invar was an expensive material (Baranek, 2012; Campbell Jr, 2003). Composite part manufacturing mold also could be made by bonding metal sheets, aluminum, steel, or Invar, to a mold frame (Sterkenburg & Wang, 2014). The frame could be made of metal or composite materials (Vangerko, 1988). An Invar/composite hybrid mold had only

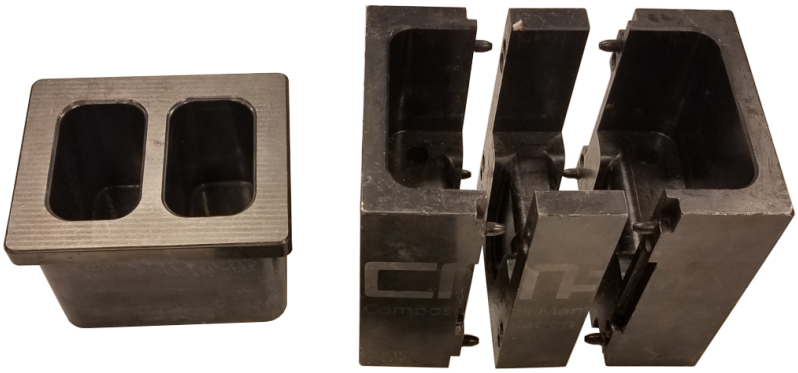

Figure 2.9. Steel composite part manufacturing mold.

50% of the weight compared to a conventional Invar mold (Stewart, 2009). Figure 2.9 showed steel composite part manufacturing molds.

Composite material

Composite materials could be used to build a mold in various ways; wet layup tooling, prepreg tooling, carbon foam tooling, and additively manufactured composite tooling (Sterkenburg & Wang, 2014). Tooling board or metal composite part manufacturing molds were often manufactured by designing the mold using computer aided design (CAD) and machining using computer numeric control (CNC) milling machine with computer aided manufacturing (CAM) technology. Differently, the traditional composite mold manufacturing process required a master mold of the part. The composite material was laid up on the master mold and cured to make a composite mold (Campbell Jr, 2003; Vangerko, 1988). Composite mold had several advantages in the composite part manufacturing process. Fiber reinforced composite materials were lightweight and low CTE (carbon fiber) (Campbell Jr, 2003; Stewart, 2009). The heating and cooling rate of the material was more suitable for composite part manufacturing than metal (Campbell Jr, 2003; Sterkenburg & Wang, 2014; Stewart, 2009). However, the surface property of a composite mold was not as good as a metal mold for the composite manufacturing

Figure 2.10. Fiberglass reinforced composite mold for composite part manufacturing.

process. Especially, the surface of the composite mold surface was not as durable as a metal mold, so the surface of the mold was more prone to get damaged (Stewart, 2009). Also, the surface of the composite mold was often rougher than metal mold due to the heterogeneous nature of composite. Chardon et al. (2017) studied building carbon fiber reinforced thermoset polymer composite mold. Chardon et al. (2017) reported that the mold surface was rough even after the post-machining process with computer numerical control (CNC) milling machine because of the broken fibers on the surface. An additional coating, such as a gelcoat, was often applied to the surface to improve durability, roughness and, aesthetic of the mold surface (Gombos & Summerscales, 2016). The matrix of composite materials tended to crack during the repeated thermal cycle (Campbell Jr, 2003). Therefore, it was important to understand the thermal behavior of the mold material before it was used for the high temperature composite part manufacturing process (Campbell Jr, 2003). Figure 2.10 showed composite mold for the composite part manufacturing process.

2.2.3 Additively manufactured composite mold

Additive manufacturing technology was one of the biggest topics in the 4th industrial revolution which marked emerging advanced technologies for today. The American Society for Testing and Material (ASTM) defined additive manufacturing as the process of bonding materials to make objects from 3D model data, usually, layer upon layer (ASTM International, 2010). The additive manufacturing process built the part layer by layer, and the part could be made with various kinds of material (Muthu & Savalani, 2016). In the part additive manufacturing process, the part was designed using CAD and virtually sliced layer by layer using a slicing software (Sudbury et al., 2017). Figure 2.11 showed part additive manufacturing process. The additive manufacturing technology allowed to manufacture more complex geometrical shaped parts and gave more freedom for part design or pattern of the part (Sudbury et al., 2017). Additive manufacturing was widely used for rapid prototyping and part manufacturing in various industries including the medical, aerospace, and automobile industry (Guo & Leu, 2013). One of the biggest advantages of additive manufacturing was material efficiency (Watson & Taminger, 2018). Only a little bit more material than what the part needed was used for manufacturing the part. On the other hand, the subtractive manufacturing process used a stock material at the beginning of the process and cut it into the final part using CNC or lathe. The amount of material waste in the subtractive manufacturing process was usually larger than the additive manufacturing process. With a subtractive manufacturing process, the average weight ratio of the final part to the original stock of the part in the aerospace industry was about 1:10 which meant only 10% of the original material was used for the final part (Watson & Taminger, 2018). However, the additive manufacturing process was not always the best choice for part manufacturing. The additively manufactured part did not have an as highly dimensional accurate surface as the subtractively manufactured part (Watson & Taminger, 2018). Also, the subtractively manufactured part had a smoother surface

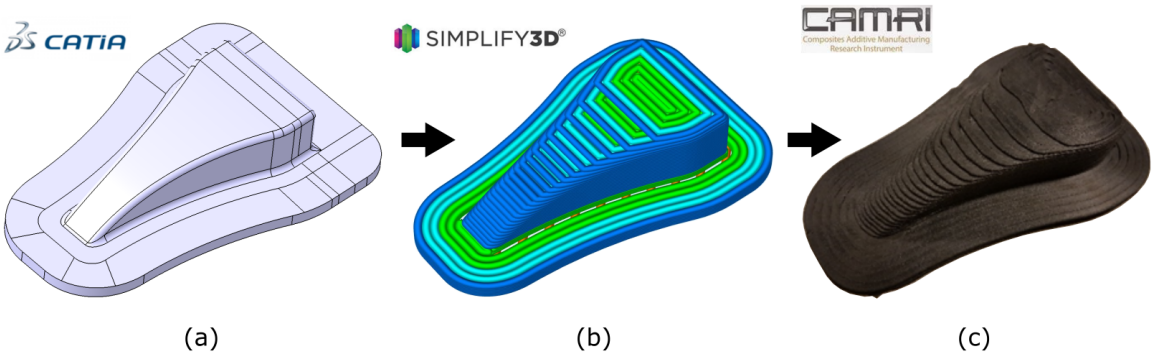

Figure 2.11. Part additive manufacturing process. (a) Part designed with CAD software, (b) virtually sliced layer by layer using slicing software, and (c) additively manufactured using additive manufacturing instrument.

finish than the additively manufactured part (Watson & Taminger, 2018). Additive manufacturing techniques usually had a longer processing time which led to higher energy consumption than subtractive manufacturing techniques. Considering both advantages and disadvantages of additive manufacturing and subtractive manufacturing, people often combined the two manufacturing methods to take advantage of both methods (Paris, Mandil, et al., 2017).

The rapid development of additive manufacturing technology allowed people to additively manufacture even a composite material (Barocio, Brenken, Favaloro, & Pipes, 2017). The extrusion deposition additive manufacturing (EDAM) method with short fiber reinforcement mixed in a thermoplastic polymer was widely used in the composite additive manufacturing industry. Different from the traditional fused deposition modeling (FDM) which used continuous filament form of printing feedstock, EDAM used pelletized feedstock for printing. Barocio et al. (2017) indicated that utilizing the pelletized feedstock material in EDAM reduced the material cost and enlarged the range of applicable printing materials. Sudbury et al. (2017) mentioned that using pelletized composite material was six times cheaper than using continuous filament material for printing composite material. The pelletized feedstock was molten in the extruder, and the molten printing material was deposited layer by layer on the printing bed through the printing nozzle. Figure

2.12 showed a schematic drawing of the EDAM process. Due to its lightweight and low CTE, the additively manufactured composite part was often used for building a mold for composite part manufacturing. Traditional composite molds were handmade by skillful technicians. Therefore, the quality of the mold varied depending on the mold making skill of the technician (Duty & Springfield, 2015; Sudbury et al., 2017). Also, handmade composite molds took a long time to make, and dimensional accuracy of the mold could not be guaranteed (Duty & Springfield, 2015; Sudbury et al., 2017). Especially, traditional large-scale molds had several manufacturing steps which made labor intensive process (Sauerbier, Anderson, & Gardner, 2018). The composite mold manufacturers used composite additive manufacturing technology to eliminate these issues (Duty & Springfield, 2015; Sudbury et al., 2017). Since the additive manufacturing technology built the part layer by layer, the surface of the additively manufactured part was not very accurate. Therefore, post finishing processes were required to create an accurate and smooth surface of the mold. Computer numerical control (CNC) milling machines were widely used for the post-machining process. Figure 2.13 showed additively manufactured composite mold before and after post-machining process.

The Composite Additive Manufacturing Research Instrument (CAMRI) was developed and built by the Purdue Composites Manufacturing and Simulation Center (CMSC) Additive Manufacturing (AM) team. CAMRI utilized EDAM technology for the fiber reinforced composite additive manufacturing process (Barocio et al., 2017). CAMRI used two different nozzle sizes, 3.175 mm diameter and 4 mm diameter. The maximum printing size of the CAMRI was 0.5 m x 0.5 m x 0.38 m, and it could print a maximum of 9.07 kg of material per hour (Barocio et al., 2017). Barocio et al. (2017) successfully printed polyphenylene sulfide (PPS) with 50% carbon fiber by weight and polyether ether ketone (PEEK) with 50% carbon fiber by weight using CAMRI and confirmed its performance as a high temperature curing composite part manufacturing mold. Figure 2.14 showed the composite additive manufacturing research instrument (CAMRI) located in Purdue

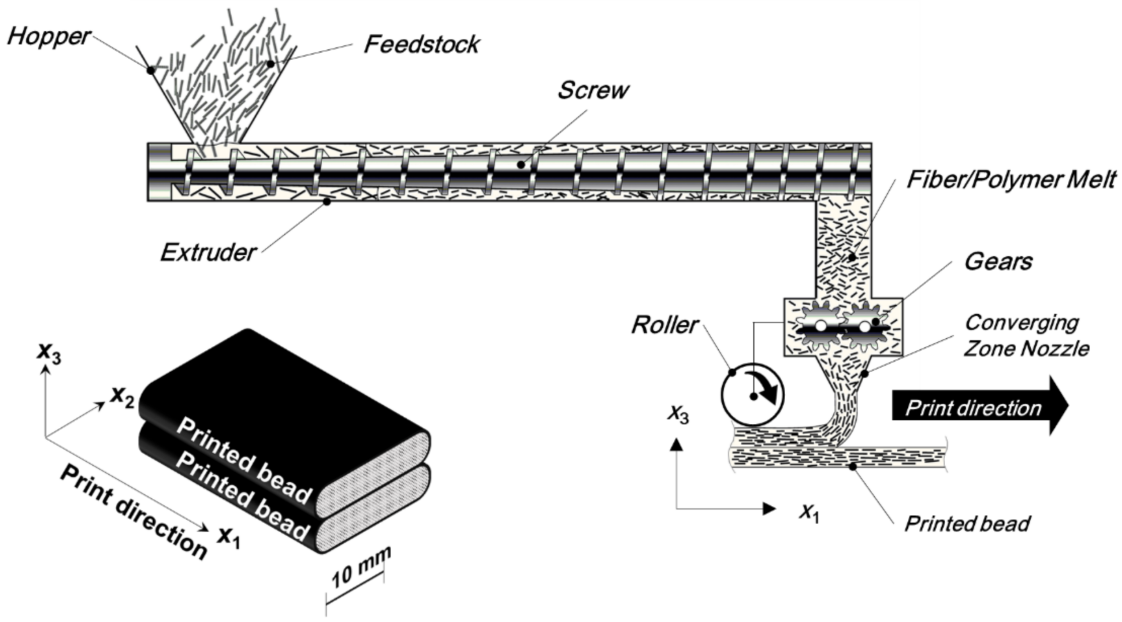

Figure 2.12. Schematic drawing of EDAM process. Adapted from "In-silico Tensile Testing of Additively Manufactured Short Fiber Composite," by M. Ramirez, 2018, p. 5. Copyright 2018 by M. Ramirez.

Figure 2.13. Additively manufactured composite mold (a) before and (b) after post-machining process.

University. Big Area Additive Manufacturing (BAAM) was developed by Cincinnati Incorporated, a partnership with Oak Ridge National Labs (Kunc et al., 2016). BAAM utilized a high speed 3-axis gantry to move the extruding nozzle (Kunc et al., 2016; Sudbury et al., 2017). BAAM also used the EDAM process with a single screw extruder and high-speed linear drive to extrude the printing material. The diameter of the extruding nozzle was between 4 mm and 7.6 mm which allowed BAAM to print the maximum of 45 kg of material per hour (Kunc et al., 2016). The capable printing size was 6 m x 2.5 m x 2 m (Sudbury et al., 2017). Hassen, Lindahl, et al. (2016) reported that they successfully manufactured a dimensionally stable high temperature autoclave composite mold using BAAM. The cost for printing the composite mold was 10 times cheaper than traditional tooling techniques and the time it took to print the mold was significantly shorter than the traditional mold manufacturing process (Hassen, Lindahl, et al., 2016; Sudbury et al., 2017). Kunc et al. (2016) printed composite molds using BAAM with two different types of polymer; PPS with 50% carbon fiber by weight (semi-crystalline) and polyethersulfone (PESU) with 25% carbon fiber by weight (amorphous). The printed molds were machined using a 5-axis gantry CNC milling machine with 12.7 mm diameter milling bit (14,500 rpm and 0.0254 mm stepover). Kunc et al. (2016) reported that the surface roughness of $R_a = 64$ μm was achieved. Hassen, Springfield, et al. (2016) built a 3D printed composite mold for room temperature curing vacuum assisted resin transfer molding (VARTM) process using BAAM. The size of the mold was 0.965 m x 0.559 m x 0.152 m. Due to the porosities inside of the printed part, the vacuum integrity of the mold surface was difficult to achieve (Hassen, Springfield, et al., 2016). Therefore, Hassen, Springfield, et al. (2016) applied additional surface coating on the surface of the mold with a standard tooling gel. The applied coating was machined and polished. The mold achieved vacuum integrity and it was used for the VARTM process (Hassen, Springfield, et al., 2016). Sudbury et al. (2017) measured the durability of the additively manufactured composite mold, built using BAAM, by measuring the number of parts pulled from

the mold before the mold was no longer serviceable. Sudbury et al. (2017) applied a different coating on the mold and used it for the composite manufacturing process. None of the coatings survived for more than five manufacturing cycles. In most cases, the coating debonded from the mold regardless of the direction of the printing (Sudbury et al., 2017). Duty and Springfield (2015) also investigated the number of parts pulled from the mold before the mold failed to measure the durability of the additively manufactured composite mold, built using BAAM. Duty and Springfield (2015) applied an epoxy coating on the surface to reduce the surface roughness of the mold and compared it to a non-coated mold. The maximum number of pulls from the coated mold was four, and from the non-coated mold was five. The coated mold failed because the coating detached from the mold. After five part pulls from the non-coated mold, the mold surface became too rough to use for composite part manufacturing (Duty & Springfield, 2015). The 3D printed composite mold showed a significantly limited number of capable part production runs compared to a traditional composite part manufacturing mold (Sudbury et al., 2017).

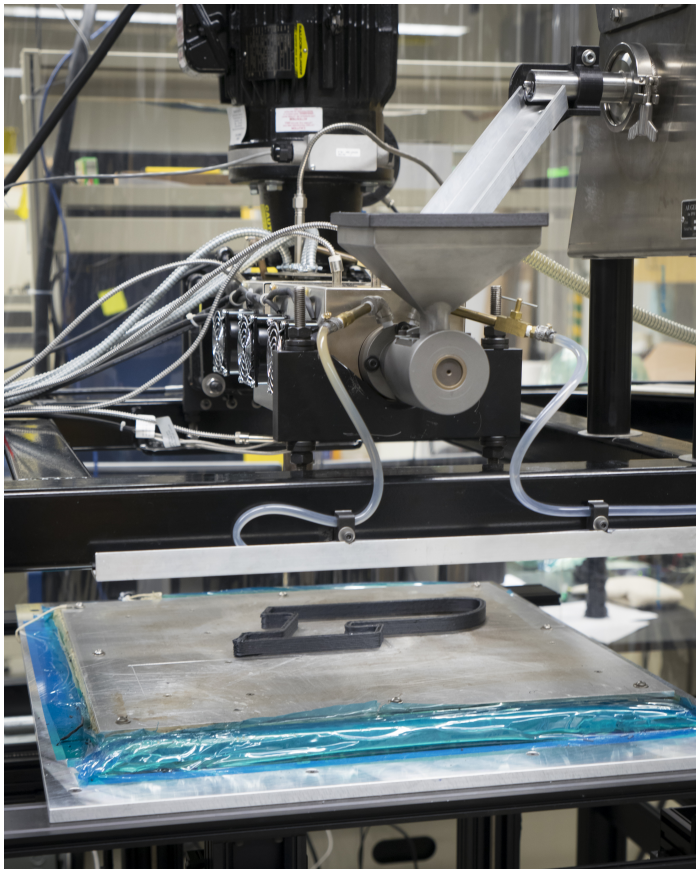

Figure 2.14. Composite Additive Manufacturing Research Instrument (CAMRI) located at Purdue University.

2.3 Coating

Coating technology for metal molds had been used for a long time already (Mercer, 2012; Nunes et al., 2017; Silva et al., 2011; Vangerko, 1988). Protective coating on metal tools increased the performance of the mold and its life expectancy (Mercer, 2012; Vangerko, 1988). Many coatings were applied to the metal mold to increase corrosion resistance, hardness, and chemical stability (Vangerko, 1988). To increase the performance of additively manufactured composite mold, such as surface hardness, abrasion resistance, and roughness, the author applied an additional coating on the mold surface. The author investigated how additional coating on the surface of the 3D printed composite mold improved the required surface property and its performance as a mold for composite part manufacturing. In the following section, the author discussed different coating technologies and coating materials used on a polymer substrate.

2.3.1 Introduction to coatings

Coating technologies were widely used in people's daily lives. A protective glass coating for the smartphone was used for improving the wear resistance of the screen. The automobile body had a coating for improving corrosion resistance and decorative purposes. The milling tool had a coating for improving hardness, abrasion resistance, and wear resistance. Many industrial parts were required to have certain surface properties, such as hardness, roughness, corrosion and wear resistance, electrical conductivity, and appearance (Asthana et al., 2006; Bach et al., 2006). However, part properties did not always meet the requirements. Therefore, coating technologies were developed to provide the required surface properties (Bach et al., 2006). A coating was a bonded layer of a different material on the surface of the substrate (Faure-Geors, 1994). The substrate was a workpiece that the coating was applied to. The additional layer of coating material was applied to the surface of the substrate to provide the required surface properties. Finding an optimal

Table 2.2. *Properties of coating. Reprinted from "Modern Surface Technology," by F.W. Bach, A. Laarmann, and T. Wenz, 2006, p. 298. Copyright 2006 by the WILEY-VCH.*

Mechanical Properties	Physical Properties	Chemical Properties
Adhesion	Thermal conductivity	Chemical composition
Hardness	Electrical conductivity	Corrosion resistance
Coating thickness	Magnetic property	Erosion endurance
Wight of coaitng	Acoustic property	
Microstructure		
Abrasion resistance		
Ductility		
Porosity		

coating technique and coating material were important. Inappropriate coating techniques and coating materials could cause a coating failure and damage the substrate. There were more than 1000 coating techniques and 40,000 - 80,000 different coating materials (Bach et al., 2006). Also, there was no such thing as a universal coating that could be an optimal choice for every application (Asthana et al., 2006). Therefore, a systematic approach was necessary to find the best coating technique and coating material for each application (Bach et al., 2006). There were many different types of coating properties that needed to be considered before the coating was applied. Table 2.2 showed a list of mechanical, physical, and chemical properties of a coating.

The property of a coating was not only affected by the coating material but also by the numerous conditions of the coating application process. For example, the adhesion strength between the coating and the substrate was one of the most important factors of coating quality. The adhesion strength of the coating was not only determined by the type of coating technique or coating material, but also by the relationship between the coating material and the substrate material, types of bonding area, pre-treatment of the substrate surface, and even the environmental

conditions, such as temperature and humidity, during the coating application process (Asthana et al., 2006; Bach et al., 2006). The coefficient of thermal expansion (CTE) mismatch between the coating and the substrate was another important factor that should be considered (Asthana et al., 2006; Vangerko, 1988). If there was a CTE difference between the coating and the substrate, the different amounts of thermal expansion at elevated temperature caused internal thermal stress between the coating and the substrate (King & Bell, 1988). During the repeated composite part cure cycles, coating failure and crack propagation of the coating and substrate could be caused by the cyclic internal thermal fatigue stress (King & Bell, 1988). Also, the coating failure and the crack propagation due to rapid temperature change which caused an internal thermal stress that was greater than interface strength was called thermal shock (King & Bell, 1988). King and Bell (1988) reported that low CTE mismatch and high coating toughness increased thermal shock resistance. By considering all these small details, the optimal coating for a part could be achieved. Lastly, the costs of the coating process also needed to be considered (Asthana et al., 2006; Bach et al., 2006; Faure-Geors, 1994). Some of the coating techniques incurred high initial cost because of the equipment. If the desired surface for the application could be achieved using a cheaper coating method, there was no reason to spend more money on expensive resources.

2.3.2 Coating techniques

There were numerous coating techniques. Therefore, it was necessary to categorize the techniques to facilitate finding an optimal coating technique for each application. The coating techniques could be categorized by the phase of coating material, coating thickness, and process temperature (Bach et al., 2006). Coating techniques could be categorized according to the phase of coating material during deposition (Bach et al., 2006). The coating material could be deposited as a gas, vapor, liquid, solid, and solution form. During physical vapor deposition (PVD) and

chemical vapor deposition (CVD) coating techniques, the coating material was deposited on the substrate in gas or vapor phase. Liquid coating or dip coating techniques used liquid phased coating material. Thermal spray, build-up brazing, soldering, and welding techniques used pasty phased coating material. Cold spray and powder electro-plating coating techniques used solid phase material. Electroplating in an aqueous solvent and electroless-plating techniques used solution phased coating material. The coating techniques could be categorized according to the thickness of the coating (Bach et al., 2006). PVD and CVD were called thin film coating technologies. They had a coating thickness between 0.001 mm to 0.1 mm. PVD usually had a slightly thicker coating than CVD. Electroplating techniques provided a coating thickness between 0.01 mm to 5 mm depending on the coating material. A thermal spray coating had a thickness between 0.1 mm to 1mm. build-up brazing, soldering, and welding technique could provide an even thicker coating (Bach et al., 2006). The process temperature of the coating application was different depending on the coating technique and coating material used. The coating process temperature must be lower than the melting temperature of the substrate. The polymer or plastic substrate had a low melting temperature. However, many coating techniques had a high coating process temperature that was even higher than the melting temperature of the polymer or plastic substrate. The coating process temperature for CVD, Thermal spraying, build-up brazing, and welding was relatively high. Cold spray, ion plating, electroplating, and electroless plating techniques had a low process temperature. Figure 2.15 showed the substrate temperature range during a coating process and coating thickness range for each coating technology.

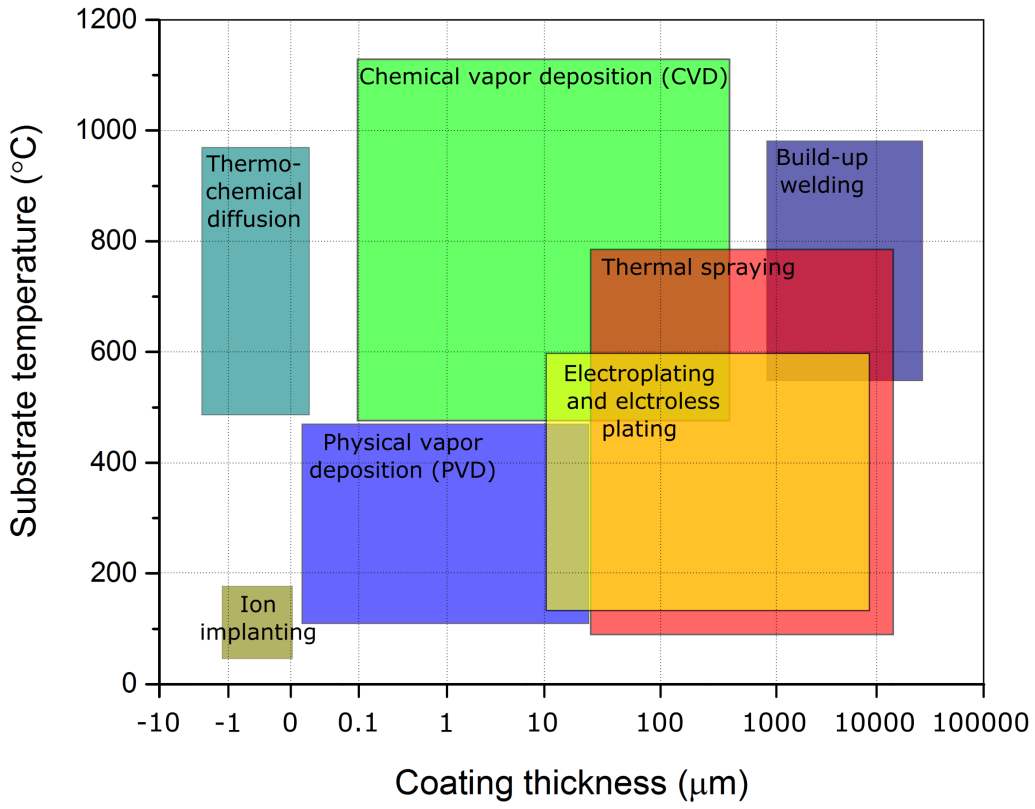

Figure 2.15. Substrate temperature and coating thickness range for each coating technique. Reprinted from "Modern Surface Technology," by F.W. Bach, A. Laarmann, and T. Wenz, 2006, p. 160. Copyright 2006 by the WILEY-VCH.

Liquid coating

The most common coating that people saw in daily lives was a paint, which was a form of liquid coating. A liquid coating technology was the easiest coating technique that was commonly used in various industries. Liquid coating materials usually had four different components; binder, pigment, carrier, and additive (Hornbaker, Keene, Krawiec, & Wilken, 2013). The binder was the main part of a liquid coating material that was left after all the carrier was evaporated. The pigment determined appearance, such as color or gloss of the coating. The carrier took up most of the liquid part of the coating material. It was mostly solvent or water. To reduce the volatile organic compound (VOC) release during liquid coating application, the use of a water-based carrier had increased (Hornbaker et al., 2013). The carrier transferred the liquid coating components to the substrate and helped them to make an even layered coating. After the liquid coating was applied to the substrate, the carrier evaporated, and the coating became a solid layer. The additive held the special properties, such as corrosion resistance or UV protection to the coating. Liquid coating techniques were relatively simple, easy, and quick. Also, the initial cost of the coating application process was low because there was no need for any expensive equipment. The liquid coating techniques were an economical and cost-effective coating method (Hornbaker et al., 2013). Usually, the substrate was pre-treated before the liquid coating application. The contaminants on the surface were removed and the surface was wiped with a solvent or pre-treatment chemical (Hornbaker et al., 2013). A liquid coating was often applied by hand brush or spray gun (Gombos & Summerscales, 2016). Manual liquid coating application required human skills to control the thickness and prevent runs and sags of coating material during the application (Suzuki, Kikuchi, Takai, Goto, & Hamada, 2015). Gombos and Summerscales (2016) introduced an in-mold gelcoating technique which applies a liquid gelcoat in the closed mold tool by injecting the coating material inside of the closed tool. Gombos and Summerscales (2016) reported that the in-mold gelcoat

technique significantly reduced the number of styrene levels in the workspace. Both thermoset and thermoplastic polymer coatings could be applied using a liquid coating technique (Asthana et al., 2006). The thermoplastic coating material was heated and melted when it was sprayed on the substrate and hardened on the substrate when it was cooled down. Commonly used thermoplastic liquid coatings were PVC, nylon, and polypropylene (Asthana et al., 2006). Thermoset coating involved a chemical reaction of the coating material during the coating application process. Commonly used thermoset liquid coatings were acrylic, epoxy, phenolic, and silicone (Asthana et al., 2006). Gelcoat was one of the most commonly used liquid coatings that were used in today's industries. Gelcoat was a thin layer of resin coat, usually, epoxy or polyester (Ahmad, Abdullah, & Abd Kadir, 2015). Gelcoat often consisted of a two-part system; resin and hardener. Gelcoat was mainly used for improving durability, reducing surface roughness, or decorative purposes (Gombos & Summerscales, 2016). Gelcoat protected the substrate from environmental damage, such as water damage, or UV light damage. Also, the gelcoat provided high gloss and homogeneous surface (Ahmad et al., 2015; Hornbaker et al., 2013). Gelcoat was often used in the composite industry for coating fiber reinforced substrates (Ahmad et al., 2015). Sometimes, additional additives were added into the liquid resin coating to provide special properties to the coating (Asthana et al., 2006; Hollaway, 1994; Hornbaker et al., 2013). For example, glass flakes in the gelcoat gave the coating had high wear or abrasion resistance (Hollaway, 1994). However, additives in the coating material could reduce its flexibility or opacity. Yan, Cai, Lu, and Miyakoshi (2017) studied the properties of epoxy lacquer coating mixed with aluminum powder. Yan et al. (2017) applied the coating with a different aluminum mass fraction to the substrate and compared them, and they reported that the infrared radiation (IR) emission and surface gloss increased when the aluminum mass fraction in the coating decreased. The adhesion strength and corrosion resistance of the coating were highest when the aluminum mass fraction was 30% (Yan et al., 2017). Liquid coating technology was often used

with other solid materials to create an additional mechanical or dimensional property for the coating. For example, a thick coating layer was difficult to make if the liquid coating material had a low viscosity. Additional fiber reinforcement needed to be added to the liquid coating material to hold the liquid coating on the surface (Chardon et al., 2017). Fiber weave, mat, or veil were often used as a solid material. Adding a fiber reinforced prepreg on the surface was a similar concept. A liquid coating with fiber reinforcement was often used with a post-machining process to meet the dimensional requirement (Chardon et al., 2017).

Vapor-phase deposition

The vapor-phase deposition technology applied a variety of materials in the vapor phase to the substrate (Asthana et al., 2006). The vapor-phase deposition technology could be divided into two big categories; physical vapor deposition (PVD) and chemical vapor deposition (CVD) (Friz & Waibel, 2003). Usually, PVD had a lower process temperature and closer tolerance than CVD (Graves, 2002). Both PVD and CVD were thin film deposition techniques which were widely used in automobile parts, metal forming, cutting tools, injection molding, and electronic semiconductor (Bach et al., 2006; Cha & Erdemir, 2015; Griffiths, Rees, Kerton, & Fonseca, 2016; Silva et al., 2011). Especially, the use of diamond-like carbon (DLC) coating had increased rapidly (Cha & Erdemir, 2015). DLC was an amorphous carbon material which could be coated less than 1 μm thick on the substrate using either PVD or CVD (Grill, 1999). Due to its good mechanical and physical properties, including wear-resistance, high hardness, and self-lubricated property, the application range of DLC coatings was getting wider and wider (Cha & Erdemir, 2015; Silva et al., 2011). Generally, the hardness of a DLC coating was around 3000 HV which was similar to an 80 - 85 Rockwell hardness measurement (Mercer, 2012). The high hardness of the DLC coating increased the scratch resistance of the coated surface (Mercer, 2012). DLC coating provided a lubricity surface which reduced

surface friction between sliding parts. DLC coating protected the substrate from a gas or moisture attack (Mercer, 2012). DLC coating was often applied to the cutting tool to improve wear resistance of the tool that reduced cutting forces and allowed to cut the material with a high feed rate (Asthana et al., 2006). DLC coating was often deposited on the substrate using plasma enhanced chemical vapor deposition (PECVD). Since the deposition temperature of the DLC coating was relatively low, around 150°C, it was possible to apply DLC coating on the substrate which had a low operable temperature. The low application temperature of the DLC coating gave less thermal stress to the substrate in the coating application process. DLC coating could be applied to complex geometrical shapes, and very thin layers of coating could be applied to the substrate (Mercer, 2012). Since thousands of parts could be coated at the same time in a modern production line, the cost for the coating process was reasonable (Cha & Erdemir, 2015).

Physical vapor deposition

In the physical vapor deposition (PVD) process, the coating material was evaporated and transformed into the gas phase and deposited on the substrate without any chemical reaction (Bach et al., 2006; Graves, 2002). The PVD technique had developed since the 1960s (Bach et al., 2006). Now, the PVD technique could be used not only for metals, alloys, or ceramics but also for glass or plastic substrates that required a low coating process temperature (Bach et al., 2006; Wang, Eberhardt, Tian, & Kück, 2006). The PVD technique was often used for coatings that provided wear resistance, release property, thermal barrier, and optical surface (Bach et al., 2006). The PVD technique could be divided into three steps. During the first step, the vapor source was emitted to vaporize the coating material. The second step was to transport the gas phase coating material to the substrate. The last step was depositing and condensing the coating material on the substrate (Graves, 2002). For the optimal coating application, the pre-treatment of the substrate surface was recommended (Cha & Erdemir, 2015). There were many methods to perform PVD coating application; evaporation, ion plating, and

sputtering (Bach et al., 2006; Faure-Geors, 1994). The evaporation PVD technique was the most widely used PVD method used in the industry (Faure-Geors, 1994). In the evaporation method, the coating material was heated and evaporated in the PVD chamber (Bach et al., 2006; Faure-Geors, 1994). The evaporated material atom was deposited on the substrate by high vacuum pressure (Asthana et al., 2006). The evaporation PVD technique provided a high deposition rate, evenly distributed coat, and strong adhesion strength between the coating and the substrate (Bach et al., 2006; Faure-Geors, 1994). Also, the evaporation PVD technique could be utilized for a substrate that had a complex shape (Bach et al., 2006). The sputtering PVD technique did not require a high vacuum system. Instead, the sputtering PVD technique utilized a process gas and high voltage source (Bach et al., 2006). The process gas, such as argon, was inserted into the chamber, and the current flowed through the coating material. If the glow discharge plasma was ignited inside of the chamber, the ionized gas particles with high kinetic energy were bombarded on the coating material (Bach et al., 2006). From the bombardment impact, the coating material particles were detached from the material and deposited on the substrate (Bach et al., 2006). Compared to the evaporation PVD technique, the sputtering PVD process could be used with a larger variety of coating materials because the coating material particles were detached from the coating material physically, not thermally (Bach et al., 2006). In the sputtering PVD process, the process temperature of the substrate was low (between 200°C and 500°C) (Faure-Geors, 1994). The sputtering PVD coating had a good coating quality and good adhesion, but the coating thickness was relatively uneven (Bach et al., 2006). The deposition rate of the sputtering PVD technique was lower than the evaporation PVD technique (Faure-Geors, 1994). In the ion plating PVD technique, an additional anode was placed in a glow discharge plasma field to generate an electromagnetic field (Bach et al., 2006; Faure-Geors, 1994). The coating material was evaporated using an evaporator, electron-beam, arc, or magnetron-sputtering. The ionized gas particles bombarded the substrate prior to coating deposition to clean the coating

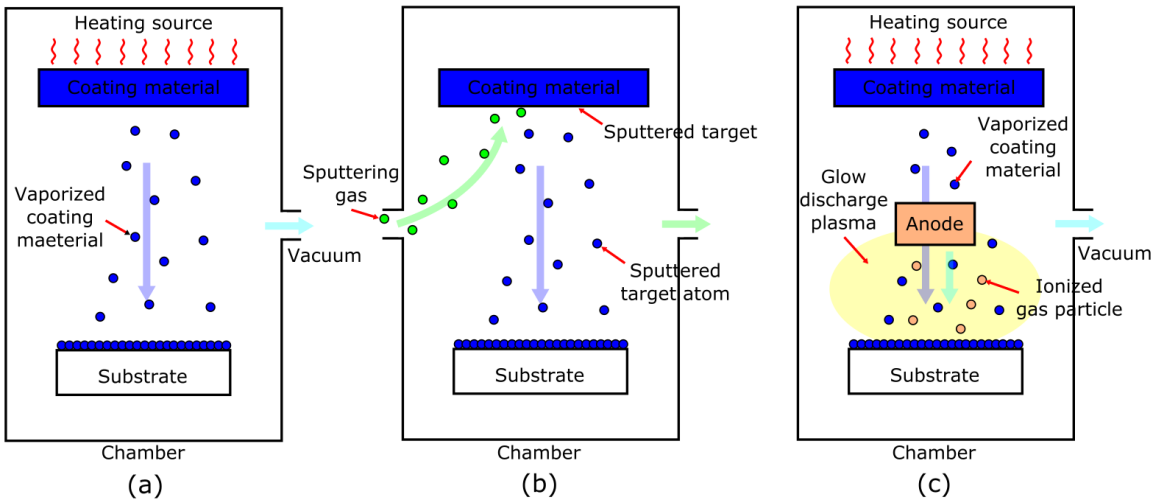

Figure 2.16. Schematic drawing of different methods of PVD (a) evaporation, (b) sputtering, and (c) ion plating.

surface. Then the evaporated coating material was deposited on the substrate. The ionized gas particles still bombarded the substrate during the deposition, and it made the coating to adhere to the substrate stronger (Bach et al., 2006). The ion plating PVD technique had a high deposition rate and good adhesion strength. Also, it required a low process temperature for coating (Faure-Geors, 1994). Even a complex shaped part could be coated using the ion plating PVD method (Faure-Geors, 1994). However, the coating thickness was relatively uneven (Bach et al., 2006). Figure 2.16 showed a schematic drawing of different methods of PVD.

PVD coating was often applied to the surface which required abrasion and corrosion resistance (Knotek, Löffler, & Bosserhoff, 1993). The part manufacturing mold was exposed to thermal and mechanical stresses during the part manufacturing process. These stresses caused the surface to crack and erode which reduced the life expectancy of the mold. Therefore, the surface coating for the mold was often applied using a PVD technique. Knotek et al. (1993) studied PVD coating with different material on the casting mold. They reported that CrN PVD coating showed more effective coating property for a die-casting mold than a Ti-based coating. Wang et al. (2006) studied the metallization of a polymer

substrate using PVD technique. They explained that the metallization of the polymer substrate was difficult because of the low surface energy of the polymer substrate. The low surface energy caused low sticking coefficients and poor metal adhesion of the surface (Wang et al., 2006). Wang et al. (2006) suggested that surface modification or an interlayer was necessary to improve the adhesion strength of the coating before the metallization of the polymer substrate. Wang et al. (2006) reported that both oxygen plasma pre-treatment and additional Ni interlayer between the coating and the substrate increased the adhesion strength between the polymer substrate and the copper coating. The adhesion strength decreased slightly after 1000 cycles of thermal shock (Wang et al., 2006).

Chemical vapor deposition

During the chemical vapor deposition (CVD) process, the coating material was deposited to the substrate by a chemical reaction with the inserted reactive gases inside of the chamber. (Asthana et al., 2006). The CVD coating technique required a high process temperature to achieve high activation energy. Some CVD techniques had a low process temperature by utilizing plasma and photon to initiate and sustain the chemical reaction (Bach et al., 2006). The chemical reaction did not always occur on the surface of the substrate, but most of the reaction occurred close to the surface because of the catalytic effect of the surface (Bach et al., 2006). The CVD technique could be operated in a low pressure or atmospheric pressure chamber. The CVD technique provided well-bonded, dense, and even thickness coating regardless of the part shape. Depending on the process pressure and reaction initiation source, the CVD techniques could be categorized into the following processes; atmospheric pressure chemical vapor deposition (APCVD), low pressure chemical vapor deposition (LPCVD), metal-organic chemical vapor deposition (MOCVD), plasma-assisted or plasma-enhanced chemical vapor deposition (PACVD or PECVD), laser chemical vapor deposition (LCVD), photochemical chemical vapor deposition (PCVD), chemical vapor infiltration (CVI), and chemical beam epitaxy (CBE) (Bach et al., 2006). Addou et al. (2016)

deposited a copper film on a carbon/epoxy composite using direct liquid injection metalorganic CVD (DLI-MOCVD). Addou et al. (2016) used various surface pre-treatments, such as atmospheric plasma treatment, UV oxidation, alkaline oxidizing solution treatment, and remote N2/O2 plasma, to improve adhesive strength, surface roughness, and wettability of the substrate. Normally, the deposition temperature range of copper using DLI-MOCVD was between 150°C and 245°C. Addou et al. (2016) reported that the optimal deposition temperature for maximum deposition growth of copper on the polymer substrate was 195°C.

Galvanotechnics

Electroplating and electroless plating were two of the oldest coating methods, but they were still commonly used in various industries (Bach et al., 2006). Both electroplating and electroless plating techniques were called Galvanotechnics. Both techniques could deposit metal and non-metal coating material on the surface of the substrate.

Electroplating

The basic principle of the electroplating technique was to move a metal ion from one to another. When the current flowed through the substrate, the substrate became a cathode. During the electroplating process, the metal ion was dissolved in the electrolyte from the anode electrolytically. The metal ion in the electrolyte was transported and deposited on the substrate (Bach et al., 2006). Figure 2.17 showed a schematic drawing of the electroplating process in aqueous electrolyte. Electroplating techniques allowed to apply the coating material on the substrate in a single operation regardless of the shape of the substrate (Asthana et al., 2006). Commonly used electroplating metals were tin, nickel, copper, chromium, silver, gold, platinum, and their alloys (Asthana et al., 2006). Nickel coating improved wear resistance and corrosion resistance of the surface. Also, it was used with chrome for decorative purposes. Copper coating sealed the surface of the substrate, so it was

often used for undercoating for other metal coatings. Chrome coating was used for cutting tools and engine components due to its low CTE, high corrosion resistance, and high strength in high temperatures (Asthana et al., 2006). The electroplating method was only useful when the substrate was electrically conductive. If the substrate was not electrically conductive, an additional conductive film should have applied before the electroplating technique. The pre-coating could be applied using various coating techniques, such as liquid coating, electroless plating, PVD, or CVD (Bach et al., 2006). Many times, the electroplating process was performed in an aqueous solution. However, the coating materials that could be electroplated on the substrate using aqueous electrolyte was limited. If the coating material had a more negative deposition potential than the substrate, the coating material could not be deposited on the substrate. In this case, the coating material should have electroplated through a non-aqueous solution which was air. Electroplating through non-aqueous solvent often had a higher process temperature, more sensitive to humidity, and more expensive than electroplating through the aqueous solution (Bach et al., 2006). The coating material which was used with the non-aqueous solution was usually in a powder form. The powder form coating material had similar components as the liquid coating material, but the powder coating material did not have a carrier. The powder form of additive, pigment, and resin was sprayed on the substrate. The powder coating material was electrostatically charged in the spray gun and attracted to the substrate which was connected to the ground (Hornbaker et al., 2013). After the deposition, the substrate was heated up in an oven to transform the powder form coating material to a liquid. And, the liquid form coating material was transformed into the solid coating when the substrate was cooled and the coating material was cured (Hornbaker et al., 2013). The properly cured powder coating provided chipping resistance, scratching resistance, UV protection, and corrosion resistance properties to the surface. The thickness was usually between 2 mm and 4 mm, but it could be up to 40 mm as needed (Hornbaker et al., 2013). The powder coating technique did not use any solvent in

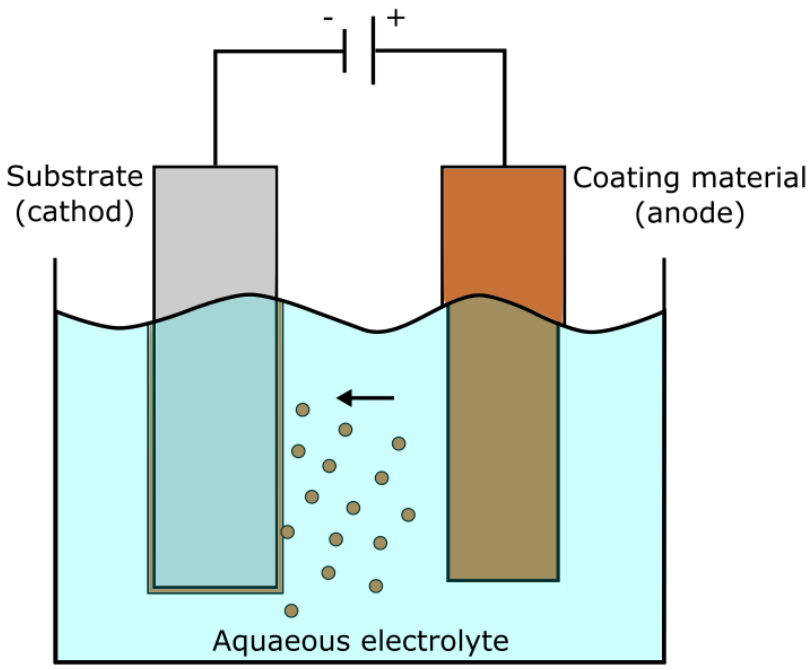

Figure 2.17. Schematic drawing of electroplating process in aqueous electrolyte.

the coating application process which made the process safer and less harmful (Asthana et al., 2006). Powder coating had a high material utilization rate which reduced material waste. Since there was no coating material mixing process, time could also be saved. Cleaning the workspace could be easily done by vacuuming the powders. If the coating was improperly applied, the applied powder on the substrate could be easily removed by using compressed air (Asthana et al., 2006). In the case of the powder coating material, the pre-treatment of the substrate was critical (Asthana et al., 2006; Hornbaker et al., 2013). The surface of the substrate was roughed with abrasive media blasting before it was coated. Depending on the coating material, sometimes, a chemical pre-treatment was necessary. The substrate needed to be rinsed and totally dried in the oven (Hornbaker et al., 2013). The powder electroplating technique released a very small amount or even no volatile organic compound (VOC) during the process (Hornbaker et al., 2013). Figure 2.18 showed a schematic drawing of the powder coating technique.

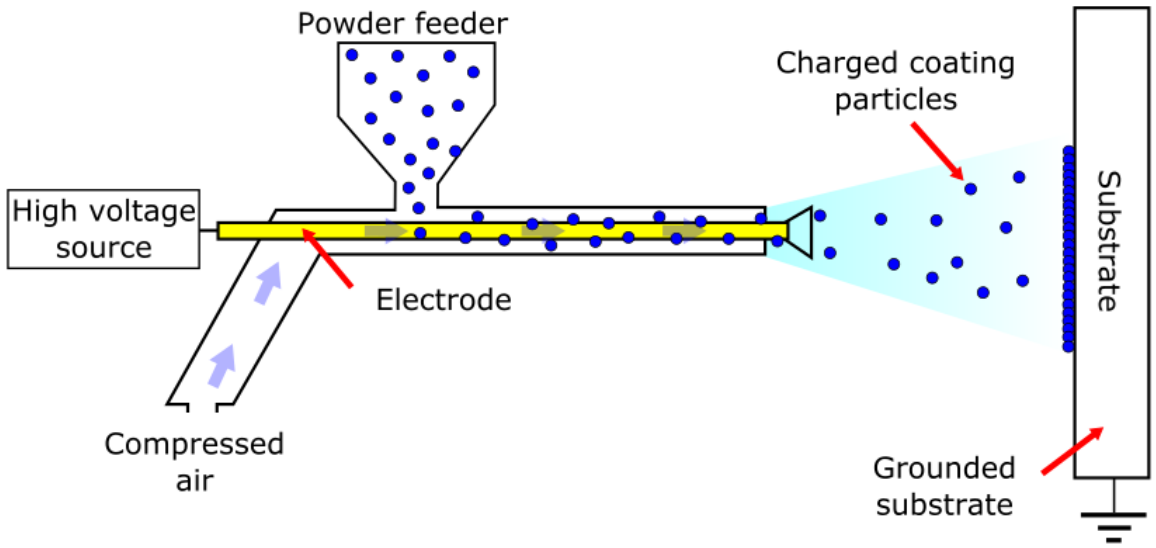

Figure 2.18. Schematic drawing of powder coating technique.

Electroless plating

Electroless plating was also called chemical plating and it could be performed without any current source (Asthana et al., 2006; Bach et al., 2006). When the standard electrode potential of the metal particle was more positively charged than the substrate, the metal ion deposited on the substrate. Also, the metal ion could be deposited by adding a reducing agent in an electrolyte which caused a catalytic reaction because of the catalytic nature of the substrate (Bach et al., 2006). For the non-metal substrate, it was required to add a catalyst treatment to the surface unless the chemical reaction could not be activated. The surface treatment had the following steps; surface cleaning, etching, neutralizing, applying catalyst, and adding accelerator (Bach et al., 2006). The coating could be deposited up to 10 μm thick using an electroless plating technique. Nickel coatings were often applied to the substrate using electroless plating techniques for higher surface hardness, wear resistance, and corrosion resistance (Asthana et al., 2006).

Thermal spray

During a thermal spray technique, the coating material was fed into the spray gun in the form of powder, wire, or rod (Asthana et al., 2006; Bach et al., 2006; Lupoi & O'Neill, 2010). The coating material was heated up in the spray gun using various energy sources such as fuel combustion, electric arc, or plasma (Asthana et al., 2006). The molten coating material was sprayed with a high-velocity gas stream and deposited on the substrate (Bach et al., 2006; Lupoi & O'Neill, 2010; Mohammadi et al., 2017). Various kinds of coating materials could be applied using a thermal spray coating technique (Bach et al., 2006). The thermal spray coating was used for providing wear resistance, corrosion resistance, thermal barrier, electrical conductivity, and magnetic property to the substrate surface (Asthana et al., 2006). Thermal spray coating technology had a very high process temperature. The flame from the thermal spray gun had a temperature between $3,000°C$ and $16,000°C$ (Amin & Panchal, 2016). Generally, The substrate was exposed to the temperature between $95°C$ and $205°C$ (Amin & Panchal, 2016; Asthana et al., 2006). The substrate was exposed to a high temperature which could cause thermal stress on the substrate (Asthana et al., 2006; Bach et al., 2006). The thermal spray coating had a high deposition rate, and the deposition could be concentrated on the local area (Bach et al., 2006). The spraying condition of the thermal spray coating technique affected the quality of the coating. Also, the pre-treatment of the substrate surface affected the adhesion strength of the coating. The pre-treatment of the substrate usually had three different steps; pre-cleaning, blasting, and post-cleaning (Bach et al., 2006). In the pre-cleaning step, contaminants and residue were removed from the surface. Then the abrasive was blasted to the surface not only for cleaning the surface, but also to increase the surface roughness and activate the surface. Roughening the surface increased the contacting area between the coating and the substrate and it improved the adhesion between the two. In the post-cleaning step, the residue from the blasting step was

cleaned (Bach et al., 2006). DIN EN 582, tensile adhesion strength test, was often used to test the adhesion strength of the coating. Depending on the way to soften the coating material and way of deposition, thermal spray coating techniques could be divided into several different types. Thermal spray coating on polymer matrix composite showed many issues, such as poor adhesion strength of the coating and matrix degradation caused by high application temperature. Rezzoug, Abdi, Kaci, and Yandouzi (2018) reported that they successfully applied protective coating on the carbon fiber reinforced polymer (CFRP) using thermal spray technique by installing a metallic mesh on the coated surface during the coating process. Rezzoug et al. (2018) reported that the coating with metallic mesh increased 50% of adhesion strength of the coating compared to the coating without the mesh, and there was not any significant mechanical strength degradation of the CFRP.

Cold spray

The basic principle of the cold spray coating technique was that the solid-phased coating material was impacted on the substrate with high velocity and deposited on the surface (Lupoi & O'Neill, 2010; Raoelison, Verdy, & Liao, 2017; Raoelison et al., 2018). Although the coating process was called cold spray, the coating process used heated and pressurized process gas to soften and accelerate the coating material particles. Different from the high-temperature thermal spray coating technique, the cold spray technique used relatively a low temperature process gas, and the coating particle was just softened instead of melted during cold spray coating process (Assadi, Kreye, Gärtner, & Klassen, 2016). The micron-sized coating material particles were injected through the supersonic nozzle with pressurized and heated process gas (Grigoriev, Okunkova, Sova, Bertrand, & Smurov, 2015). Nitrogen and helium were commonly used process gases (Alhulaifi, Buck, & Arbegast, 2012; Assadi et al., 2016; Grigoriev et al., 2015; Raoelison et al., 2018). Figure 2.19 showed a schematic drawing of cold spray coating application

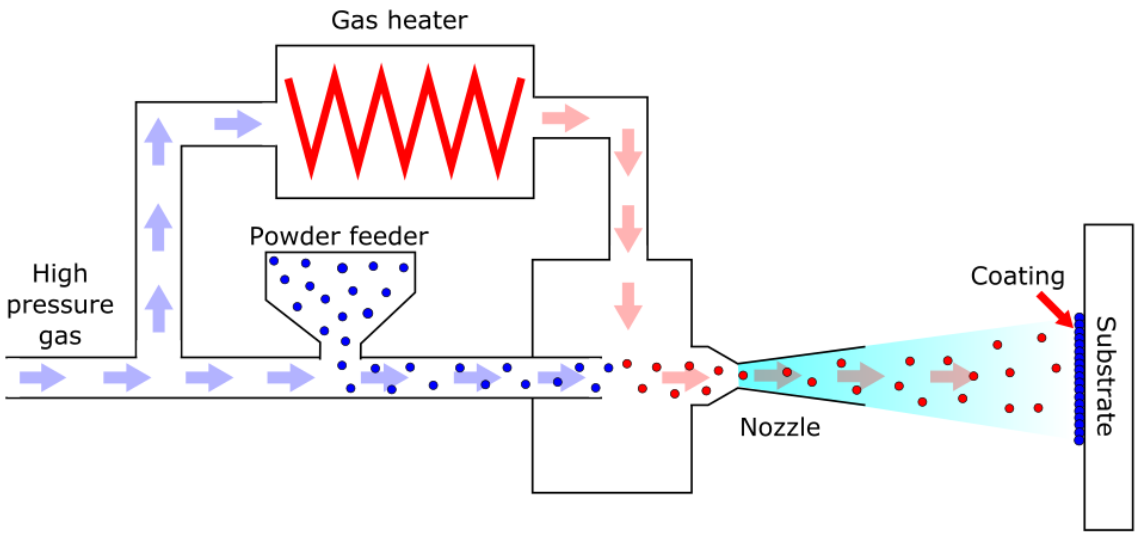

Figure 2.19. Schematic drawing of cold spray technique.

process. The velocity of the particle reached between 500 m/s and 1200 m/s, and the temperature of the particle reached up to 1000°C (Alhulaifi et al., 2012; Assadi et al., 2016; Grigoriev et al., 2015). The coating material particle with high kinetic energy impacted the substrate. Because of the high kinetic energy, the particle deformed plastically when it impacted the substrate (Assadi et al., 2016; Grigoriev et al., 2015; Lupoi & O'Neill, 2010; Raoelison et al., 2017). The bonding between the first coating layer and the substrate was caused by the plastic deformation of the coating material. The bonding between coating layers was more like a metallurgical bonding (Raoelison et al., 2017, 2018). The cold spray was a relatively inexpensive coating technique and easy to perform (Lupoi & O'Neill, 2010). Cold spray technology was widely used not only for coating but also for additive manufacturing or repairing (Assadi et al., 2016; Raoelison et al., 2017).

During the cold spray coating process, the substrate was exposed to a lower temperature compared to other thermal spray techniques. It created less oxidation, thermal stress, deformation, and thermal shock to the substrate (Assadi et al., 2016; Grigoriev et al., 2015; Yin et al., 2018). Since the coating material was not melted during a cold spray coating process, the original property of the material was

retained (Raoelison et al., 2017, 2018; Yin et al., 2018). Also, temperature sensitive materials could be used as a coating material and the substrate with cold spray coating technique (Alhulaifi et al., 2012; Assadi et al., 2016; Grigoriev et al., 2015). Pre-treatment of the substrate before the coating was necessary for a better coating quality. The substrate was often pre-treated by roughing the surface where the coating was applied. Sandblasting or grinding could be used for the metal substrate, and degreasing and cleaning could be used for glass or polymer substrate. Heating the substrate was another pre-treatment method. The heated surface of the substrate during the deposition increased the deposition efficiency. Also, texturing the surface improved the deposition strength (Raoelison et al., 2018). The coating parameters during the coating process affected the properties of the coating. Inappropriately applied coating material caused high porosity, low adhesion strength, and high residual stress of the coating (Assadi et al., 2016). Depending on the coating material, substrate material, and desired coating properties, proper coating process parameters should have set for optimal coating results. Especially, the velocity of the particle should have set to the critical value of impact velocity. The critical value of impact velocity referred to the velocity that was high enough to deposit the coating particle on the substrate, but not too high to avoid erosion of the substrate (Alhulaifi et al., 2012). The coated part was heat-treated after the coating process to remove micro-pores in the coating by recrystallizing the deposited coating particles. Annealing helped to reduce the interlayer boundaries and improve the properties of coating (Yin et al., 2018). Yin et al. (2018) reported that an annealing process significantly improved tensile strength, ductility strength, elastic modulus, electrical conductivity, and thermal conductivity of the coating (Yin et al., 2018). Annealing in a higher temperature for a longer period was more efficient to remove voids in the coating, However, the hardness of the coating could be decreased because of the recrystallization of the particles (Yin et al., 2018).

Usually, the cold spray coated surface was rough. Therefore, a cold spray coating process was often used with a post-machining process (Yin et al., 2018). An

extra material was applied on the surface and it was machined to fulfill the dimensional requirement of the part. One of the properties of a cold sprayed coating was a heterogeneous deposition. Some areas were denser, and some areas had more porosity than other areas. The heterogeneous deposition of the coating applied the variation of the mechanical and thermal load to the milling tool during the machining process (Yin et al., 2018). The inconstant density and porosity of the coating caused inconstant tool engagement and disengagement, which could lead to tool wear (Yin et al., 2018). If the coating was applied inappropriately, the coating could be damaged during the machining process because of the weak inter-particle bonding. Even with well-performed machining, the porosity inside of the coating could be exposed to the machined surface. Also, the applied stress during machining could cause delamination between the coating and the substrate. Yin et al. (2018) reported that the machinability of the cold spray coated part depended on the density and ductility of the coating. The machining parameters, such as rotation per minute (RPM), feed rate, and cut depth, should have considerably set to avoid cracks, fractures, and delamination of the coating during the machining process (Yin et al., 2018). Also, annealing the coating before machining reduced the surface roughness of the finished part because the annealing improved inter-particle bonding (Yin et al., 2018). Some applications required a metallization of the surface of the polymer substrate to create special surface properties, such as electrical conductivity, thermal conductivity, electromagnetic surface, and erosion resistance (X. Zhou, Chen, Liu, Wu, & Zhang, 2011). Lupoi and O'Neill (2010); X. Zhou et al. (2011) explained that there were many coating techniques to deposit molten material to the substrate; PVD, CVD, electroplating, thermal spray, or laser cladding. However, the cold spray was the most suitable coating technique when the metallic coating was deposited on the polymer surface. Other coating techniques had high equipment cost and coating application cost, and the size of the substrate was limited by the size capability of the coating equipment. Electroplating had a low adhesive force and low stability coating (X. Zhou et al., 2011). Electroforming

had long application times and it generated pollution. Thermal spray used high temperature which could give thermal stress to the substrate that could cause substrate deformation. Also, Lupoi and O'Neill (2010) reported that the thermal spray coating on the polymer surface had a high porosity because the nature of thermal spray coating would not let the coating material completely bond to the substrate (X. Zhou et al., 2011). Metal particles with high kinetic energy often eroded the polymer surface instead of adhering during the cold spray process because of the low hardness of the polymer surface (Che, Chu, Vo, & Yue, 2017; Lupoi & O'Neill, 2010). However, many publications showed the application of the cold sprayed coating to the polymer substrate (Raoelison et al., 2018). Raoelison et al. (2018) explained that cold spray coating on the polymer substrate could be achieved by either using a low temperature or using nano-sized coating particles. Raoelison et al. (2018) reported that 5 μm to 50 μm size coating material particle and the gas pressure between 1 MPa and 3 MPa were the optimal settings for depositing the coating material on the polymer substrate using cold spray technique. Also, the preheat temperature of the process gas should have lowered than 500°C because of the thermal sensitivity of polymer substrate (Raoelison et al., 2018). Since the velocity of the coating particle and the process temperature during the cold spray technique for the polymer substrate was relatively low, the bonding strength of the coating could be weaker. Soft metals, such as tin, zinc, and aluminum were preferred for the metallization of the polymer substrate (Raoelison et al., 2018). Che, Chu, et al. (2017) studied metallizing a carbon fiber reinforced polymer using cold spray coating technique. They reported that the deposition efficiency of the coating process was not good when they used tin particles as the coating material. However, when they used tin particles mixed with zinc and copper particles, the deposition efficiency of the process increased significantly (Che, Chu, et al., 2017). Lupoi and O'Neill (2010) tested the deposition compatibility of metallic coating particles on a non-metal substrate using cold spray technology. Lupoi and O'Neill (2010) successfully deposited 45 μm - 100 μm thick tin coating on

the polymer substrate by optimizing nozzle parameters. Lupoi and O'Neill (2010) reported that tin could be deposited because the weight of the particle was low. However, copper particles had a high particle weight, so it eroded the polymer surface (Lupoi & O'Neill, 2010). Sturgeon, Dunn, Celotto, and O'Neill (2006) successfully deposited aluminum particles on a carbon fiber reinforced polymer. Sturgeon et al. (2006) reported that they used He gas as the process gas and they raised the gas temperature to 300°C. Che, Vo, and Yue (2017) coated carbon fiber reinforced polymer substrate with aluminum, copper, and tin particle using cold spray coating technique under various spraying parameters and conditions. Che, Vo, and Yue (2017) reported that it was impossible to deposit the coating particle on the substrate using a high-pressure cold spray technique because the surface of the substrate was eroded by the coating particle. The continuous coating deposition on the carbon fiber reinforced polymer substrate was achieved by utilizing low-pressure spray with 0.41 MPa gas pressure and a high gas temperature (300°C) (Che, Vo, & Yue, 2017). Raoelison et al. (2018) explained that it was difficult to deposit polymer particles on the substrate using a cold spray coating technique. The interfacial shear and dragging force during the deposition process would not allow the coating material to be deposited on the substrate. Even if the coating material particle was deposited on the surface, it was detached when the next particle impacted it (Alhulaifi et al., 2012; Raoelison et al., 2018). Alhulaifi et al. (2012) reported that the cold spray coating technique with a polymer coating material was achieved by using shock waves. The process gas pressure was set to 0.5 MPa and the process temperature was set to 275°C (Alhulaifi et al., 2012). Figure 2.20 showed a scanning electrode microscope (SEM) image of deposited copper powder on the carbon fiber reinforced polymer laminate using the cold spray technique.

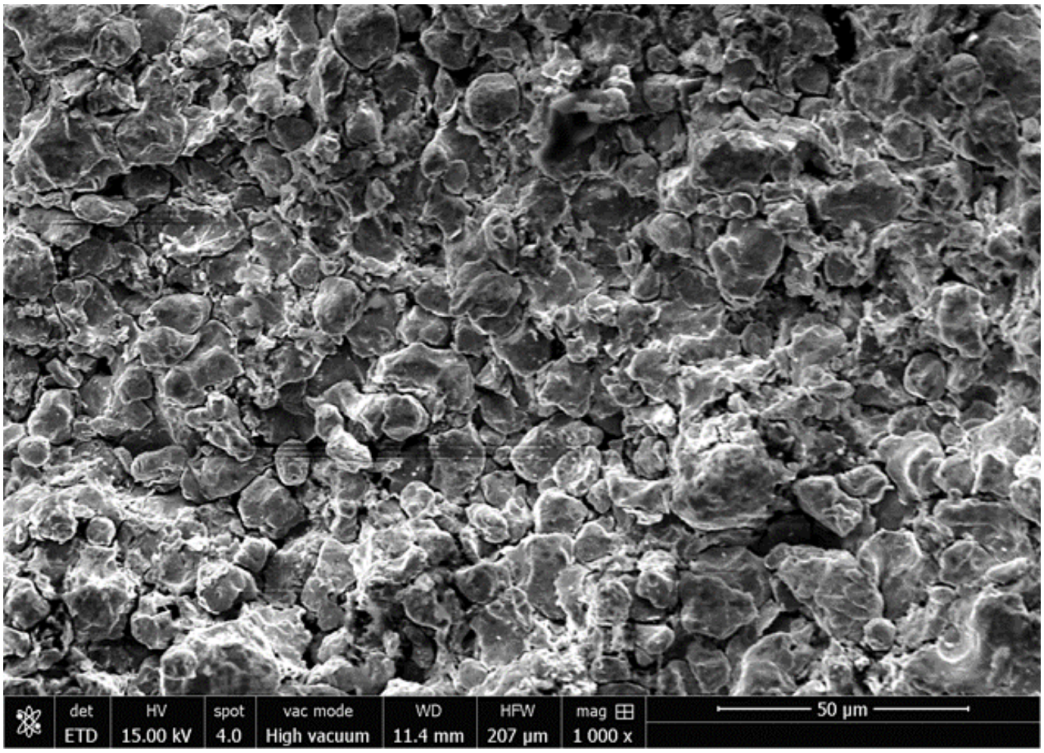

Figure 2.20. Scanning electrode microscope (SEM) image of deposited copper powder on the carbon fiber reinforced polymer composite laminate using cold spray technique. Reproduced with permission (Tsai et al., 2020).

Sol-gel coating

The Sol-gel coating technique provided a non-metallic and inorganic coating on the substrate. The basic principle of sol-gel technology was forming an oxide network through hydrolysis and polycondensation of a molecular precursor in the liquid (Innocenzi, 2019). The sol was a colloidal system, which was made of two or more components, in the fluid medium (Innocenzi, 2019). The gel was a colloidal or polymer network in semi-solid nature (Innocenzi, 2019). The sol-gel coating technique started from the formation of a sol from a precursor. The precursor was usually an inorganic metal salt or a metal alkoxide. Then the sol was transformed to gel through sol-to-gel transition. Both precursor-to-sol and sol-to-gel transition were due to hydrolysis and condensation (Innocenzi, 2019). The sol-gel technology

could be formed differently depending on the drying process after the sol-to-gel transition. The sol-gel could be a solid ceramic, spray coating, nanoparticle, or aerogel (Bach et al., 2006). The sol-gel technology was often used for coating. The physical properties of the coating, such as hardness, porosity, and density, were determined by the condition during sol-gel synthesis (Bach et al., 2006). Ph. level of sol determined the shape of the nanoparticle which was made during synthesis. The shape of the nanoparticle determined the network of the particle when the sol transformed into gel. Based on the network of the particle, the coating could be porous or dense (Bach et al., 2006). The sol-gel coating had a high purity and low process temperature (Bach et al., 2006). Therefore, the sol-gel coating process could be applied to various substrates, including metal, glass, or plastic, even if they had a low operating temperature. Sol-gel coating technology was often used in optical sensors and the medical field (Bach et al., 2006). Sol-gel coating could be applied to the substrate using the following methods; dipping, spinning, spraying, electrodeposition, glazing, brush painting, roller coating, screen printing (Bach et al., 2006).

2.4 Summary

The author described basic information related to composite materials, composite manufacturing processes, and composite mold in this chapter. The author also explained different coating techniques and coating technologies. Previous related researches were introduced to better understand the topic. This chapter established the foundation for the research design which was introduced in the next chapter.

CHAPTER 3. METHODOLOGY

The author described the research framework and experimental design in this chapter. This chapter included all the experimental procedures, such as material characterization, test specimen manufacturing, coating application, coated surface property test, and coating evaluation.

3.1 Substrate material thermal characterization

To find an applicable coating technique and coating material for the additively manufactured carbon fiber reinforced composite mold, the thermal properties of the substrate should have analyzed first. Many coating techniques required high coating application temperature. If the coating application temperature was higher than the substrate maximum allowable temperature, the substrate could be deformed permanently during the coating application process. Therefore, the maximum allowable temperature of the substrate should have investigated before deciding what type of coating technique and coating material were used. For this study, the glass transition temperature (T_g), was used to determine the maximum allowable temperature of the substrate material. The glass transition temperature was the temperature where the polymer changes from a glassy state to a plastic state (Baur, Ruhrberg, & Woishnis, 2016). Therefore, a thermal analysis was performed to find the glass transition temperature of the substrate material. Two different types of equipment were used for the thermal analysis; differential scanning calorimeters (DSC) and dynamic mechanical analysis (DMA). A semi-crystalline polymer, polyphenylene surfide (PPS) reinforced with 50% by weight of carbon fiber (Techmer Electrafil© XT1 3DP) was used in this work.

3.1.1 Differential scanning calorimeters (DSC)

A Differential scanning calorimeters (DSC) allowed measuring the heat flow that entered or left from a small sample of material as a function of time and temperature and served to investigate the thermal property of the material (Groenewoud, 2001). DSC could be used to determine the glass transition temperature (T_g), melting temperature (T_m), or crystallization temperature (T_c) (Groenewoud, 2001). The heat capacity of the polymer was different below and above the T_g. Usually, material above T_g had a higher heat capacity. Different heat capacity of the material above and below the T_g allowed DSC to measure different heat flow from the material below and above T_g (ASTM International, 2015a). The following equation represented the general DSC response;

$$\frac{dQ}{dt} = C_p \frac{dT}{dt} + f(T, t) \tag{3.1}$$

where dQ/dt represented heat flow from the DSC sample, C_p represented heat capacity of the sample, dT/dt was heating rate, and $f(T, t)$ represented heat caused by the kinetic processes of the sample. TA Instruments© Q100 DSC was used for the test. To make a DSC test sample, a small carbon fiber reinforced PPS composite pellet was placed inside an aluminum hermetic pan and a lid was installed and sealed. The author made sure that the pellet inside of the container did not deform the container while the lid was installed. The weight of the pellet inside of the container was measured and put into the test setup. The DSC sample was placed inside the furnace of the DSC. Figure 3.1 showed the DSC sample and the DSC sample in the DSC furnace. The temperature of the furnace was programmed to (1) equilibrating at 25°C, (2) ramping at 30°C/min to 330°C, (3) isothermal for 5 minutes, (4) ramping at 30°C/min to 25°C. The DSC test result was analyzed using TA Universal Analysis software. The glass transition temperature was identified in accordance with ASTM D3418, standard test method for transition temperatures and enthalpies of fusion and crystallization of polymers

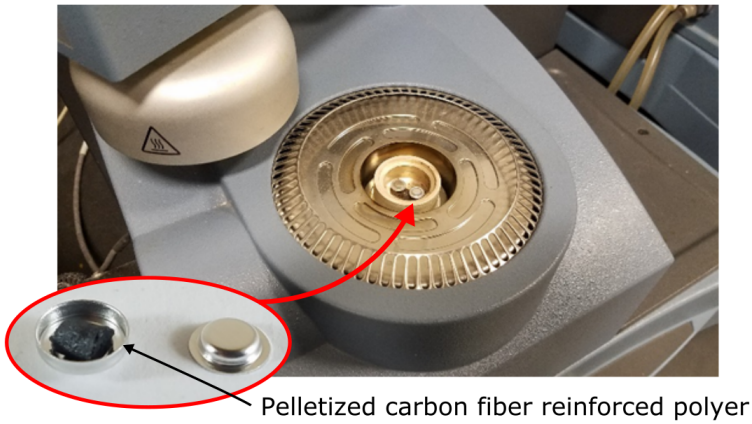

Figure 3.1. DSC sample with the pelletized carbon fiber reinforced polymer inside of the aluminum hermetic pan and TA Instruments© Q100 DSC.

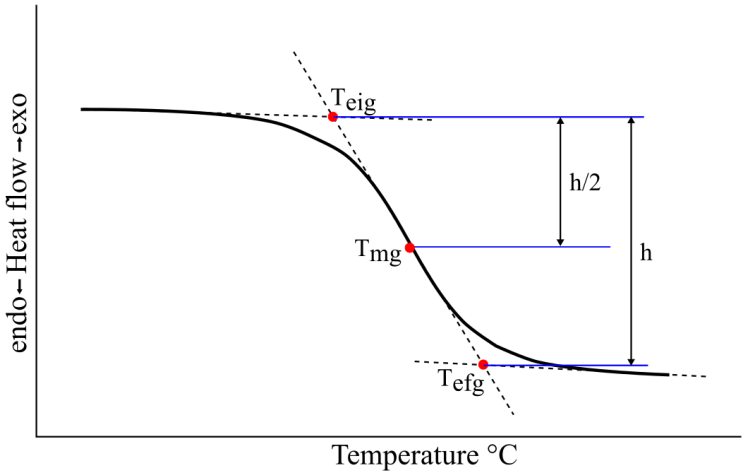

Figure 3.2. T_{eig}, T_{efg}, and T_{mg} in the glass-liquid transitioning area in the DSC result (ASTM International, 2015a).

by differential scanning calorimetry (ASTM International, 2015a). The glass transitioning area of the DSC result was identified and T_{eig} and T_{efg} were measured where T_{eig} was extrapolated onset temperature and T_{efg} was extrapolated end temperature. Then T_{mg}, midpoint temperature between T_{eig} and T_{efg} was calculated and determined as a glass transition temperature of the material as showed in Figure 3.2 (ASTM International, 2015a).

3.1.2 Dynamic mechanical analysis (DMA)

Dynamic mechanical analysis (DMA) allowed characterizing the thermomechanical as well as the thermoviscoelastic behavior of a material. This was achieved through the application of controlled temperature, strain, or stress conditions or histories (ASTM International, 2015c; Barsoum, 2015). DMA applied sinusoidal deformation to the DMA sample to measure viscoelastic moduli, storage modulus, and loss modulus of the sample at different temperatures using the following equation (Barsoum, 2015);

$$E' = \frac{\sigma_0}{\gamma_0} cos(\delta) \tag{3.2}$$

$$E'' = \frac{\sigma_0}{\gamma_0} sin(\delta) \tag{3.3}$$

where $E^{'}$ and $E^{''}$ were storage modulus and loss modulus respectively. σ_0 was stress amplitude and γ_0 was strain amplitude, and δ was the phase angle between the deformation and sample response due to the viscoelastic nature of the polymer (Barsoum, 2015). The mechanical property of a polymer was changed from a glassy state to an elastic state above T_g due to the change of the polymer chains. Therefore, it showed drastic change of viscoelastic moduli, storage modulus, and loss modulus below and above T_g. DMA could be used to find the T_g by finding the temperature where the modulus of the sample changed (Barsoum, 2015). TA instruments© Q800 DMA was used for the test. The DMA test sample was manufactured from additively manufactured carbon fiber reinforced PPS composite plate. The plate was be machined into the sample size for a 3-point bending test, using a computer numerical control (CNC) milling machine and an abrasive waterjet. The size of the test sample was 50 mm x 12.09 mm x 2.98 mm. The test sample was installed in the 3-point bending test fixture of the DMA. Figure 3.3 showed the DMA sample and the 3-point bending test fixture in DMA. The DMA test was set to oscillate at 0.05 strain with 1 Hz, and the temperature was set to

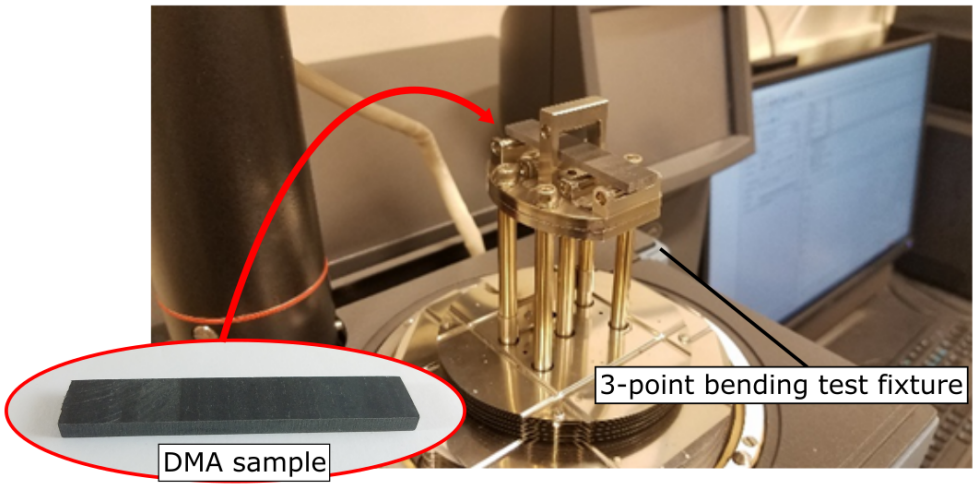

Figure 3.3. DMA sample and 3-point bending test fixture in TA instruments© Q800.

ramp to 200°C with 5°C/min ramp rate from 25°C. The DMA test results was analyzed using TA Universal Analysis software. The T_g of the material was identified in accordance with ASTM D7028, standard test method for glass transition temperature (DMA T_g) of polymer matrix composites by dynamic mechanical analysis (DMA) (ASTM International, 2015c). At the T_g, the storage modulus of polymer material decreased dramatically. Therefore, in the storage modulus versus temperature plot, two tangent lines were made in the portion where the storage modulus decreased dramatically as showed in Figure 3.4. Then, the temperature where two tangent lines met was determined as a T_g of the material. After the T_g of the carbon fiber reinforced PPS composite was obtained from DSC and DMA tests, the coating technique and coating material which had a coating application temperature lower than the T_g of the material had chosen.

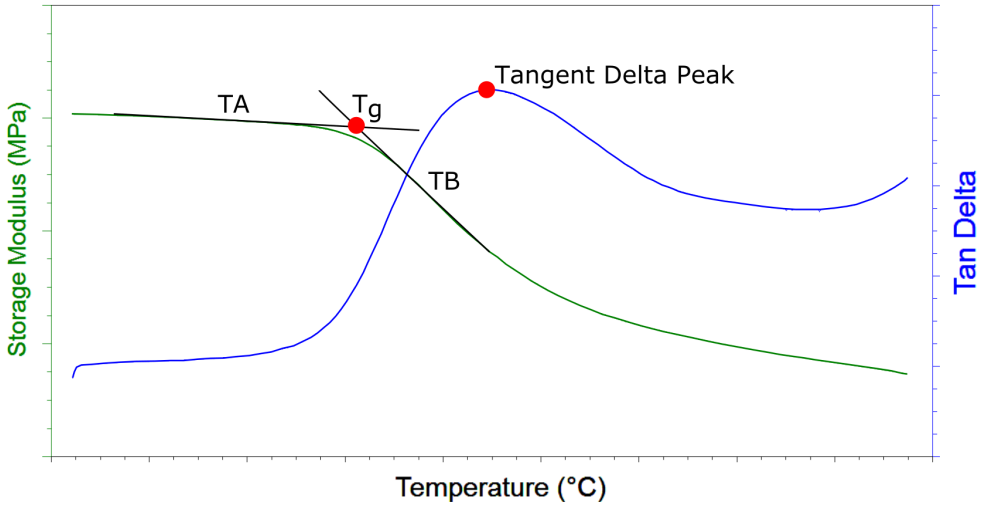

Figure 3.4. DMA test result; storage modulus versus temperature plot and glass transition temperature determined by the two tangent lines (ASTM International, 2015c).

3.2 Test specimen preparation

3.2.1 Part printing process

To investigate the performance of the coating on the additively manufactured fiber reinforced composite mold for the composite part manufacturing process and compared with the non-coated mold, many different surface property tests, such as surface hardness test, abrasion resistance test, roughness test, demolding test, CTE test, coating adhesion test, and mold life experiment test, were prepared in this study. For each test, test specimens were needed to be manufactured. The test specimens were additively built using Composite Additive Manufacturing Research Instrument (CAMRI) located at Purdue University as showed in Figure 3.5. CAMRI had developed and built by Purdue Composites Manufacturing and Simulation Center (CMSC) Additive Manufacturing (AM) team. CAMRI utilized extruder deposition additive manufacturing (EDAM) technology for the fiber reinforced composite additive manufacturing process (Barocio et al., 2017). The

general additive manufacturing process of CAMRI was described as follow; (1) the pelletized fiber reinforced thermoplastic polymer was inserted into the hopper of the machine, (2) the material feeder inside of the hopper fed the material into the extruder with specific feeding rate, (3) the screw in the extruder rotated and delivered the material forward to the nozzle, (4) heating resources attached on the outside of the extruder raised the material temperature and melted it while the material moved toward the nozzle, (5) the melted material was extruded out through the nozzle by the extruder gear pump, (6) the extruded material was compacted using a tamper and the print bed moved to position the bead to the desired location (Barocio et al., 2017). For the printed material, polyphenylene sulfide (PPS) with a 50% carbon fiber content (Techmer Electrafil© XT1 3DP) was used. Figure 3.6 showed pelletized carbon fiber reinforced polyphenylene sulfide (PPS) composite (50% carbon fiber by weight).

The pelletized carbon fiber reinforced PPS composite was put into the dryer to remove the moisture inside of the material. The pellets were dried at 130°C for 4 hours (Barocio et al., 2017). The dried material was put into the hopper of CAMRI. CAMRI printed the test specimen with a 4 mm diameter nozzle which printed a 6.15 mm bead width and 1.5 mm bead height. Three different models were designed to make the test specimen; 2-bead wall, demolding test tool, and mold life experiment tool. 2-bead wall was used to manufacture the test specimen which had flat plate shape, such as surface hardness, abrasion resistance, roughness, and coating adhesion tests. The size of the 2-bead wall model was 330.2 mm x 12.3 mm x 330.2 mm which consisted of 2 beads along its width direction (6.15 mm * 2 = 12.3 mm). However, the printed 2-bead wall was machined to 6.15 mm width in the test specimen machining process. Figure 3.7 showed orthographic projection of the machined 2-bead wall panel with the dimensions. The author wanted the demolding test tool to have a high demolding force during the test, so it was easier to notice the difference on the demolding force between the non-coated and coated composite tools. To make the demolding test tool which had high demolding force, a pillar

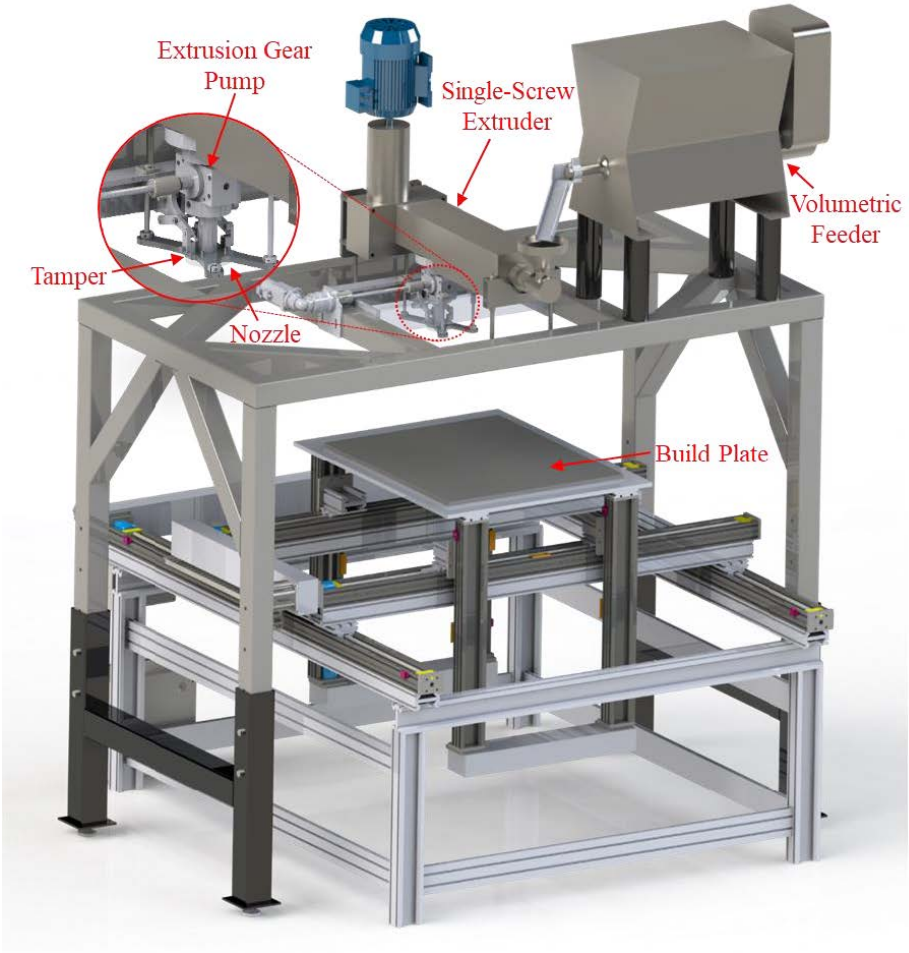

Figure 3.5. Composite additive manufacturing research instrument (CAMRI) located at Purdue University.

Figure 3.6. Pelletized carbon fiber reinforced polyphenylene sulfide (PPS) composite (50% carbon fiber by weight).

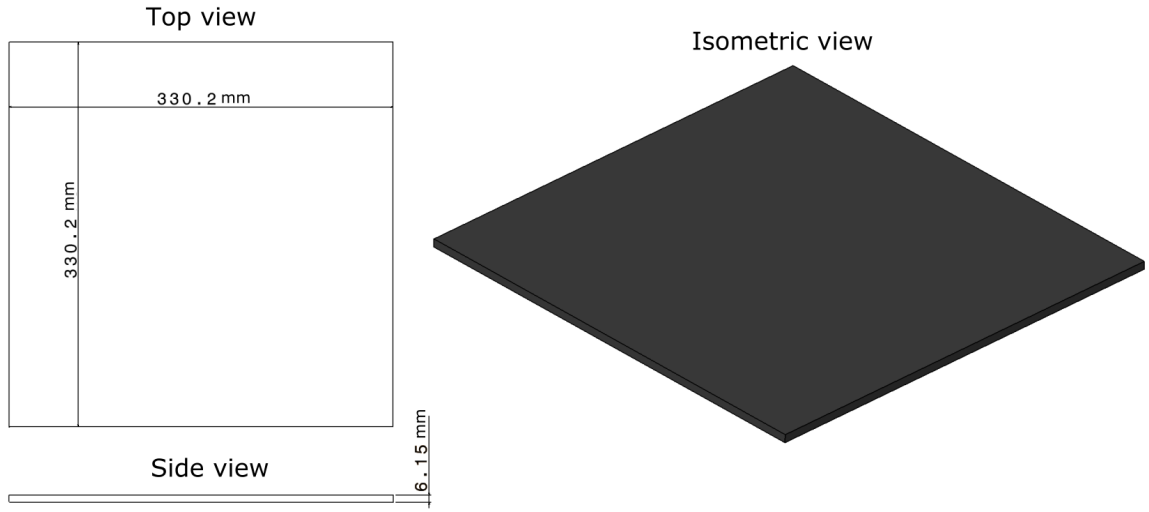

Figure 3.7. Orthographic projection of the machined 2-bead wall with the dimensions.

shaped tool design was chosen. The composite material was laid on the side of the pillar, so there was a frictional shear stress between the tool and the part during the demolding process. Also, the composite material was laid on the top of the tool for a part ejecting process. The cylindrical shape tool with edge fillet on the top was designed to minimize a stress concentration of the part when it was demolded. When the composite material laid on the demolding test tool was cured in an elevated temperature and cooled down, the composite material shrank and generated normal force against the tool. The composite material with higher CTE shrank more and generated a higher normal force. The square bottom section was designed to be used to support the tool while the composite part was demolded during the demolding test. Also, it was used to facilitate the printed tool to be fixed in a vise during the machining process. There was a hole all the way through the tool for an ejector pin and there was a pocket which had a slightly larger diameter than the hole on the top of the tool for an ejector plug. Figure 3.9 showed the orthographic projection of the demolding test tool with dimensions.

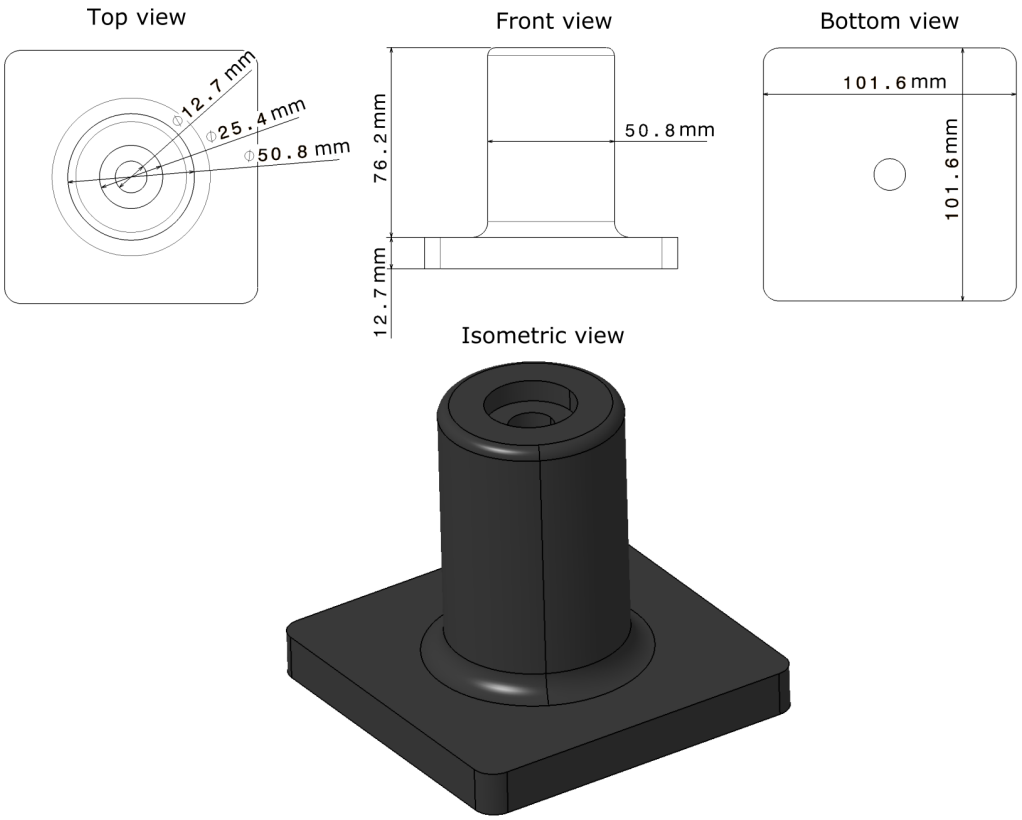

Figure 3.8. Orthographic projection of the demolding test tool with dimensions.

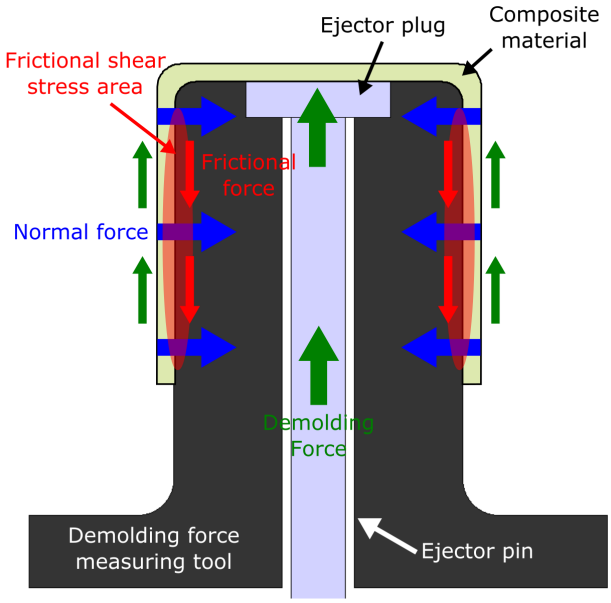

Figure 3.9. Orthographic projection of the demolding test tool with dimensions.

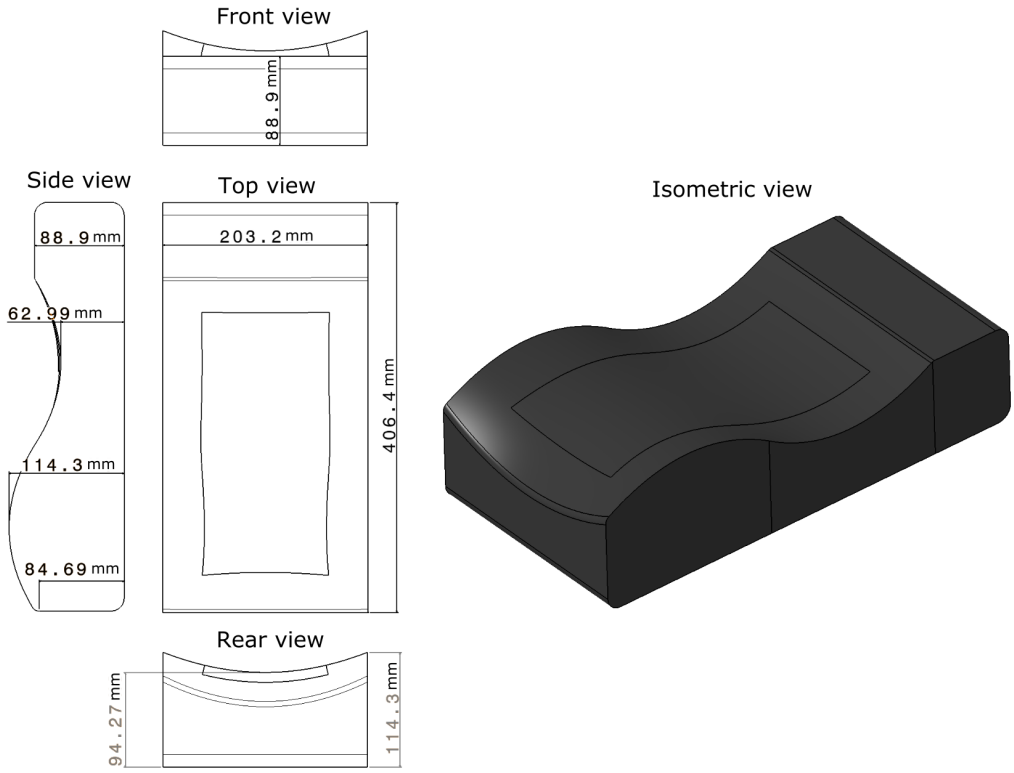

Figure 3.10. Orthographic projection of the mold life experiment tool with dimensions.

The mold life experiment tool was designed to have a curvy surface on the top of the tool. The curvy surface of the tool caused internal stress due to the CTE mismatch in the radial and hoop direction of the surface which could lead to change of the tool shape in the repeated composite part curing cycles. The curvy surface on the top of the tool provided some complicated geometrical shape of the tool, but, at the same time, it was not very difficult to layup plies on the tool. Also, the shape of the tool was simple enough to measure the surface using a 3D laser scanning device easily. Beside the curvy surface, the tool had a flat section on the top of the tool to have space for a vacuum port. The part trim line was added on the top curvy surface of the tool. The part trim line had a 38.1 mm offset from each edge of the curvy surface. Figure 3.10 showed the orthographic projection of the mold life experiment tool with dimensions.

The printed parts were required to be annealed to relieve the thermal residual stress inside of the parts (Basgul et al., 2020). The printed parts were placed inside of the oven and heated up to about 20°C - 30°C above the T_g of the material for 2 hours for annealing (Basgul et al., 2020).

3.2.2 Microstructure investigation of the printed material

The microstructure of the printed part was investigated by observing the cross-sectional area of the printed bead. In the microstructural analysis of the printed part, the void content inside of the printed material was investigated. Void content in composite material affected the mechanical strength of the structure negatively (Mehdikhani, Gorbatikh, Verpoest, & Lomov, 2019). Also, the void inside of the printed part could be exposed to the outer surface when it was machined. The void on the surface of the composite part manufacturing mold negatively affected the performance of the mold (Mohammadi et al., 2017). The void content inside of the printed part was calculated using the following equation;

$$V_v = \frac{\beta_v}{\beta_t} \tag{3.4}$$

where V_v was the volume fraction of voids, β_v was the area of the void and β_t was the full cross sectional area of the part. To observe the cross-sectional area of the printed part, a microscope sample of the printed part was made. The printed part was cut into a small sample size and potted in a resin to make a microscope sample. After the resin was cured, the cross-sectional plane of the part was ground and polished. The cross-sectional area of the part was observed using a microscope with 10X magnification. The microscopic image was taken and analyzed using an image processing software, ImageJ. The thresholding technique in the image processing software was used to measure the area of the voids inside of the bead. Figure 3.11 showed the microscope and microscope sample.

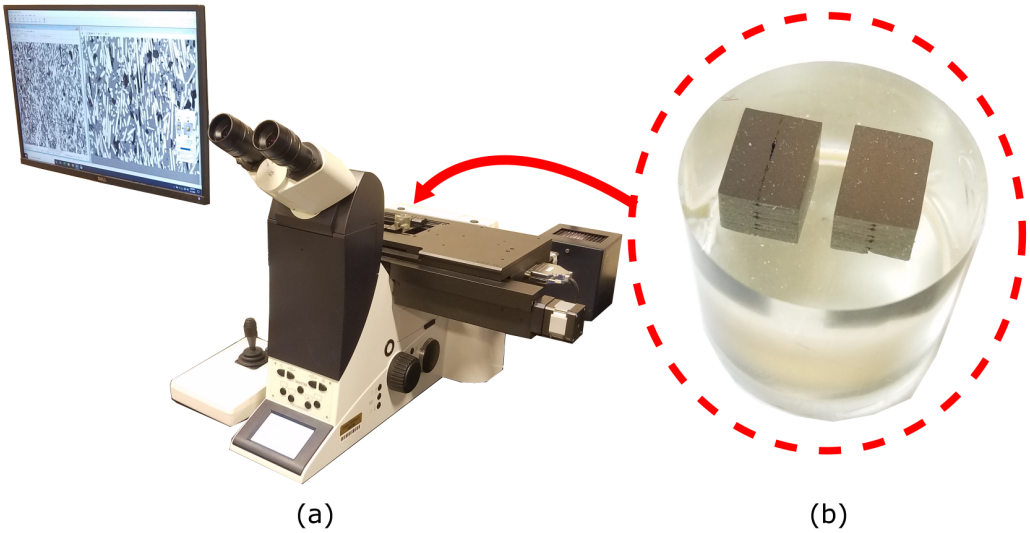

Figure 3.11. (a) Inverted microscope and (b) resin potted microscope sample.

3.2.3 Test specimen machining process

Since the surface of the printed part had a non-smooth surface, it could not be used as a test specimen right after it was printed. Therefore, the printed part was required to be machined to fabricate the experimental tool and make an individual test specimen. In this study, the computer numerical control (CNC) milling machine was mainly used to machine the parts as showed in Figure 3.12. Since there were no specified CNC machining parameters, such as surface feet per minute (SFM) and inch per tooth (IPT), for machining the carbon fiber reinforced PPS, that was used to print the part in this research, from the tool manufacturer, an additional experiment was designed and performed to investigate an optimal SFM and IPT for machining carbon fiber reinforced PPS.

SFM represented the speed of the cutter traveled across the workpiece (Koepfer, 1996). SFM was a parameter which determined rpm of the cutter using the following equation (Koepfer, 1996; Sheikh-Ahmad, 2009);

$$N = \frac{v}{\pi D} \tag{3.5}$$

Figure 3.12. Computer numerical control (CNC) milling machine.

where N was the spindle speed, revolution per minute (rpm), v was the cutting speed, surface feet per minute (SFM), and D was the diameter of the tool. Improper SFM could cause high heat due to the rubbing friction between the cutter and the workpiece (Sheikh-Ahmad, 2009). High heat on the cutting tool could soften the tool and caused the dull edge of the tool. High heat during the machining also could damage the workpiece by burning for thermoset polymer workpiece and by melting for thermoplastic polymer workpiece (Sheikh-Ahmad, 2009). IPT was a chip load that represented amount of material removed by each tooth of the cutter per revolution (Koepfer, 1996). IPT was a machining parameter that determined the feed rate of the cutter using the following equation(Koepfer, 1996; Sheikh-Ahmad, 2009);

$$F = Nfn \tag{3.6}$$

Where F was feed rate, f was the feed per tooth value (IPT), and n was the number of the tooth of the tool. If the IPT was too high, the cutter could have poor chip evacuation which could lead to tool breakage. If the IPT was too low, it caused rubbing between the cutting tool and the workpiece which could damage the tool and poor machined surface quality (Sheikh-Ahmad, 2009). Different SFM and IPT

Table 3.1. *Design of experiment (DOE) table for the experiment to investigate an optimal SFM and IPT for machining carbon fiber reinforced PPS.*

Various SFM with fixed IPT		
Case	SFM	IPT
1	250	0.001
2	500	0.001
3	1000	0.001
4	1500	0.001
5	1963	0.001

Various IPT with fixed SFM		
Case	SFM	IPT
1	500	0.001
2	500	0.0025
3	500	0.005
4	500	0.0075
5	500	0.01

were used to machine the test specimen and the machined surface quality of the test specimen was investigated using a stereoscope and surface roughness tester. The stereoscope was used to observe any surface defects due to the machining process, and the surface roughness tester was used to measure surface finish quality of the machined surface of the test specimen. Five different levels of SFM were tested; 250, 500, 1000, 1500, and 1963. While the different SFM was tested, IPT was fixed to 0.001. Among the five different levels of SFM, the one which created a surface with the least surface defect observed by a stereoscope and the least surface roughness value was determined. Then, the five different levels of IPT were tested while the SFM was fixed to the predetermined SFM; 0.001, 0.0025, 0.005, 0.0075, and 0.01. The machined surface with different IPT levels was observed using a stereoscope and measured with roughness tester to find an optimal IPT. 12.7 mm diameter end mill was used for the milling tool.

After the optimal SFM and IPT were decided, the 2-bead wall, demolding test tool, and mold life experiment tool were machined. Since the printed 2-bead wall did not have any flat and smooth face that could be used to fix the part to the CNC for the machining, a surface planer was used first to make one side flat before it was machined in the CNC. A 50.8 mm diameter face mill with 6-tooth was used to machine the plate in the CNC. To minimize the intra-bead void exposed on the machined surface of the 2-bead wall, the 2-bead wall was machined up to the middle of the bead. Therefore, a half bead amount (about 3 mm) from the top and bottom of the part was machined. Figure 3.13 showed the surface of the 2-bead wall before

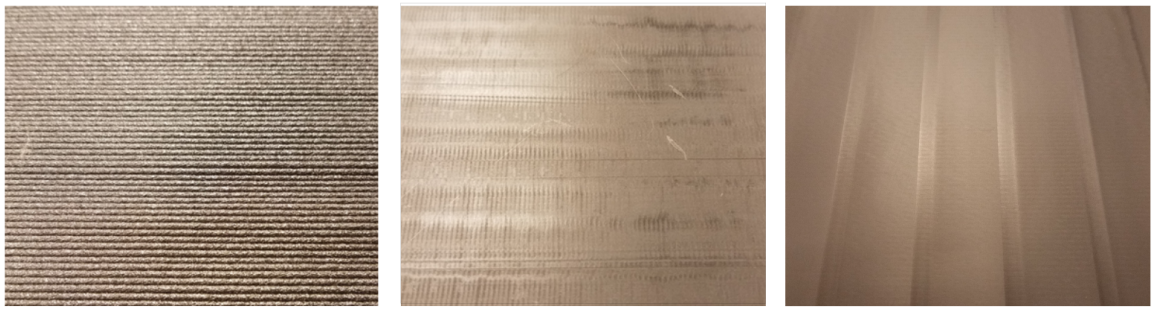

Figure 3.13. Surface of the 2-bead wall plate (a) after 3D printed, (b) after machined with the planer, and (c) after machined with CNC.

machining, after machining with the planer, and after machining with the CNC. Once milling the surface of the 2-bead wall plate finished, an abrasive waterjet was used to cut the panel to create the individual test specimens. The surface hardness, surface abrasion resistance, and surface roughness test specimen was a square shape with the size of 101.6 mm x 101.6 mm, and the coating adhesion test specimen was also square shape with the size of 38.1 mm x 38.1 mm. The surface abrasion resistance test specimen had a 6.35 mm diameter hole in the middle of the test specimen to be installed on the turntable platform of the surface abrasion resistance tester (ASTM International, 2014). The demolding test tool and the mold life experiment tool also had no smooth face to fix it to the CNC. Therefore, the demolding test tool was first bolted on an aluminum plate and the contour of the bottom flat section of the tool was machined. Then the tool was detached from the aluminum panel and directly fixed in the vise for the rest of the machining operations. The mold life experiment tool was not detached from the printing bed plate after printing. The print bed plate was directly fixed on the vacuum pod in the 5-axis CNC to machine the bottom surface of the tool. After the bottom of the tool was machined, the tool was detached from the printing bed plate and directly fixed on the vacuum pod for the rest of the machining operations.

3.3 Thermal analysis of the coating material

The author had found a liquid coating that had a thermoset polymer coating with ceramic particles as a coating material candidate for this study. This coating material could be applied to the substrate by the liquid spray coating technique. The liquid spray coating technique was simple and did not require any heavy equipment to apply the coating material that led to a low initial cost. Also, the size of the substrate was barely restricted with liquid spray coating technique. According to the coating manufacturer, the recommended coating application temperature was 148.89°C. However, the manufacturer reported that if the substrate material could not withstand in the high temperature, the coating material could be cured in between 65.56°C and 82.22°C for 2 hours alternatively. Also, the coating manufacturer reported that the maximum allowable temperature of the coating was 260°C which was high enough for high-temperature composite prepreg curing processes (180°C). Even though the general information of the coating material was provided by the coating manufacturer, it was necessary to verify the thermal characteristic of the coating material to use it in this study. The degree of cure of the coating material in the recommended temperature cycle from the manufacturer was investigated using DSC. Since the coating material was thermoset polymer, each polymer cross-linking released heat when the coating material cured. Therefore, the degree of cure of the coating material could be calculated using the following equation;

$$\alpha(t) = H(t)/H_R \tag{3.7}$$

where $\alpha(t)$ represented the degree of cure as a function of time, and $H(t)$ and H_R represented the heat released as a function of time and the total heat of reaction, respectively. DSC measured heat flow in and out from the sample during the temperature change, the exothermic reaction due to the coating material curing could be measured using DSC. Therefore, the coating curing temperature cycle was

Figure 3.14. (a) Thermogravimetric analysis (TGA) instrument and (b) TGA sample holder with the coating material.

tested to check whether it provided enough degree of cure for the coating material. The coating material was mixed with the catalyst and the mixed coating material was inserted into the DSC sample container. The weight of the mixed coating material inside of the container was measured and put into the test setup. The DSC sample was placed inside the furnace of the DSC. The temperature of the furnace was programmed to (1) ramping at 2.78°C/min to 82.22°C, (2) isothermal for 2 hours, (3) ramping at 2.78°C/min to 25°C. The DSC test result was analyzed using TA Universal Analysis software. The coating operable temperature was investigated using a thermogravimetric analysis (TGA) as showed in Figure 3.14. TGA was an equipment which measured the weight change of the sample due to decomposition kinetics in temperature change. Thermal degradation of the polymer could be analyzed using TGA by measuring the weight loss of the material in a tested temperature cycle. The cured coating material sample was placed in a TGA and the composite part curing temperature cycle was programmed to check there was any significant thermal degradation of the coating material during the composite part curing temperature cycle. The temperature cycle was programmed to (1) ramping at 2.78°C/min to 180°C, (2) isothermal for 2 hours, (3) ramping at 2.78°C/min to 25°C. The TGA test result was analyzed using TA Universal Analysis software.

3.4 Coating application process

The coating material was applied to the machined additively manufactured carbon fiber reinforced PPS composite parts in accordance with the coating application guide from the coating manufacturer. After the parts were machined, they were cleaned with compressed air and wiped with isopropyl alcohol to remove any contaminants, oil, or solvents on the part surface. Then, the parts were placed into the oven and heated up to 80°C for 2 hours to remove any moisture inside of the parts. A visual inspection was performed to verify that there was no evidence of any contaminants, oil, or moisture on the surface. If there were any evidence of contaminants, the parts were re-cleaned thoroughly, dried, and checked again. The coating material was mixed with a catalyst with the specific ratio and filtered with a mesh paint strainer to remove any contaminants from the coating material. The filtered coating material was poured in a high-volume & low-pressure (HVLP) spray gun with a 0.8 mm tip. The pressure for the spray gun was set to 0.17 MPa - 0.21 MPa and the spray gun was set to have a 50.8 mm to 76.2 mm wide spray pattern from 76.2 mm to 127 mm away from the substrate. The coating manufacturer recommended to apply 1 or 2 coats of coating material with 0.0127 mm to 0.0254 mm of total coating thickness. Figure 3.15 showed a picture of liquid coating application with a high-volume & low-pressure (HVLP) spray gun. If there were any runs and sags during the coating application process, the applied coating material was cleaned with isopropyl alcohol and restarted from the part cleaning process. After the coating was applied, the coated parts were placed in the oven for the coating material curing process. The coated parts were heated up to 82°C and soaked for 2 hours to cure the coating material. Figure 3.16 showed the coating application process diagram.

Figure 3.15. Liquid coating application with a high-volume & low-pressure (HVLP) spray gun.

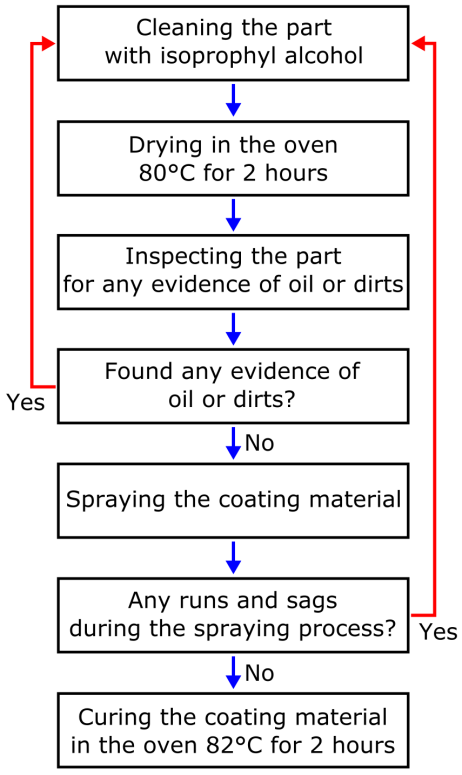

Figure 3.16. The coating application process diagram.

3.5 Surface property tests

In the following sections, the durability and surface performance of the coated surface were measured. The durability of the surface was measured using a surface hardness test and abrasion resistance test. The surface performance of the coated surface was measured using a surface roughness test and demolding test. The surface friction of the coated and non-coated surface was analyzed by conducting demolding test of the non-coated and coated composite tools. Not only the surface properties of the coated surface, but also the sustainability and life of the coating were important for the mold. Therefore, a CTE, coating adhesion strength, and life of the coating were investigated in the following sections.

3.5.1 Surface hardness test

The surface hardness of the additively manufactured carbon fiber reinforced PPS composite test specimen was tested using a Barcol impressor in accordance with ASTM D2583-13a, the test method for indentation hardness of rigid plastics by means of a Barcol impressor (ASTM International, 2013). Barcol hardness test was a static hardness test which used an impressor to indent the surface of the material with a specific load (Hashmi, 2016; Tabor, 2000). The depth of the indent was measured to determine the hardness level of the material surface (Tabor, 2000). Qualitest GYZJ-934-1 was used for a Barcol impressor. In total, four test specimen were prepared; two non-coated and two coated composite test specimens. 50 different surface hardness measurements from each test specimen, that made total 100 hardness measurements for each non-coated and coated test specimen, were collected. Accordance to ASTM D2583-13a, each measurement had a minimum distance of 3.175 mm from the edge of the test plate and between each measurement (ASTM International, 2013). The surface hardness data of the non-coated and coated composite test specimen was analyzed and compared using a statistical analysis tool. A two-sample t-test was performed with a 0.05 significance level to

Figure 3.17. Barcol Impressor.

investigate if there was any significant surface hardness improvement after the coating was applied.

$$H_0 : \mu_n = \mu_c \qquad H_a : \mu_n < \mu_c \tag{3.8}$$

where μ_n and μ_c represented the average surface hardness level of the non-coated and coated composite respectively. In addition, the surface hardness level of an aluminum 6061-T6 and a 1020 steel, which were commonly used metal for mold manufacturing, were measured to compare the hardness of an additively manufactured carbon fiber reinforced PPS composite to the hardness of a traditional metal. 50 surface hardness measurements were made from each aluminum and steel test specimen.

3.5.2 Surface abrasion resistance test

The abrasion resistance test measured the abrasion resistance of the material surface. The abrasion resistance test was performed in accordance with ASTM D4060, standard test method for abrasion resistance of organic coatings by the Taber abraser (ASTM International, 2014). A Teledyne Taber abraser model 503 was used for an abrasion tester as showed in Figure 3.18(a). The abrasion resistance tester had a turntable, abrasion wheel, and vacuum system. The abrasion resistance

test specimen was mounted on the turntable and fixed using a clamping nut on the middle of the turntable. Two Taber abrasion wheels were placed on the top surface of the test specimen with a specific load which could be adjusted by putting a weight on the abrasion wheel. In this study, CS-10 Calibrase resilient wheels and 500 g of load on each wheel were used. When the turntable rotated, the abrasion wheels were rotated driven by the rotation of the test specimen. The rub-wear action between the test specimen and the abrasion wheels abraded the surface of the test specimen as showed in Figure 3.18(b) (Izdebska, 2016). The vacuum system cleaned abraded particles on the test specimen during the test. For the surface abrasion resistance data, the weight change of the test specimen corresponding to the number of abrasion cycles was used. In total, 2000 abrasion cycles were tested for each test specimen. The weight change of the test specimen was measured after every 200 abrasion cycles. Taber wear index, which represented the rate of wear, for each test specimen and compared. The Taber wear index was calculated using the following equation (ASTM International, 2014);

$$I = [(w_a - w_b) * 1000]/c \tag{3.9}$$

where I represented Taber wear index, w_a was the weight of the test specimen before abrasion, w_b was weight of the test specimen after abrasion, and c was the number of abrasion cycles. One non-coated and one coated composite abrasion resistance test specimen were prepared, and 10 wear index could be calculated from each test specimen. The wear index data of the non-coated and coated composite test specimen were compared using a two-sample t-test with a significance level of 0.05 to investigate if there was any significantly decreased Taber wear index after the coating was applied.

$$H_0 : \mu_n = \mu_c \qquad H_a : \mu_n > \mu_c \tag{3.10}$$

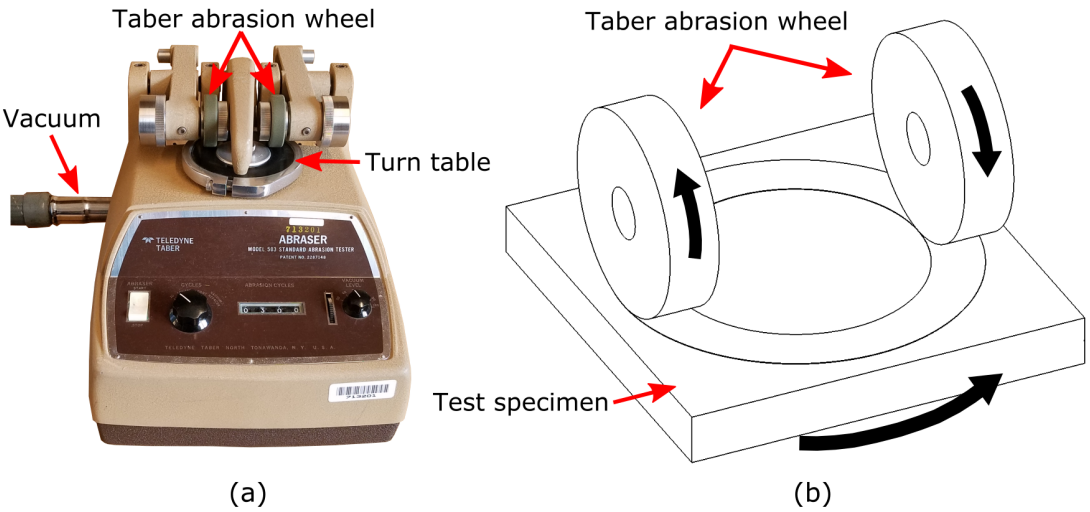

Figure 3.18. (a) Taber surface abrasion resistance tester and (b) schematic drawing of surface abrasion resistance test.

where μ_n and μ_c represented the average wear index of the non-coated and coated composite respectively. In addition, aluminum 6061-T6 and 1020 steel test specimen were tested using the same setting to compare the wear index of the coated and non-coated additively manufactured carbon fiber reinforced PPS composite to the wear index of traditional metal.

3.5.3 Surface roughness test

In this study, the surface roughness test was performed in accordance with ASTM D7127, standard test method for measurement of surface roughness of abrasive blast cleaned metal surfaces using a portable stylus instrument (ASTM International, 2018). The Mitutoyo surf tester SJ-210 was used for the surface roughness test as showed in Figure 3.19. The roughness tester measured a deviation in the normal direction of the surface which represented the irregularity of the surface. The surface roughness tester measured various parameters; arithmetical mean roughness (R_a), mean roughness depth (R_z), and maximum roughness depth (R_{max}) (Gadelmawla et al., 2002). In this study, arithmetical mean roughness (R_a)

Figure 3.19. Surface roughness tester.

was used to compare the surface roughness level of the test specimen (Hashmi, 2016). R_a was calculated using the following equation;

$$R_a = \frac{1}{n}\sum_{i=1}^{n}|y_i| \tag{3.11}$$

where n was the number of samples and y_i was a deviation from the sample mean line (Gadelmawla et al., 2002). The roughness tester was set to have a 2.5 mm cutoff length and 12.5 mm sampling length for the test. The roughness was measured in the direction which was orthogonal to the creases on the machined surfaces that was the same as machining direction. Two non-coated and two coated composite test specimen were prepared. For each test specimen, 20 roughness measurements were collected. A total of 40 roughness measurements were collected for the non-coated and coated composite surface. A statistical analysis tool, two-sample t-test with a 0.05 significance level was performed to investigate any significant surface roughness (R_a) decrease after the coating was applied to the test specimen.

$$H_0 : \mu_n = \mu_c \qquad H_a : \mu_n > \mu_c \tag{3.12}$$

where μ_n and μ_c were the average surface roughness level (R_a) of the non-coated and coated composite respectively.

3.5.4 Demolding test

A demolding force was the force required to detach a cured part from the mold. The demolding force was an important property of the part-manufacturing mold because a high demolding force could damage the mold and the part during the part demolding process. The demolding force was closely related to the surface property of the mold. Therefore, in this experiment, composite part-manufacturing molds were built and used in a composite part manufacturing process. The force required to demold the part from the mold was measured and compared. The demolding test tool with a part ejecting system was designed, additively manufactured, and machined. Figure 3.20 showed the design of the demolding test tool with the part ejecting system. The cured composite part was demolded from the tool by pushing the part through the ejecting pin hole. The demolding test tool had an ejector plug in the circular pocket on the top of the tool. The ejector plug prevented the resin smeared inside of the part ejecting system of the tool during the composite part curing cycle. The ejector plug was machined using aluminum 6061-T6. One non-coated and one coated tool were prepared and tested. The surface of both tools was treated using Chemlease 15 Sealer EZ and Chemlease R&B semi-permanent mold release. The mold sealer and release were applied in accordance with the application instructions from the manufacturer.

Since the author wanted to have a high demolding force of the tool during the demolding test, the author used a woven fiber glass reinforced prepreg for the composite layup plies to increase the demolding force intentionally. Generally, fiber glass had a higher coefficient of thermal expansion (CTE) than carbon fiber (Chawla, 1987). Therefore, once the composite part was cured and cooled, the fiber glass composite part shrank more than the carbon fiber reinforced composite tool that gave a higher normal force of the composite part toward the tool. CATIA V5 CAD software was used to design the lay-up ply as showed in Figure 3.21. The composite ply was designed to lay on the top and side of the tool. Due to the

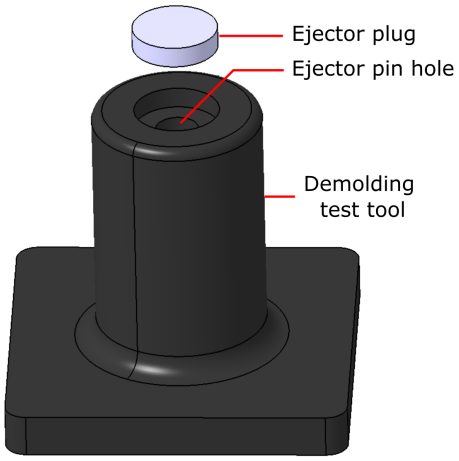

Figure 3.20. Design of the demolding test tool with the part ejecting system

geometrical shape of the tool, the composite ply had to have darts for draping the ply on the tool. Eight plies were laid on the tool with $[0/90/30/60]_2$ orientation to distribute the darts evenly across the tool surface. Also, additional plies were laid on the top of the tool to prevent the part from bending during the demolding process. After the composite plies were all laid, it was vacuum bagged and cured in an autoclave with a cure cycle that had a 2-hour soak at 180°C with 586 kPa of pressure as showed in Figure 3.22. After the composite part was cured, the tool was installed in an MTS universal testing machine for the demolding test. An ejector pin was placed inside of the ejector pin hole of the tool and pushed the ejector plug to demold the part from the tool. The MTS machine recorded the force applied to the ejector pin and its displacement during the test. Each tool had a total of 10 part production cycle. The demolding force for each production run was recorded and analyzed to compare the demolding characteristic of the non-coated and the coated composite tools. A statistical analysis was performed using a two-sample t-test with a significance level of 0.05 to investigate any significantly decreased required demolding force with the coating on the tool.

$$H_0 : \mu_n = \mu_c \qquad H_a : \mu_n > \mu_c \tag{3.13}$$

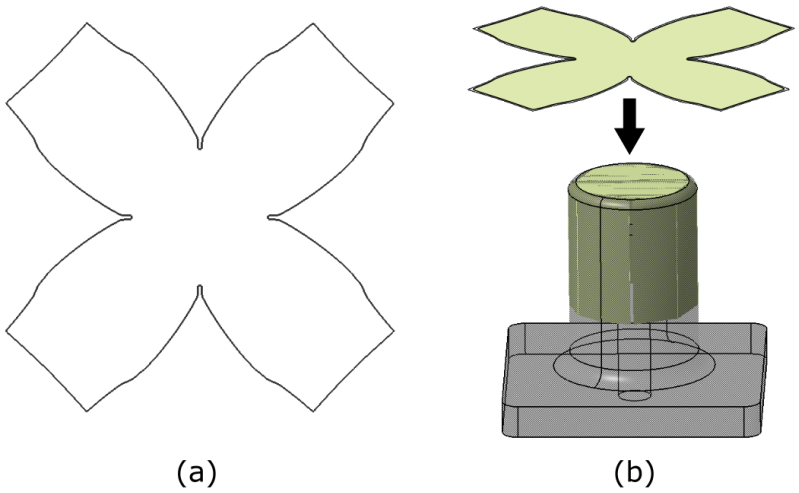

Figure 3.21. (a) Composite layup design for the demolding test and (b) schematic drawing of ply laid up on the demolding test tool.

where μ_n and μ_c were average force required to demold the composite part from the non-coated tool and coated tool respectively. Also, a Pearson correlation test, with 0.05 significance level was performed between the required demolding force and the number of the production cycle for the non-coated and coated tool to investigate how the required demolding force of the non-coated and coated tool changed over the production cycles using the following hypothesis;

$$H_0 : \rho = 0 \qquad H_a : \rho \neq 0 \tag{3.14}$$

where ρ was the population correlation between the required demolding force and the number of the production cycles. The surface quality of the tool after each production cycle was investigated using a surface roughness tester. Also, the surface of the tool was inspected visually and using a stereoscope after each production cycle to detect any tool surface damage during the demolding process.

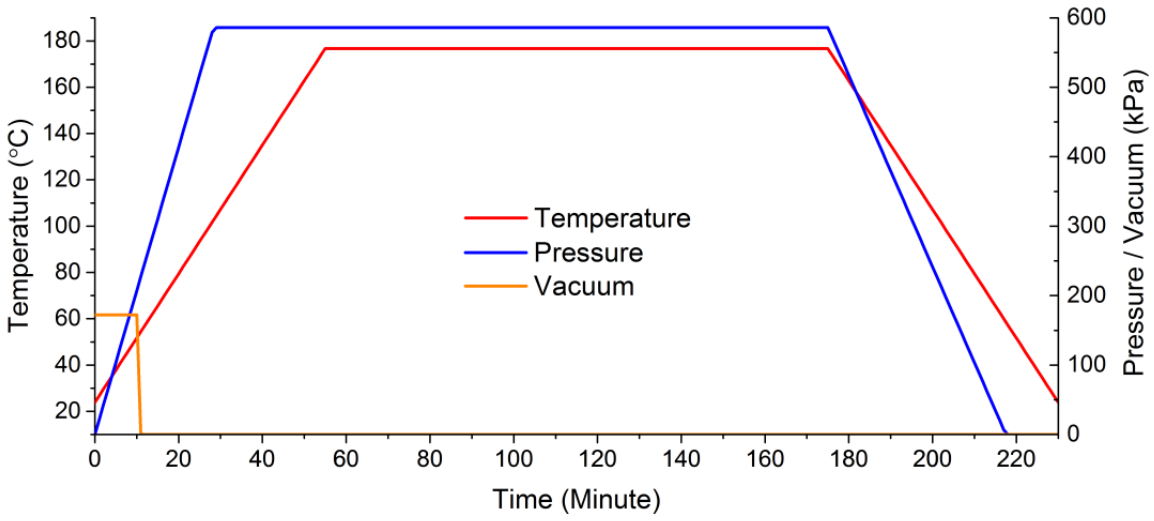

Figure 3.22. The composite part curing cycle (temperature, pressure, and vacuum) using the autoclave

3.5.5 Coefficient of thermal expansion (CTE) test

Thermal fatigue was a fatigue failure caused by the repeated thermal stresses. Thermal fatigue was one of the biggest factors that caused the debonding of the coating from the substrate because the coefficient of thermal expansion (CTE) mismatch between the coating and substrate caused shear stress at the bonding area at elevated temperature (Humfeld Jr, 1997). Since the composite part manufacturing mold was used for repeated composite part production cycle in elevated temperature, it was important to verify that the coating could withstand thermal fatigue during the production cycle. To understand the thermal fatigue between the additively manufactured carbon fiber reinforced PPS composite and the coating material, their CTE needed to be measured first.

To measure the CTE of the materials, digital image correlation (DIC) technology was used in this study. DIC was a technique that used multiple images and analyzed them to measure displacement and strain on the surface of the test specimen. The CTE test was performed for the non-coated composite test specimen and the coating material. The CTE mismatch between the substrate material and

the coating was investigated by comparing the CTE difference between the two. The composite CTE test specimen was made from 1 bead thick face machined additively manufactured carbon fiber reinforced PPS composite plate. The plate was machined to 25.4 mm x 25.4 mm using an abrasive waterjet. Since the additively manufactured carbon fiber reinforced PPS composite had anisotropic property, the CTE in all 1 (printing direction), 2 (in-plane transverse direction), and 3 (stacking direction) direction were calculated. Two composite CTE test specimens, one for 1&2 direction and one for 1&3 direction, were tested. The coating material CTE test specimen was manufactured by potting the coating material in a mold which had a 25.4 mm diameter. The cured coating material was sliced to 2.45 mm thick using a sectioning wheel. The coating material was an isotropic material, so only one test specimen was tested. The DIC technique required a speckle pattern on the surface of the test specimen. Therefore, the cut CTE test specimens were dried and the speckle pattern was applied using white flat spray paint on the top surface of the test specimen as showed in Figure 3.23(a). The speckled CTE test specimen was placed inside of a hot stage. A DIC camera with a 35 mm lens was installed and positioned above the top glass of the hot stage to record the speckles on the top surface of the test specimen inside of the hot stage. The light source and lens exposure were adjusted to get a good focus on the speckle pattern on the test specimen with the minimized uncertainty value in the DIC image. Figure 3.23(b) showed the CTE test setting. Once the CTE test started, the DIC camera took a picture of the speckles every 30 seconds. The CTE test temperature cycle for the printed PPS composite was programmed to go up to 270°C, and the CTE test temperature cycle for the coating material was programmed to go up to 200°C. The hot stage was programmed to have 4°C/min ramp rate for both heating and cooling. In addition, the temperature of the hot stage was programmed to soak for 5 minutes for every 10°C of temperature change to measure the strain change of the speckles when the temperature got stable

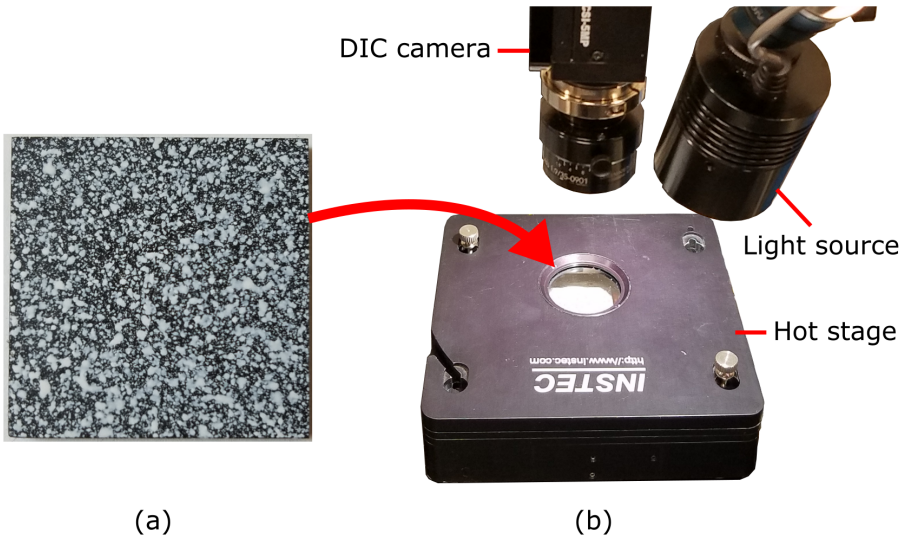

Figure 3.23. (a) The speckled CTE test specimen and (b) CTE test setting.

instead of measuring the strain change during the temperature ramping. Figure 3.24 showed the programmed temperature setup of the hot stage during the CTE test.

The recorded DIC images were imported into VIC 2D, an image processing software, to obtain strain change of the speckles. The strain change data from DIC was synchronized to the temperature change data from the hot stage. The strain change data points from every temperature soaking section (every 10°C) were extracted and averaged. These averaged strain changes for every 10°C were used to make a strain change versus temperature plot. Then the CTE of the test specimen was calculated using the following equation;

$$\alpha_i(T) = \frac{\triangle\varepsilon_i(T)}{\triangle T}, i = 1, 2, 3 \tag{3.15}$$

where $\alpha_i(T)$ was CTE of the test specimen in i direction at temperature T. $\triangle\varepsilon_i(T)$ was the strain change in i direction during $\triangle T$, temperature changes. $i = 1$ was the printing direction, $i = 2$ was the in-plane transverse direction, and $i = 3$ was the stacking direction.

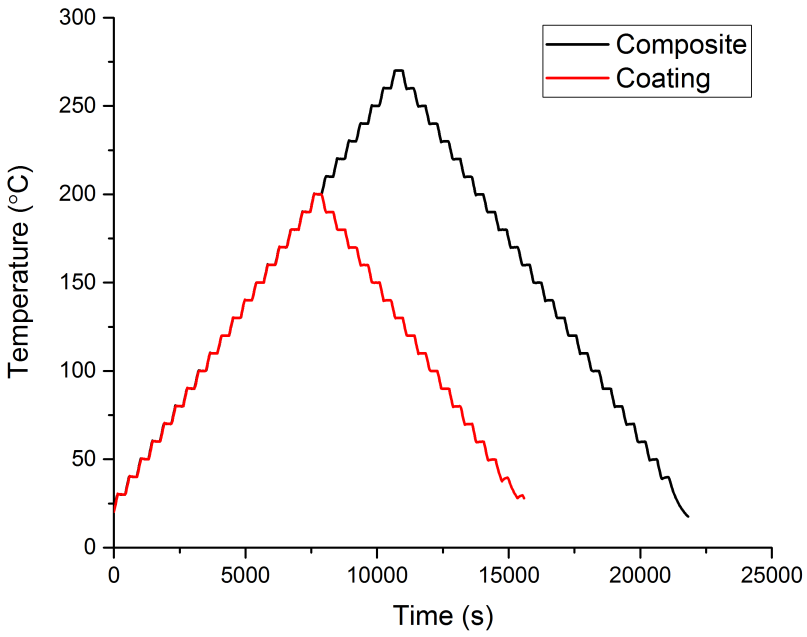

Figure 3.24. The programmed temperature for the CTE test

3.5.6 Coating adhesion test

The coating adhesion test measured the adhesion strength between the coating and the substrate material. The adhesion strength of the coating was an important factor which affected the life of the coating. Coatings often failed due to the low adhesion strength between the coating and substrate. The composite mold was exposed to various forces, such as the shear forces resulting from CTE mismatch between the substrate and coating material during the curing process, and frictional shear and peel stresses (normal stress) resulting from part demolding. Therefore, it was important to verify that the coating adhered to the mold firm enough, so it could be used for composite part manufacturing mold surface. Also, the composite part manufacturing mold underwent a repeated temperature cycle which could cause thermal fatigue between the mold and the coating. Therefore, the adhesion strength between the mold and the coating corresponding to the number of composite part manufacturing temperature cycle was investigated. In this study, the adhesion strength of the coating was tested using a pull-off adhesion test

(ASTM International, 2017). The adhesion test specimen was cut from the 2-bead wall panel and the size of the test specimen was 38.1 mm x 38.1 mm. After the test specimen was cut, the coating was applied to the top surface of the test specimen. In the adhesion test, the number of temperature cycles was set as a variable, and 0 to 10 temperature cycles were tested. The temperature cycle was programmed to (1) ramping at 2.78°C/min to 180°C, (2) isothermal for 2 hours, (3) ramping at 2.78°C/min to 25°C. 10 test specimen were prepared and tested for each cycle. After the temperature cycle, a pull-off test dolly was bonded on the top of the test specimen. The pull-off test dolly was 25.4 mm high aluminum 6061-T6 cylindrical shaped rod with 19.05 mm diameter. On the top of the dolly, there was a threaded hole to connect the dolly to the pull-off testing fixture. The bonding surface of the dolly was sandblasted and cleaned before it was bonded. the bonding area of the test specimen was also lightly sandblasted and cleaned. Two-part mix urethane adhesive was used to bond the dolly to the top of the test specimen. To keep the dolly centered and aligned to the test specimen while the dolly was bonded, 3D printed pull-off test dolly bonding jig was designed and used. Figure 3.25 showed the coating adhesion test specimen preparation process. After the adhesive was fully cured, the coating around the dolly was trimmed using a hole saw to keep the coating adhesion test area consistent for all test specimens (ASTM International, 2017). The pull-off test was performed using an MTS universal testing machine and a customized pull-off test fixtures. The top fixture had a threaded rod that connected to the pull-off testing dolly and held it while the bottom fixture pulled the test specimen as showed in Figure 3.26. The pull-off test condition was set in accordance with ASTM D4541, standard test method for pull-off strength of coatings using portable adhesion testers (ASTM International, 2017). The pulling rate was set to 0.5 mm/min and 20 data were collected per second. The pull-off test data was analyzed and compared by finding a maximum pull-off strength of the coating which was calculated using the following equation (ASTM International, 2017);

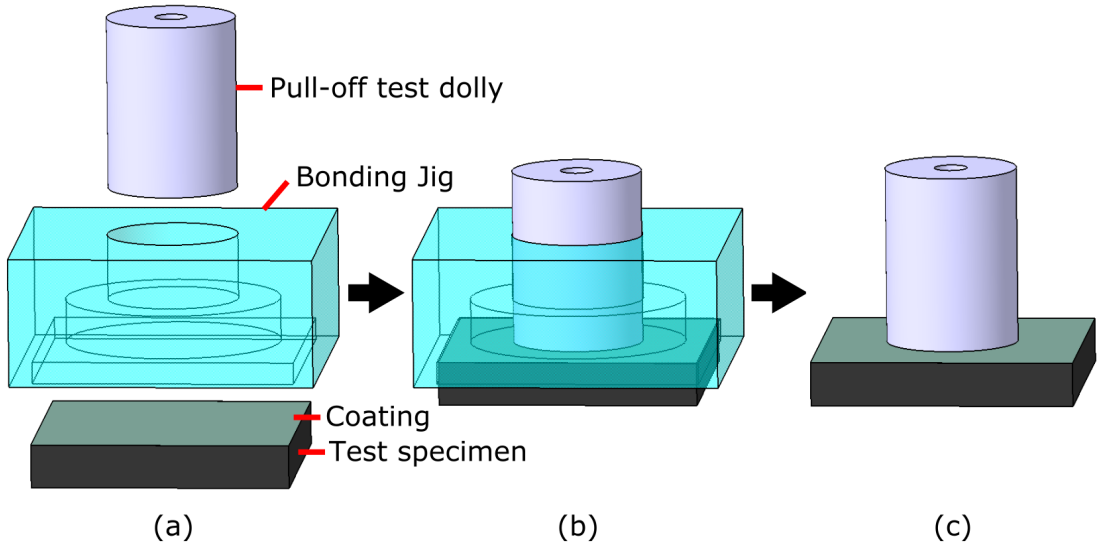

Figure 3.25. The coating adhesion test specimen (a) before bonding with the pull-off test dolly, (b) bonding with the dolly using the bonding jig, and (c) after removing the jig after bonding.

$$X = 4F_{max}/\pi d^2 \tag{3.16}$$

where X was maximum pull-off strength of the coating, F_{max} was maximum load before the coating fails, and d was the diameter of the bonding area. The maximum pull-off strength of each test specimen was recorded and the relationship between the coating adhesion strength and the number of cure cycles was demonstrated. A Pearson correlation test, with 0.05 significance level was performed between the maximum pull-off strength of the coating and the number of the production cycle to investigate how the strength of the coating changed over the production cycles using the following hypothesis;

$$H_0 : \rho = 0 \qquad H_a : \rho \neq 0 \tag{3.17}$$

where ρ was the population correlation between the maximum pull-off strength of the coating and the number of the production cycles.

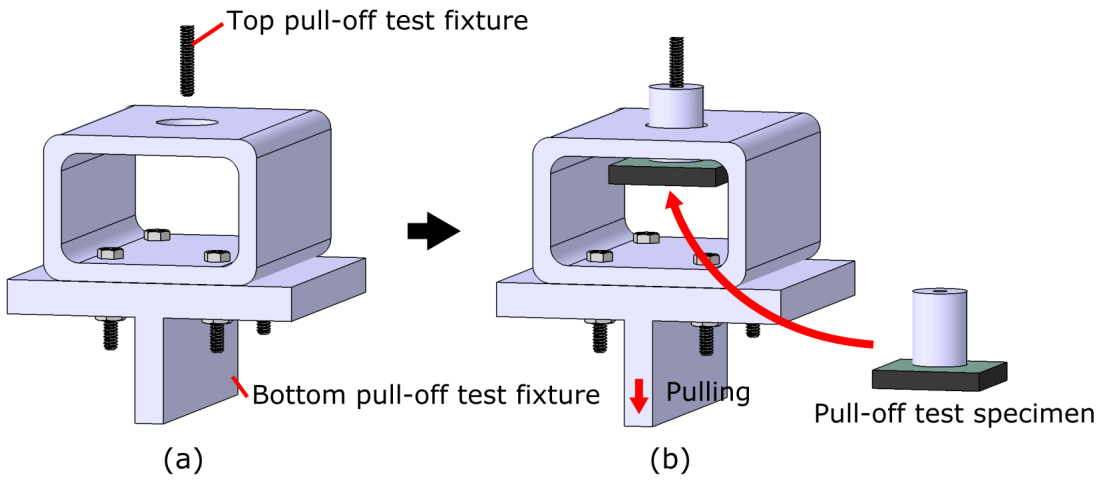

Figure 3.26. Schematic drawing of (a) the top and bottom pull-off test fixture and (b) the pull-off test specimen in the test fixture.

3.5.7 Coating sustainability and mold life experiment

In coating sustainability and mold life experiment, the sustainability of the coating material on the additively manufactured fiber reinforced composite mold, and how the coating affected the life of the mold were investigated. The mold life experiment tool was additively manufactured and used for a number of composite part manufacturing cycles. The coated tool was used to test the sustainability of the coating on the tool. Also, it was compared to the non-coated tool to study how the coating affected the life of the tool. One non-coated and one coated tool were prepared. The surface of the non-coated and coated mold life experiment tool was prepared with Chemlease 15 Sealer EZ and Chemlease R&B semi-permanent mold release. The layup ply was designed to have a 6.35 mm offset to the part trim line as showed in Figure 3.27. The designed ply was cut using an automatic cutting table. Four plies of the plain weave carbon fiber reinforced epoxy prepreg, HEXCEL 299 947-321 TY II CL A/AGP 193PW/3501-6, with $[0]_4$ orientation was laid on the top of the tool. After the composite plies were all laid, it was vacuum bagged and tested for air leak. It was important to verify that the tool was fully airtight because the air leak decreased the applied vacuum pressure to the plies which could

lead to improper composite part consolidation during the curing process (Campbell Jr, 2003). Air leak of the tool was tested in accordance with ASTM D5687, standard guide for the preparation of flat composite panels with processing guidelines for specimen preparation. The vacuum pressure level was monitored and checked whether it had no vacuum pressure dropping more than 3.5 kPa in any five-minute period (ASTM International, 2015b). The composite part was cured in an autoclave with a cure cycle that had a two-hour soak at 180°C with 586 kPa of pressure as showed in Figure 3.22. After each composite part manufacturing cycle, the cured composite part was demolded, and the mold life experiment tool was inspected visually to detect any surface defects. Also, geometrical surface data from the top surface of the tool was measured using 3D laser scanning device, FARO Arm Edge model 14000, as showed in Figure 3.28. The collected data was analyzed to investigate the geometrical shape change of the tool in the repeated composite part manufacturing cycle. A Pearson correlation test, with 0.05 significance level was performed to investigate if there was any relationship between the amount of the geometrical deviation of the tool and the number of production cycle using the following hypothesis;

$$H_0 : \rho = 0 \qquad H_a : \rho \neq 0 \tag{3.18}$$

where ρ was the population correlation between the geometrical deviation of the tool and the number of the production cycle. The sustainability of the coating was evaluated by inspecting the coated tool during multiple composite part manufacturing cycles. The surface visual inspection, air leak test, and shape change deviation analysis of the coated tool were compared to the non-coated tool to analyze how the coating affected the life of the composite part manufacturing mold.

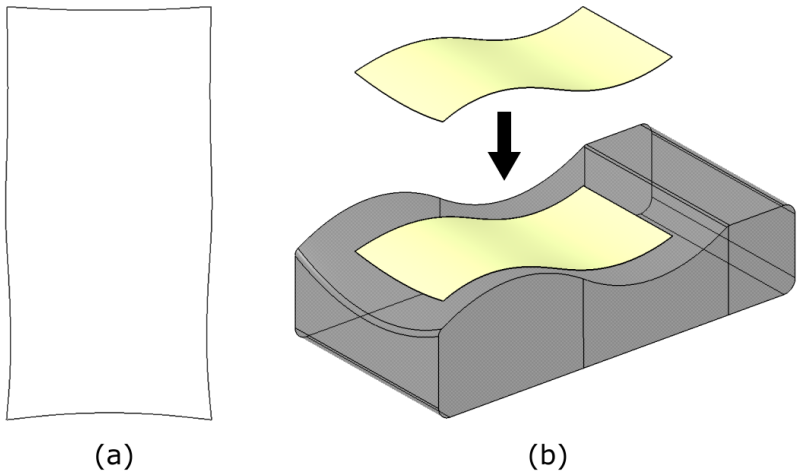

Figure 3.27. (a) Ply design for the mold life experiment tool and (b) schematic drawing of the ply laid up on the tool.

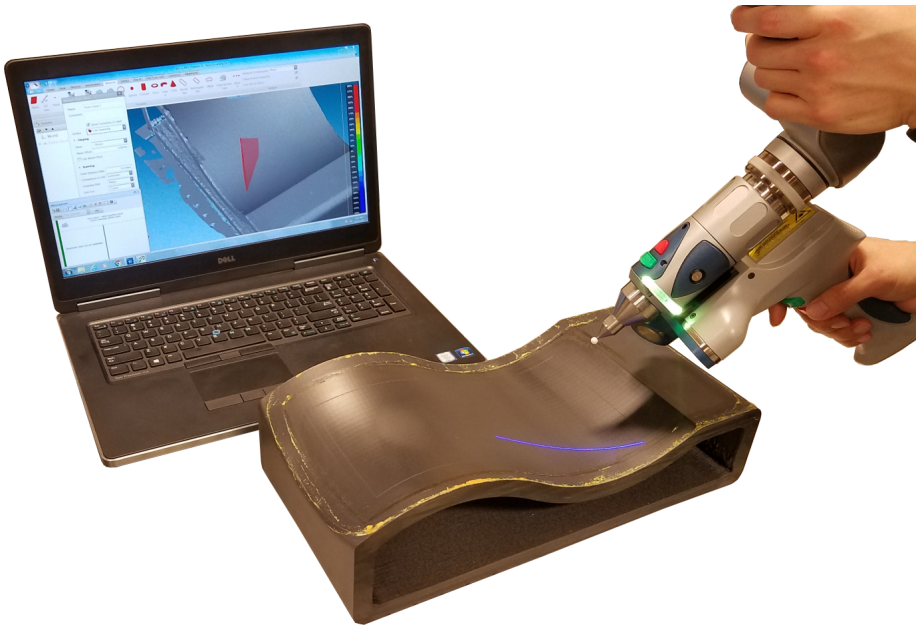

Figure 3.28. Surface measuring of the mold life experiment tool using 3D laser surface scanning technology.

3.6 Summary

This chapter provided the experimental framework and procedures of the experiment. In this chapter, the process of material thermal characterization for testing the coating applicability, test specimen preparation, coating application, and various surface property tests were introduced. The following chapter presented the results from the experiments presented in this chapter.

CHAPTER 4. RESULTS

In this chapter, the author reported the experimental data, data analysis, and discussion for the experimental results. This chapter included the results of the substrate and coating material thermal characterization, test specimen printing and machining process, coating application process, and coating performance tests, such as surface hardness test, abrasion resistance test, roughness test, demolding test, CTE test, coating adhesion test, and mold life experiment test.

4.1 Substrate material thermal characterization

4.1.1 Differential calorimeter (DSC)

The thermal characteristic of the carbon fiber reinforced PPS sample was investigated using the differential calorimeter (DSC). The heat flow, temperature, and time data were exported from DSC and analyzed. Figure 4.1 showed the DSC results, heat flow and temperature data in a time plot. The author was able to identify the glass transition temperature, crystallization temperature, and melting temperature of the material in the plot by finding the area where the heat flow transition had occurred. The cold crystallization, due to the lack of crystallization in the pellet material, was identified at the temperature of 131.53°C, the melting temperature was identified to be 289.20°C, and the non-isothermal crystallization temperature was identified to be 234.28°C. In the glass transition area, T_{eig}, T_{efg} and T_{mg} were identified in accordance with ASTM D3418 as showed in Figure 4.2. T_{eig}, T_{efg} and T_{mg} were determined to be 93.46°C, 97.66°C, and 95.91°C respectively. T_{mg}, 95.91°C was estimated as the glass transition temperature (T_g) of the substrate material.

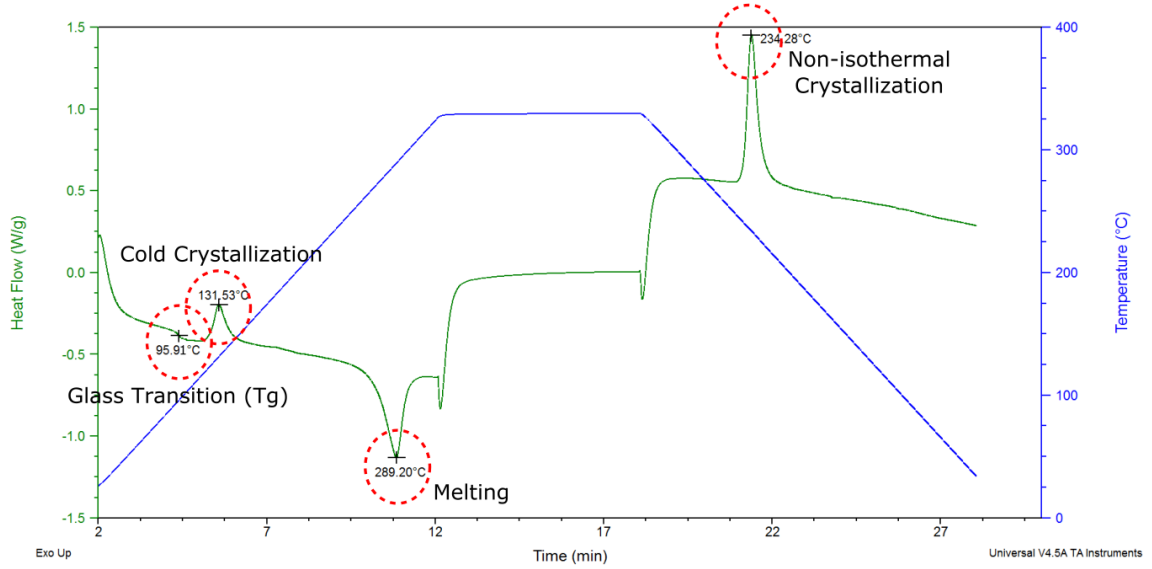

Figure 4.1. DSC thermal analysis result of the substrate material.

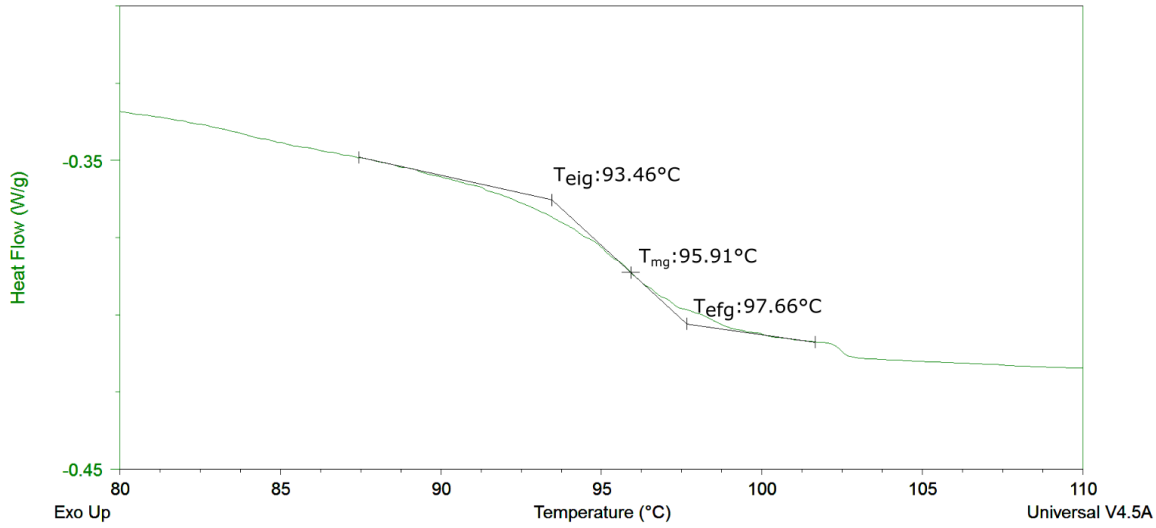

Figure 4.2. Glass transition area in the DSC thermal analysis result of the substrate material with identified T_{eig}, T_{efg}, and T_{mg}.

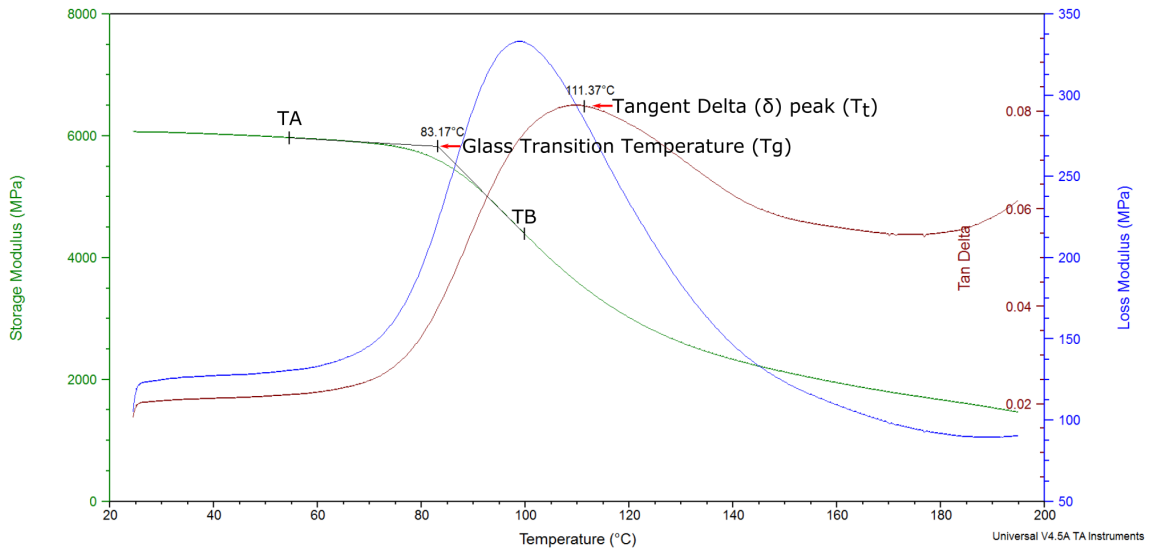

Figure 4.3. DMA result that had storage modulus, loss modulus, and tangent delta corresponding to the temperature change.

4.1.2 Dynamic mechanical analysis (DMA)

The thermal characteristic of the carbon fiber reinforced PPS sample was also investigated using the dynamic mechanical analysis (DMA). The storage modulus, loss modulus, tangent delta, and temperature data were exported from DMA and analyzed. Figure 4.3 showed the DMA result plot, storage modulus, loss modulus, and tangent delta corresponding to the temperature change. Two tangent lines where the storage modulus decreased dramatically, TA and TB, were identified. The point where the two tangent lines intersected, 83.17°C was identified and estimated to be the glass temperature (T_g) of the substrate material. The tangent delta peak (T_t) was identified to be 111.37°C. The glass transition temperature of the substrate material estimated in DSC was 95.91°C and the glass transition temperature of the substrate material estimated in DMA was 83.17°C. Therefore, the maximum allowable temperature was estimated to the range between 83.17°C and 95.91°C.

4.2 Test specimen preparation

4.2.1 Part printing process

Three different types of specimens were additively manufactured using Composite Additive Manufacturing Research Instrument (CAMRI). The first specimen type was a 2-bead wall. The 2-bead wall was used to fabricate flat test specimen for surface hardness test, abrasion resistance test, roughness test, and coating adhesion test. The second specimen type was a demolding test tool, and the last specimen type was a mold life experiment tool. Simplify3D was used to slice the CAD model and generate G-code for printing. For all specimens, the same printing conditions, such as printing temperature and printing speed, were used. Figure 4.4 showed the printing temperature condition which was used in this study. The printing speed of 5500 mm/min was used for all test specimen. The 2-bead wall was set to have one outline/perimeter shell for all layers and three 2-bead walls were printed at the same time as showed in Figure 4.5. The total printing time of three 2-bead walls was 1 hour 24 minutes. The demolding test tool was printed with two different processes. The bottom section, which had a square contour, was set to have eight outline/perimeter shells (between 0 mm and 15 mm high), and a cylinder section was set to have four outline/perimeter shells (between 15 mm and 92 mm high) as showed in Figure 4.6. The total printing time of the demolding test tool was 8 minutes. The mold life experiment tool was set to have no top and bottom solid layer. The outline/perimeter shells were set to three to all layers height. Figure 4.7 showed the sliced mold life experiment tool for 3D printing and the printed tool. The total printing time of the mold life experiment tool was 1 hour 11 minutes. For thermal stress relaxation of the part, all printed parts were annealed in an oven with the following temperature cycle; (1) ramping to 130°C by 2.78°C/min, (2) soaking at 130°C for 2 hours, and (3) ramping to 25°C by 1.11°C/min. Once the test specimens were annealed, they were ready to be machined.

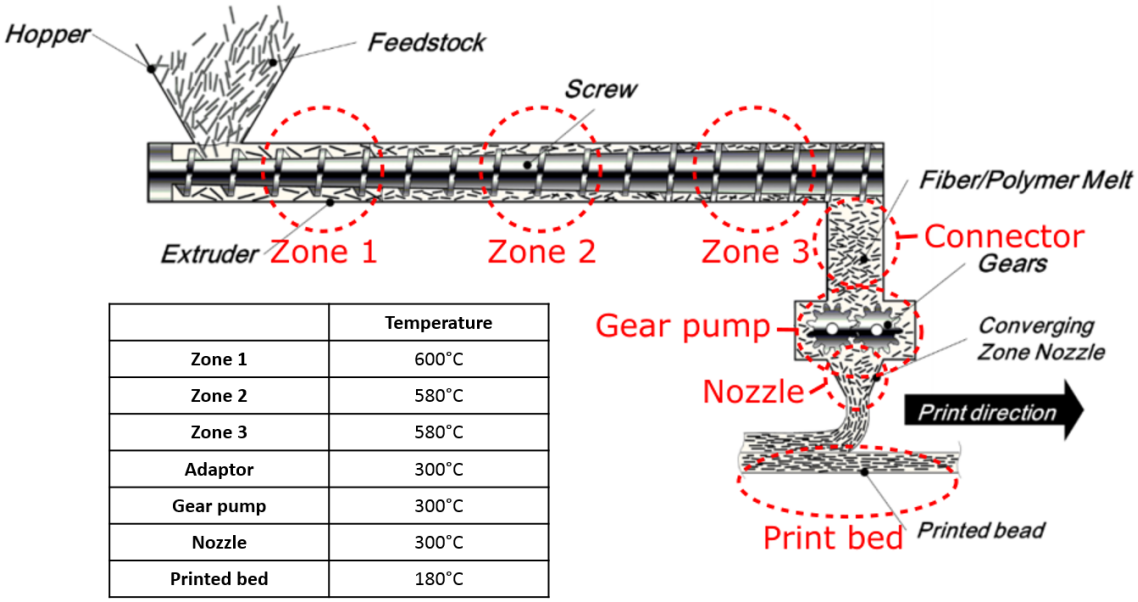

	Temperature
Zone 1	600°C
Zone 2	580°C
Zone 3	580°C
Adaptor	300°C
Gear pump	300°C
Nozzle	300°C
Printed bed	180°C

Figure 4.4. Printing temperature condition chart for printing the carbon fiber reinforced PPS composite. Reprinted from "In-silico Tensile Testing of Additively Manufactured Short Fiber Composite," by M. Ramirez, 2018, p. 5. Copyright 2018 by M. Ramirez.

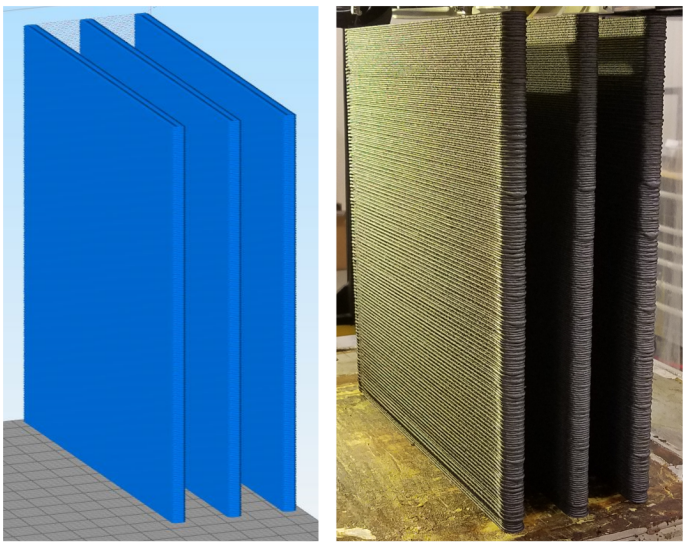

(a) (b)

Figure 4.5. (a) Three 2-bead walls slicing image, and (b) the printed three 2-bead walls.

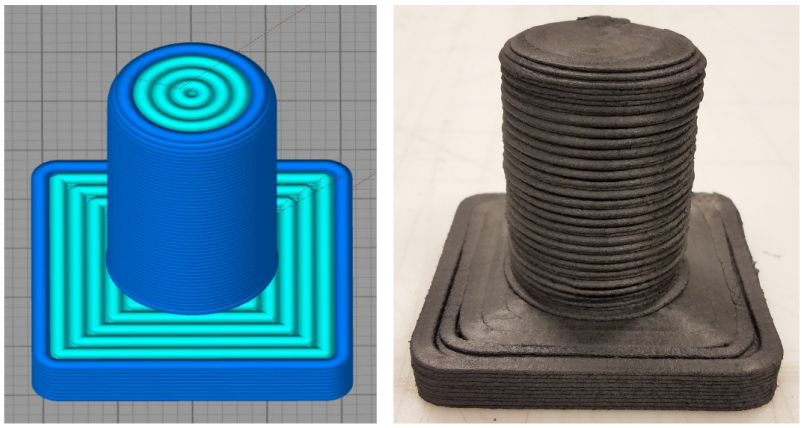

Figure 4.6. (a) Demolding test tool slicing image, and (b) the printed Demolding test tool.

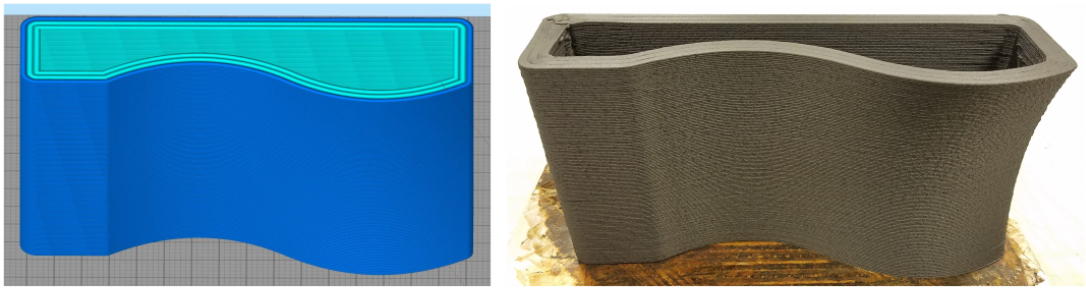

Figure 4.7. (a) Mold life experiment tool slicing image, and (b) the printed Tool life experiment mold.

4.2.2 Microstructure investigation of the printed material

To investigate the microstructure of the printed material, the printed part was cut, polished, and observed using a microscope. The microscopic image of the cross-sectional area of the bead showed the reinforced carbon fiber, PPS thermoplastic polymer matrix, inter-bead voids, and intra-bead voids. The fiber volume fraction and inter-bead void content of the bead were estimated using an image-based technique with the software, ImageJ. The threshold technique was used to calculate an area of fiber, matrix, and voids in the microscopic image as showed

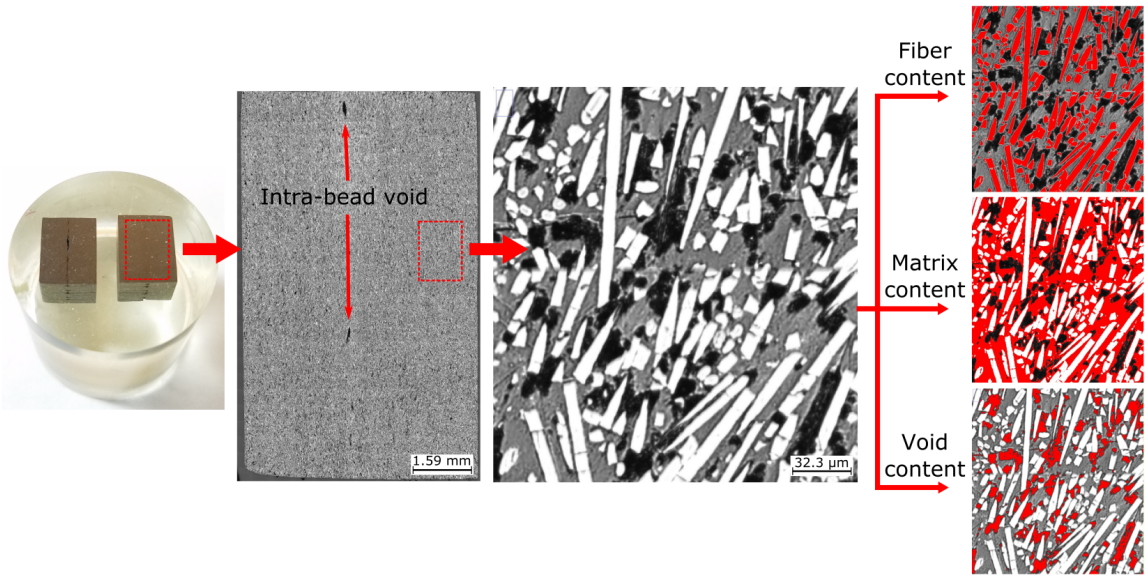

Figure 4.8. Microscopic image of cross-sectional area of the printed 2-bead wall, and the application of image threshold technique for calculating fiber, matrix, and void content in the material.

in Figure 4.8. The fiber volume fraction of the printed bead was estimated to be approximately 36%, and the inter-bead void of the printed bead was estimated to be approximately 15%. The fiber volume fraction and the void content which were measured using image threshold technique were highly dependent on the perspective of the user and polishing quality of the microscope sample. The size of the intra-bead void was larger than the size of the inter-bead void. The size and the number of intra-bead voids varied depending on the location of the bead in the part, that was affected by the compaction method and additive manufacturing process conditions. Figure 4.9 showed different amounts of intra-bead voids in different 2-bead wall test specimen.

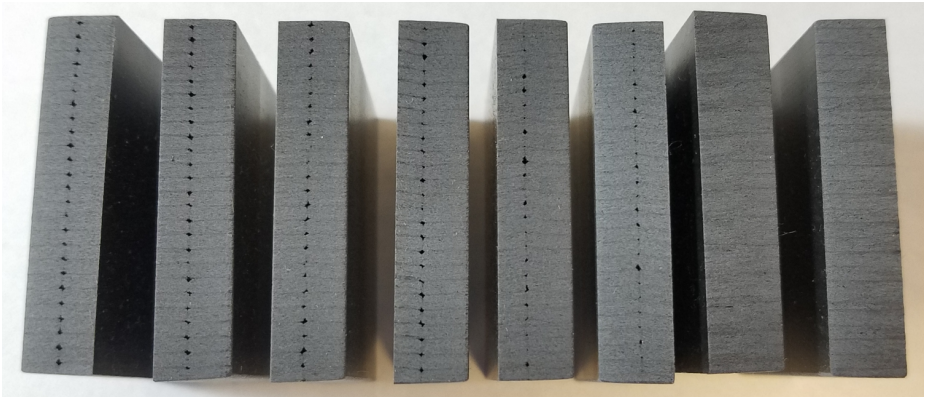

Figure 4.9. Different amounts of intra-bead voids in different 2-bead wall specimen.

4.2.3 Test specimen machining parameters

The annealed parts were machined using a 3-axis and a 5-axis computer numerical control (CNC) milling machine. To determine machining parameters suitable for the printed fiber reinforced polymer, such as revolution per minute (rpm) and feed rate of the milling tool that provided a high-quality surface finish of the part, different rpm and feed rates were tested. To find the optimal rpm and feed rate for machining, various surface feet per minute (SFM) and inch per tooth (IPT) values were used to machine the test specimen and their surface finish was investigated using a stereoscope and roughness tester. If there were surface defects caused by the machining process, such as fiber pullout, fiber breakage, or melted polymer on the surface, they could be observed in the stereoscopic image as showed in Figure 4.10. First, different SFM values, 250, 500, 1000, 1500, and 1963 were tested with a fixed 0.001 IPT. Figure 4.11 showed the stereoscopic images of the test specimen which were machined with various SFM and fixed 0.001 IPT. The stereoscopic image of the test specimen machined with 250 and 500 SFM did not show any distinctive surface defect. However, the stereoscopic image of test specimen machined with 1000, 1500, and 1963 SFM showed surface defects and the amount of surface defect increased as the machining SFM increased. Table 4.1 showed the average surface roughness and standard deviation of test specimen

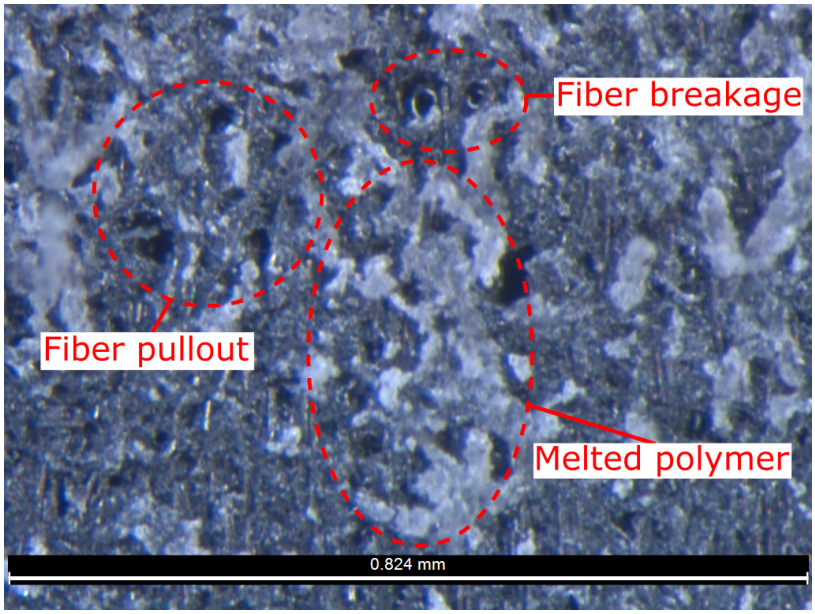

Figure 4.10. Stereoscopic image of the surface defects on the 3D printed composite (PPS with carbon fiber reinforcement) due to the machining process (9X magnified).

Table 4.1. *Average surface roughness and standard deviation of the test specimen machined with various SFM and fixed 0.001 IPT.*

	250 SFM	500 SFM	1000 SFM	1500 SFM	1963 SFM
Average Ra (μm)	0.73	0.76	1.01	2.00	2.96
Standard deviation	0.24	0.12	0.09	0.56	0.40

machined with various SFM and fixed 0.001 IPT. The surface roughness of the test specimen increased as the machining SFM increased. Based on the surface quality investigated using stereoscopic image and the surface roughness value, the author decided to use 500 SFM for the machining because the average surface roughness of the test specimens which were machined with 250 SFM and 500 SFM was similar, but 500 SFM provided a smaller standard deviation.

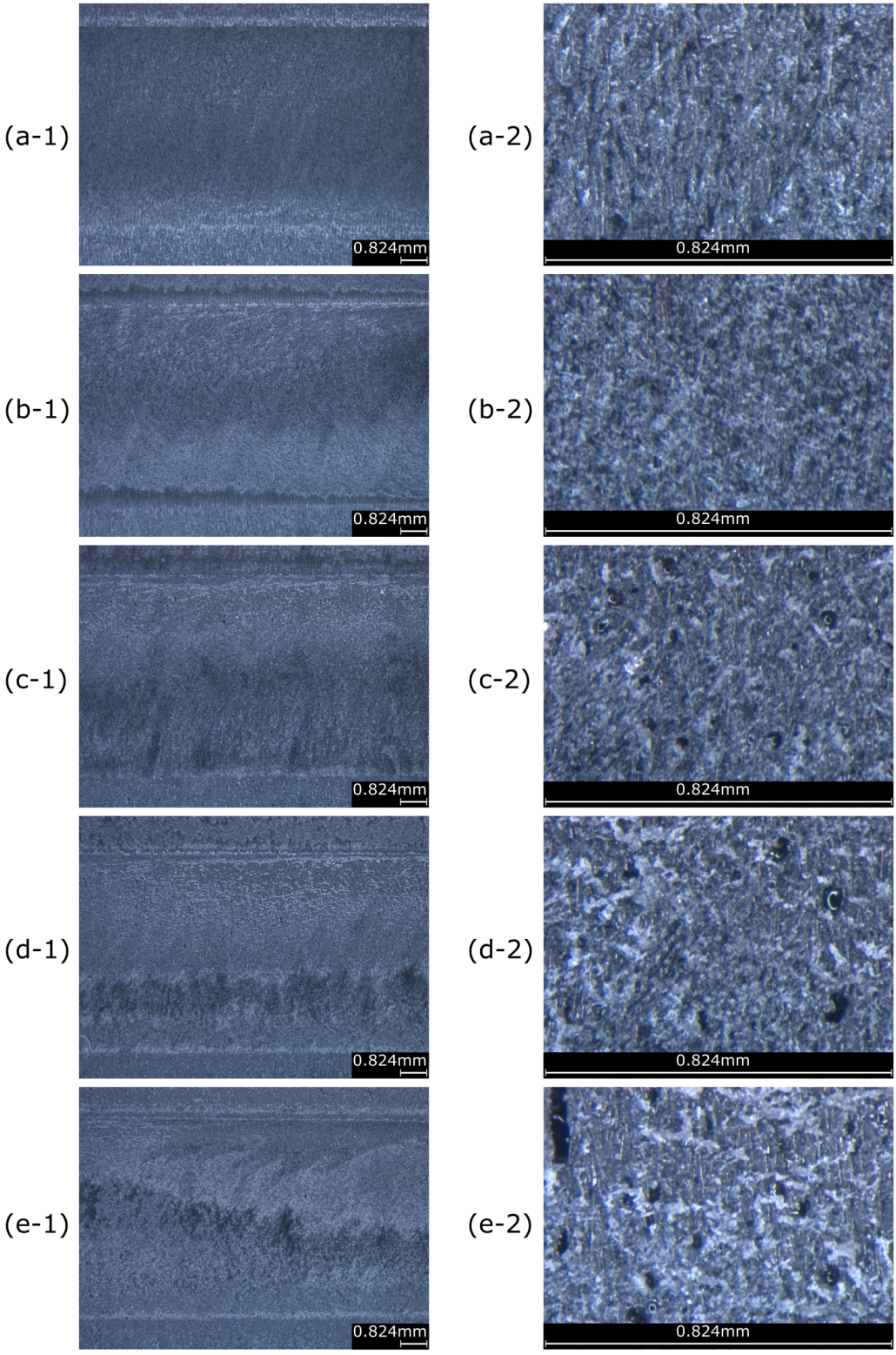

Figure 4.11. Stereoscopic images of the test specimens which were machined with (a) 250 SFM, (b) 500 SFM, (c) 1000 SFM, (d) 1500 SFM, and (e) 1963 SFM and fixed 0.001 IPT. The first column was 0.7X magnified image and the second column was 9X magnified image.

Table 4.2. *Average surface roughness and standard deviation of the test specimen machined with various IPT and fixed 500 SFM.*

	0.001 IPT	0.0025 IPT	0.005 IPT	0.0075 IPT	0.01 IPT
Average Ra (μm)	0.76	0.69	0.57	1.22	0.82
Standard deviation	0.12	0.11	0.17	0.12	0.16

Then, different IPT values, 0.001, 0.0025, 0.005, 0.0075, and 0.01 were tested with a fixed 500 SFM. Figure 4.12 showed the stereoscopic image of test specimens which were machined with various IPT and fixed 500 SFM. The stereoscopic image of the test specimen machined with a low IPT value, 0.001 and 0.0025, showed small amounts of melted polymer on the machined surface. Test specimen machined with a high IPT value, 0.0075 and 0.01 had surface voids due to fiber pullout and fiber breakage. Table 4.2 showed the average surface roughness and standard deviation of the test specimen machined with various IPT and fixed 500 SFM. The surface roughness of the test specimen decreased as the machining IPT increased until 500 IPT and the surface roughness increased for the test specimen machined with 0.0075 IPT and 0.01 IPT. Based on the surface quality investigated using stereoscopic image and surface roughness value, the author decided to use 0.005 IPT for the machining. For this research, all the printed parts were machined with 500 SFM and 0.005 IPT. In addition, compressed air was used to cool the milling tool and the test specimen during the machining process.

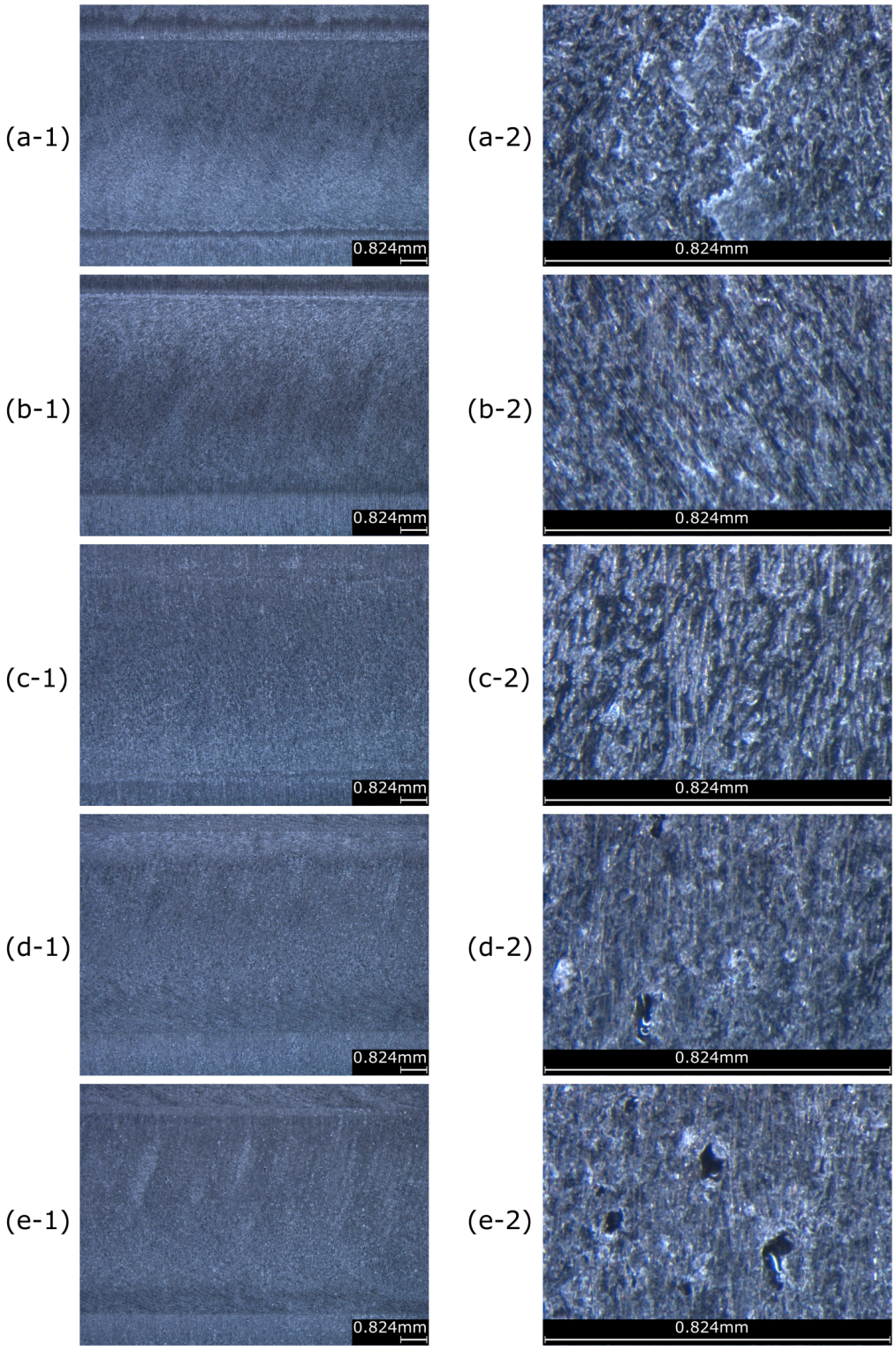

Figure 4.12. Stereoscopic images of the test specimens which were machined with (a) 0.001 IPT, (b) 0.0025 IPT, (c) 0.005 IPT, (d) 0.0075 IPT, and (e) 0.01 IPT and fixed 500 SFM. The first column was 0.7X magnified image and the second column was 9X magnified image.

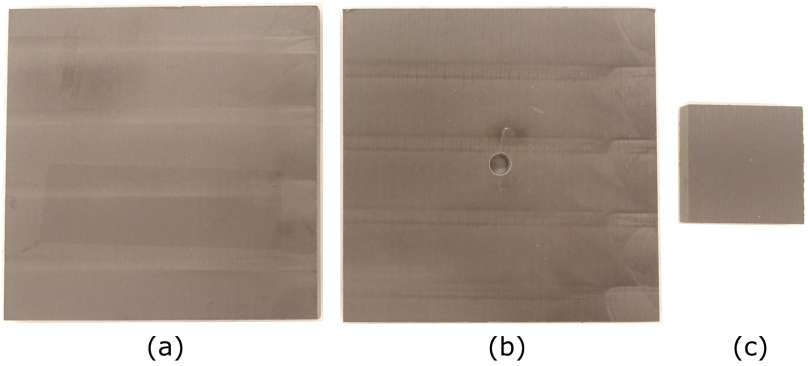

Figure 4.13. The machined (a) surface hardness/roughness test specimen, (b) surface abrasion resistance test specimen, and (c) coating adhesion test specimen.

4.2.4 2-bead wall machining

The annealed 2-bead wall was flattened with a planer to create one flat side, so that it could be fixed in the CNC milling machine for the machining operation. The planer removed about 2.54 mm from only one side of the wall. The cut panel was affixed in the CNC milling machine on top of vacuum pods. The top surface of the 2-bead wall was machined using a 50.8 mm diameter face mill cutter. 3.048 mm of the material was machined from the top surface. The face machining was divided into 3 levels to prevent that high loads were applied to the milling tool and the part during the machining process. The depth of cut for each level was 1.27 mm, 1.27 mm, and 0.508 mm. Then, the panel was flipped and 0.508 mm of the material on the other side was machined. The face machined 2-bead wall was cut into individual test specimen using the abrasive waterjet. The hardness, abrasion resistance, and roughness test specimens were cut into 101.6 mm x 101.6 mm coupons. The abrasion resistance test specimen had a 6.35 mm diameter hole in the middle of the test specimen to be able to fix it on the abrasion tester. The adhesion test specimen was cut into 38.1 mm x 38.1 mm coupons. The cut test specimens were cleaned using isopropyl alcohol and dried at 80°C for 2 hours. Figure 4.13 showed hardness, abrasion resistance, roughness, and adhesion test specimen cut from the 2-bead wall.

4.2.5 Demolding test tool machining

The annealed demolding test tool had a non-smooth side surface which made it difficult to be clamped using a vise in the CNC milling machine. Therefore, a square bottom section of the tool was drilled and fixed on an aluminum plate first. The aluminum plate was aligned and fixed in the CNC using the vacuum pod, and the contour of the bottom square section and top face of the cylindrical section were machined. A small pocket on the top surface was machined to make it easier to find the machining work offset (center of the pocket) for the next machining processes. The machining operations as showed in Figure 4.14(a)-(c) were performed when the tool was fixed on the aluminum plate. Since the bottom square section of the tool had a smooth surface now, it could be directly clamped to the vise in the CNC machine. The CNC touch probe was used to find a work offset by measuring the middle of the pocket made in the previous machining process. The rest of the surface was machined using profile contouring, spiral milling, pocketing, drilling, and isoparametric machining operations. The machining operations as showed in Figure 4.14(d)-(h) were performed when the tool was fixed on the vise. The tool was cleaned with isopropyl alcohol, dried, and inspected. An ejector plug was manufactured from aluminum 6061-T6. Figure 4.15 showed the machined demolding test tool.

4.2.6 Tool life experiment mold machining

After the mold life experiment tool was printed, the tool was not detached from the print bed plate and it was annealed with the print bed plate. The tool was fixed on a vacuum pod in the 5-axis CNC milling machine. The bottom and two sides of the tool were machined flat using a multi-axis sweeping operation as showed in Figure 4.16(a). Then, the tool was detached from the print bed plate and fixed in the 3-axis CNC milling machine using vacuum pods.

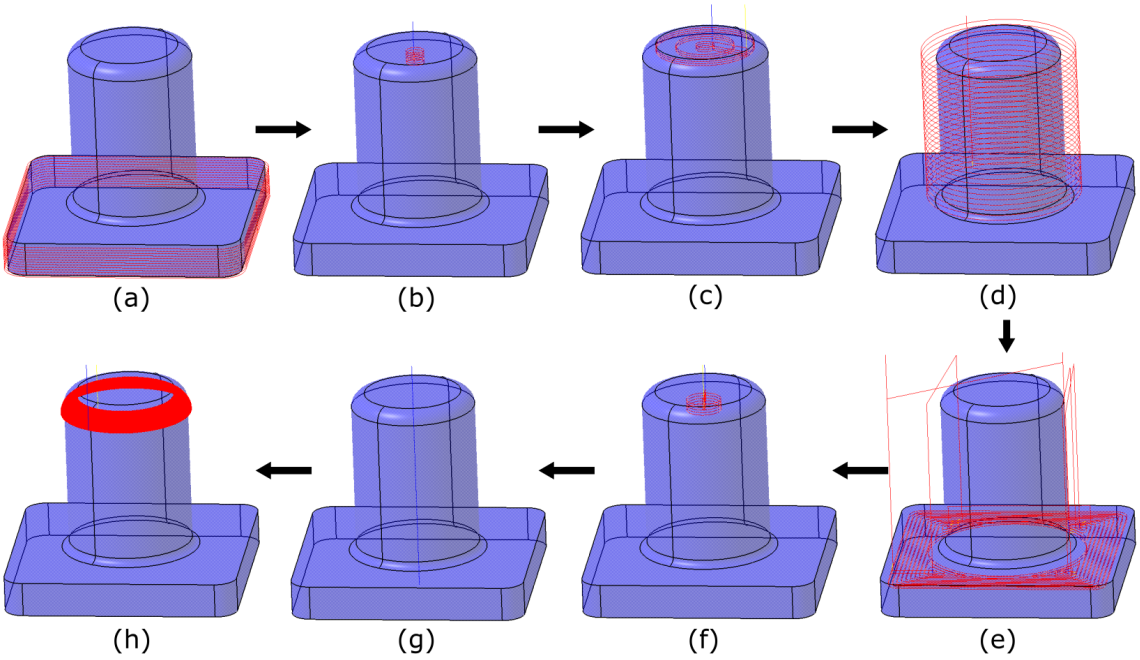

Figure 4.14. Machining process of the demolding test tool. (a) Profile contouring 1, (b) pocketing 1, (c) facing, (d) profile contouring 2, (e) spiral milling, (f) pocketing 2, (g) drilling, and (h) isoparametric machining operation.

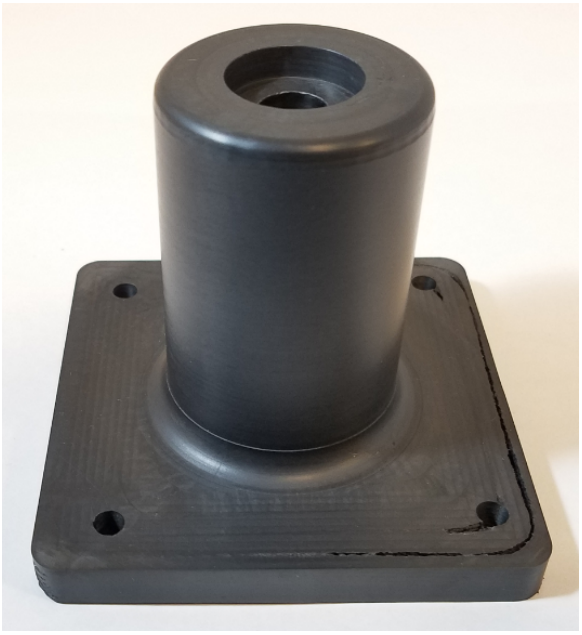

Figure 4.15. The machined demolding test tool.

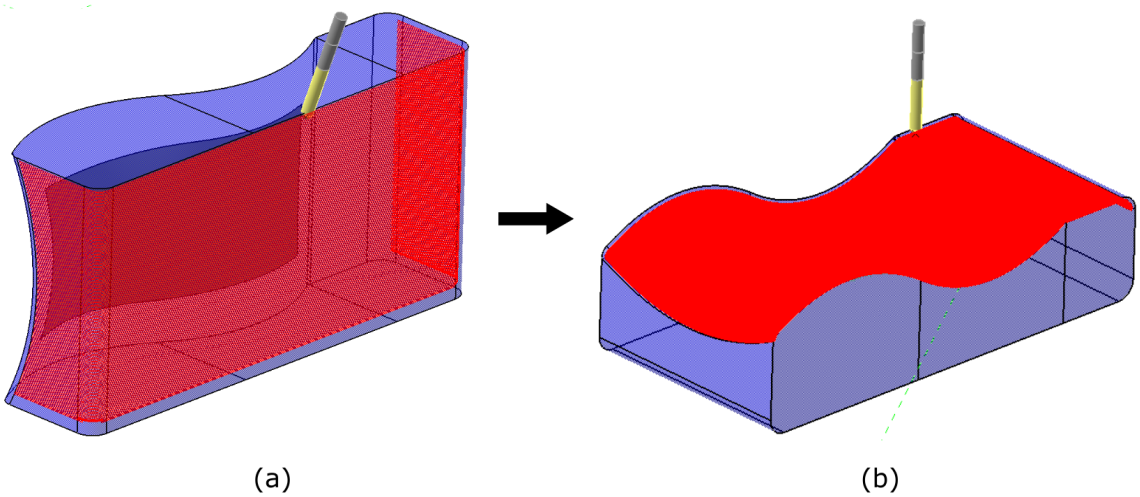

Figure 4.16. Machining process of the mold life experiment tool. (a) Bottom and the side of the tool machining using a 5-axis CNC milling machine. (b) Top surface machining using a 3-axis CNC milling machine.

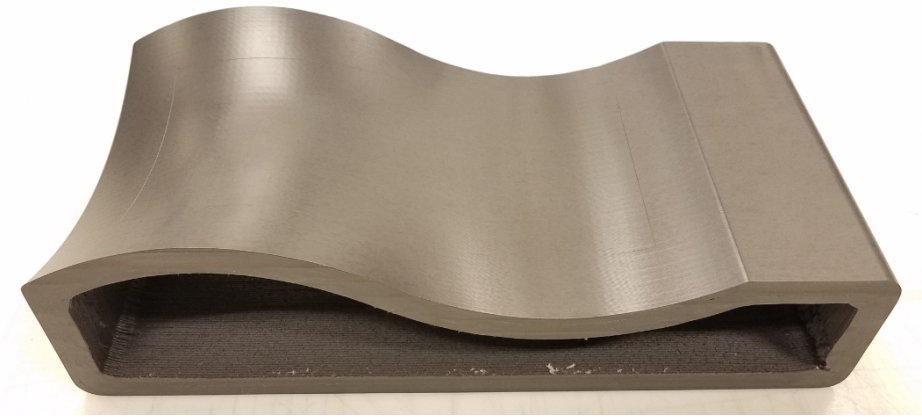

Figure 4.17. The machined mold life experiment tool.

The top surface was machined using a sweeping operation with a 9.525 mm diameter ball end mill and 0.00254 mm scallop height as showed in Figure 4.16(b). The part trim line was engraved using an engraving tool. The machined tool was cleaned with isopropyl alcohol, dried, and inspected. Figure 4.17 showed the machined mold life experiment tool.

4.3 Coating material thermal characterization

4.3.1 Differential calorimeter (DSC)

A commercially available thermoset polymer coating with ceramic particles was chosen as a candidate for the coating material in this research. To investigate the coating material was suitable to coating for additively manufactured carbon fiber reinforced PPS composite mold for composite part manufacturing, thermal characteristic of the coating material was studied. First, degree of cure of the coating material in coating curing temperature cycle was tested. According to the coating material manufacturer, the recommended cure temperature of the coating material was 148.89°C for 1 hour. However, the coating manufacturer reported that the coating material could be cured in 65.56°C - 82.22°C for 2 hours for the plastic substrate material which could not withstand the high coating application temperature. To investigate if the alternative cure cycle provided enough degree of cure of the coating material, the degree of cure of the coating material in the alternative cure temperature cycle was tested using DSC. The coating material and a catalyst were mixed in the specific ratio, and the mixed coating material was placed in a DSC test sample container. The DSC was set to run the following temperature cycle; (1) ramping up to 82.22°C with 3°C/min, (2) soaking to 82.22°C for 2 hours, and (3) ramping down to 30°C with 3°C/min. The heat flow from the coating material during the alternative cure cycle showed that most of the curing was accomplished during the first hour of the soaking period, and the coating material seemed fully cured in two hours as showed in Figure 4.18. Therefore, it was verified that the coating material could be cured fully on the mold at 82.22°C, which was lower than the maximum allowable temperature of the substrate material, range of 83.17°C - 95.99°C that was estimated in the previous section.

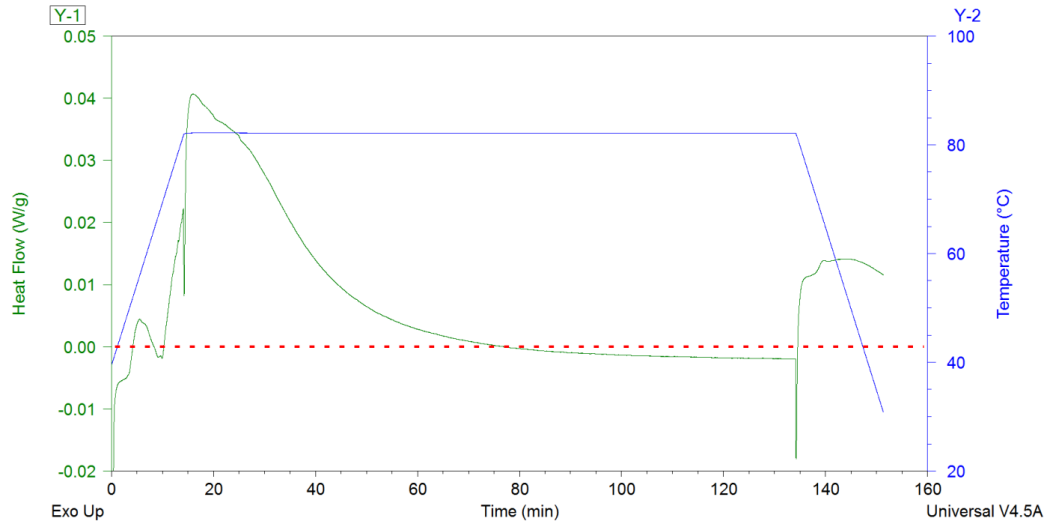

Figure 4.18. DSC thermal analysis result of the uncured coating material; heat flow from the coating material during the alternative coating cure cycle.

4.3.2 Thermal degradation analysis using thermogravimetric analysis (TGA)

Not only the coating curing temperature, but also the coating operable temperature was investigated. The coating manufacturer reported that the coating material could be stable up to 260°C. To verify that the coating material could withstand the temperature cycle during the composite part curing process, the thermal degradation of the coating material was tested using a TGA. A piece of coating material was inserted in the TGA and weighted. The composite part curing temperature cycle, which was used in this research; (1) ramping up to 2.78°C/min to 180°C, (2) soaking at 180°C for 2 hours, and (3) ramping down to 20°C with 2.78°C/min was applied to the coating material in the TGA. The TGA measured a weight change of the coating material during the temperature cycle. Figure 4.19 showed the TGA result of the coating material during the one temperature cycle. The TGA result showed an irregular weight loss at the beginning stage of the temperature cycle. The irregular weight change in the beginning of the temperature cycle could be attributed by the sample repositioning inside of the TGA or the moisture evaporating in the sample. Therefore, the weight loss of the coating

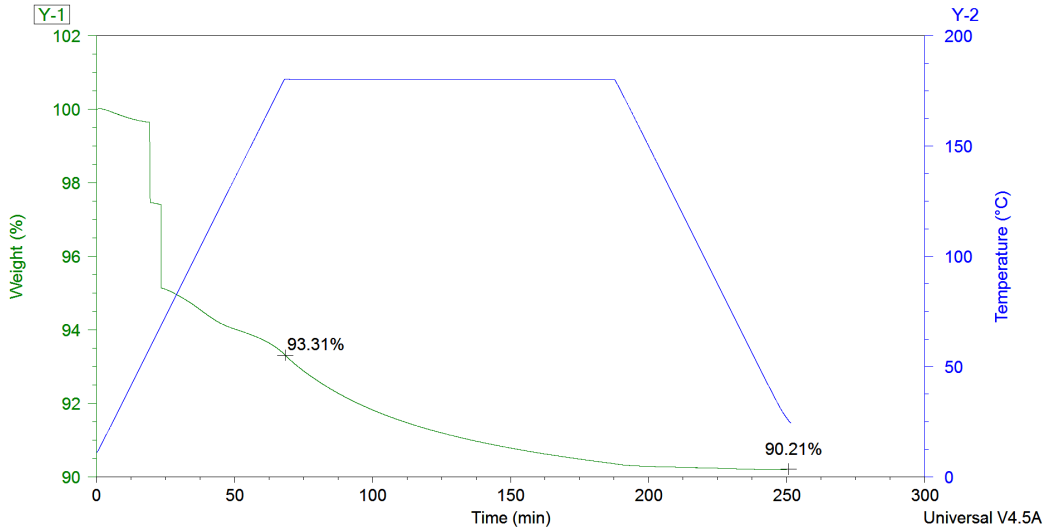

Figure 4.19. TGA thermal degradation analysis; weight change of the coating material during the composite cure temperature cycle.

material was calculated from when the weight change got stable, from when the temperature reached 180°C. The result showed that the coating material had a 3.1% of weight loss (93.31% - 90.21%) during the composite part curing temperature cycle. Not only thermal degradation of the coating material during one temperature cycle, but also during repeated temperature cycles were investigated. Thermal degradation of the coating material in a three-repeated temperature cycle was tested. Each temperature cycle was the same as the one temperature cycle from the previous test. Figure 4.20 showed the TGA result of the coating material during the three repeated temperature cycles. The weight loss in the first cycle was a 2.8% (97.54% - 94.74%), the weight loss in the second cycle was a 0.7% (94.74% - 94.04%), and the weight loss in the third cycle was a 0.39% (94.04% - 93.65%). It was showed that the thermal degradation, weight loss, of the coating material in the composite part manufacturing temperature cycle, which was used in this research, was only 3% and it got closer to 0 in the repeated cycle. Since the coating curing temperature and the operable temperature of the coating material met the requirements for this research, the author decided to use this coating material for this study.

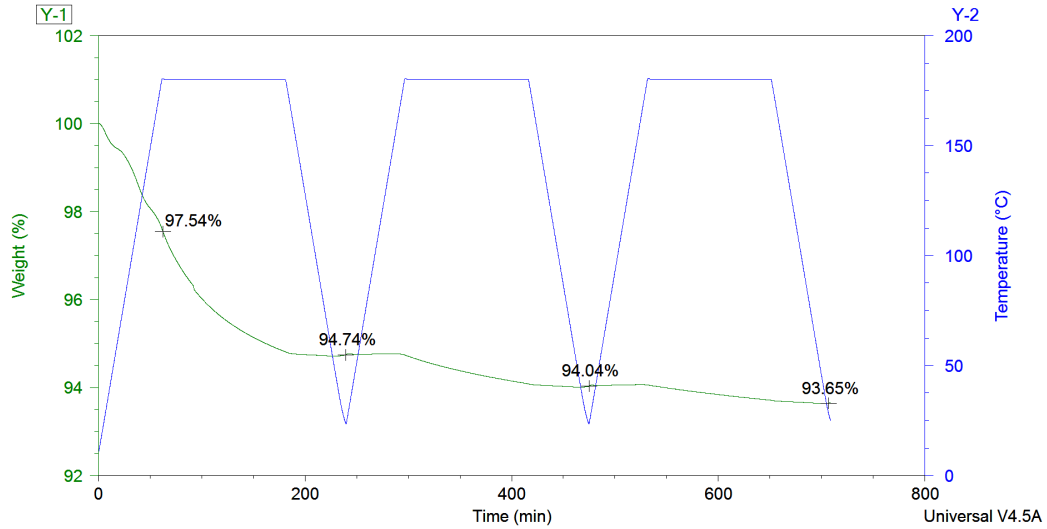

Figure 4.20. TGA thermal degradation analysis; weight change of the coating material during the 3 times repeated composite cure temperature cycle.

4.4 Coating application

The coating application process was performed in accordance with the coating application guide provided by the coating material manufacturer. The machined part was cleaned with isopropyl alcohol and dried at 80°C for 2 hours. The surface of the part was visually inspected to make sure there was no evidence of any oil or solvent. The coating material was mixed with a catalyst thoroughly in the specific ratio in accordance with the coating application guide. The mixed coating material was sprayed on the part surface using a high-volume, low-pressure (HVLP) spray gun. Two even coats of the coating material were applied on the part and it was cured in the oven at 82°C for 2 hours. The coating quality was investigated visually and using a stereoscope as showed in Figure 4.21. The cross-sectional area of the coated test specimen was observed using a microscope to check the bonding quality between the coating and the substrate as showed in Figure 4.22. There was no evidence of debonding between the coating and the substrate. The thickness of the coating was approximately 10 μm.

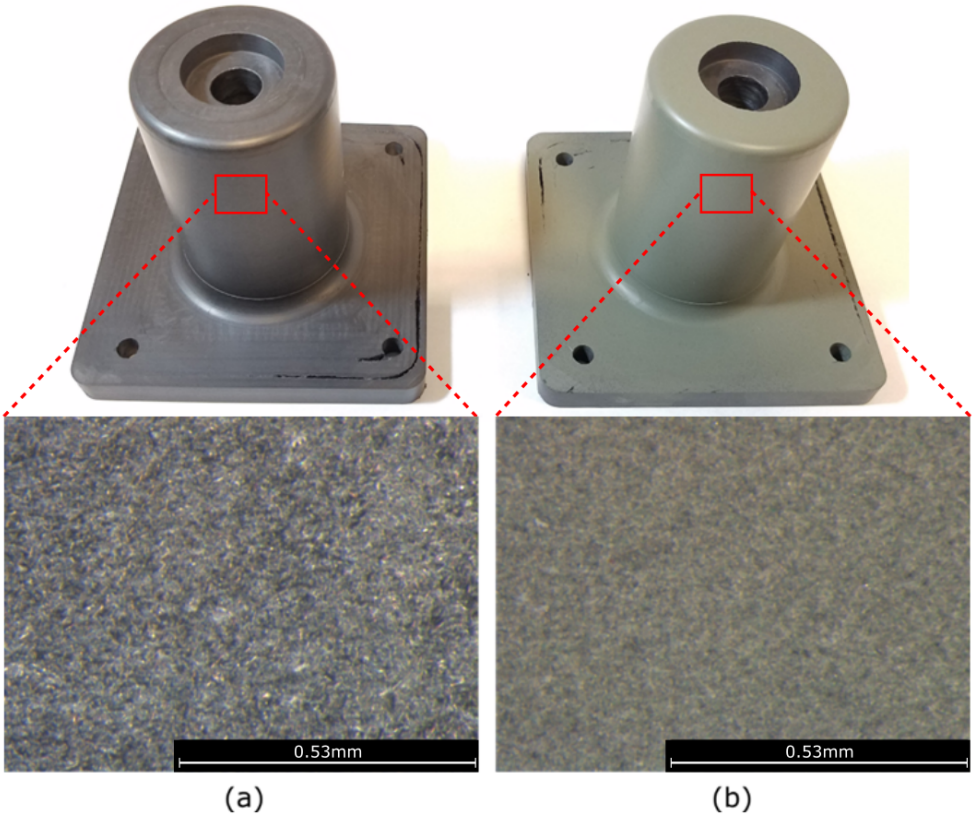

Figure 4.21. Stereoscopic image of the (a) non-coated and (b) coated test specimen.

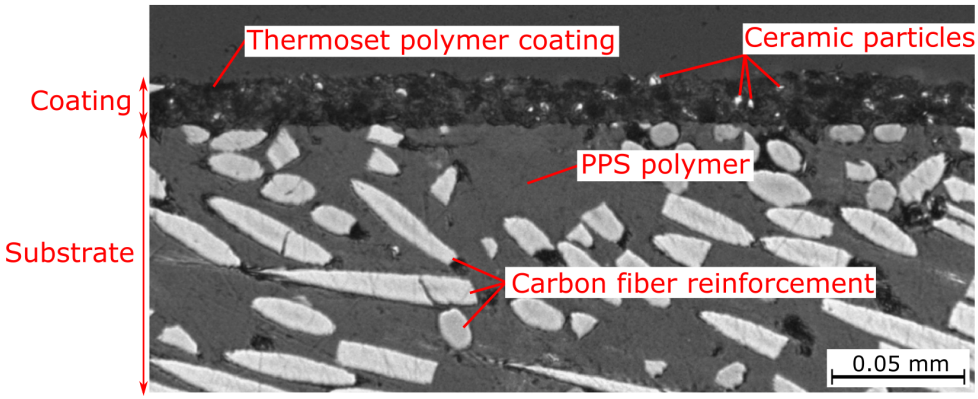

Figure 4.22. Microscopic image of cross-sectional area of the coating applied on the substrate.

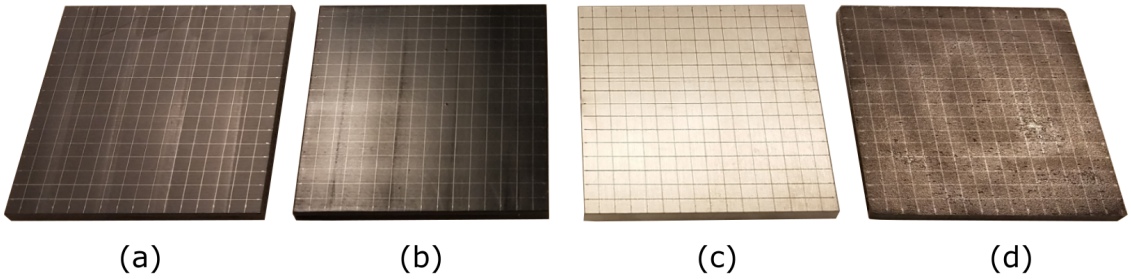

Figure 4.23. The hardness test specimen; (a) non-coated composite, (b) coated composite, (c) aluminum 6061-T6, (d) 1020 steel.

4.5 Surface property testing

4.5.1 Surface hardness test

The hardness test was performed on two non-coated composite, two coated composite, one aluminum 6061-T6, and one 1020 hot rolled steel test specimens. The grid with a 6.35 mm gap between lines was made as a guide for the hardness measurement. Using this grid, it was made sure that none of the hardness measurements was tested within 3.175 mm from other measurements or the edge of the test specimen in accordance with ASTM D2583-13a. Figure 4.23 showed the hardness test specimen with the grid lines. 50 Barcol hardness measurements were collected from each test specimen. Table 4.3 showed the average Barcol hardness of each test specimen group and standard deviation. Figure 4.24 showed a bar graph of the average Barcol hardness of each test specimen group with a standard deviation bar.

The average Barcol hardness of the coated composite specimen was 23.38% lower than the non-coated composite test specimen. A statistical hypothesis test, two sample t-test, with a 0.05 significance level was performed under the following hypothesis;

$$H_0 : \mu_n = \mu_c \qquad H_a : \mu_n < \mu_c \tag{4.1}$$

Table 4.3. *Average Barcol hardness and standard deviation of each test specimen.*

	Number of measurement	Average Barcol hardness	Standard deviation
Non-coated	100	22.67	2.30
Coated	100	17.37	2.35
Aluminum 6061-T6	50	79.80	0.49
1020 steel	50	89.62	0.75

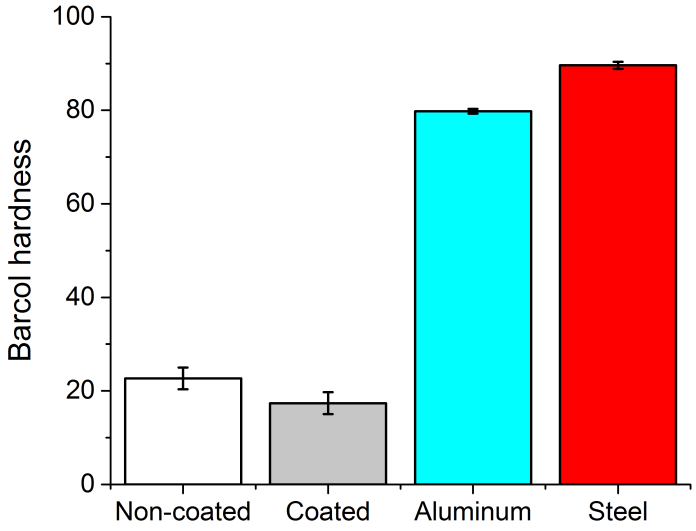

Figure 4.24. Bar graph of average Barcol hardness with a standard deviation bar for each test specimen.

where μ_n and μ_c represented the average surface hardness level of the non-coated and coated composite respectively. The two-sample t-test result reported that it failed to reject the H_0 because the p-value was greater than the significance level, 0.05 (p-value=1). Therefore, the t-test concluded that hardness of the coated test specimen (M=17.37, SD=2.35) was not significantly higher than hardness of non-coated test specimen (M=22.67, SD=2.30); $t(198) = 16.13$, p-value=1. The average Barcol hardness of the aluminum and steel test specimen was much higher than the composite test specimen.

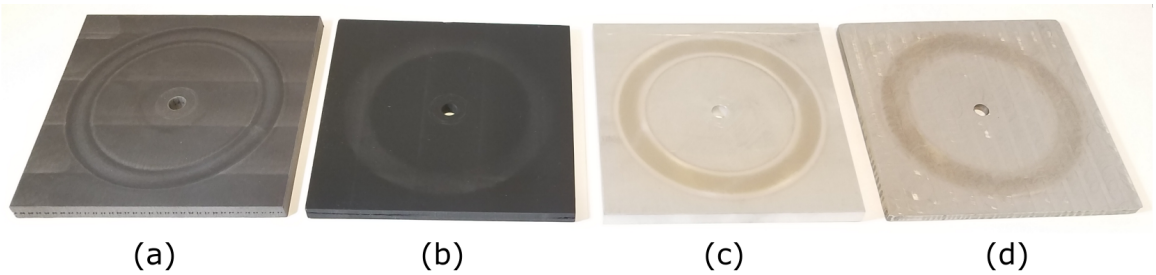

Figure 4.25. The surface abrasion resistance test specimen after 2000 abrasion cycles; (a) non-coated composite, (b) coated composite, (c) aluminum, and (d) steel test specimen.

4.5.2 Surface abrasion resistance test

The abrasion resistance test was performed on one of each non-coated and coated composite, aluminum 6061-T6, and 1020 hot rolled steel test specimens. The initial weight of each test specimen was measured and the test specimen was installed on the Taber abrasion tester. The abrasion test was performed with two CS-10 Calibrase resilient wheels, and 500 g of load was applied to each wheel. The Calibrase wheels were resurfaced using S-11 refacing disc every 1000 abrasion cycle and before testing the next test specimen. Each abrasion resistance test specimen was abraded 2000 cycle total. Figure 4.25 showed the test specimen after 2000 cycle abrasion test. After every 200 abrasion cycles, the test specimen was lightly brushed to remove abraded particles on the test specimen surface, and the weight of the test specimen was measured. In total, 11 weight measurements for each test specimen, including its initial weight, were collected and 10 wear index values were calculated by finding a weight difference between before and after every 200 abrasion cycle. Table 4.4 showed the average wear index and standard deviation of each test specimen. Figure 4.26(a) showed the weight change of each test specimen for every 200 abrasion cycles during the abrasion resistance test, and Figure 4.26(b) showed a bar graph of the average wear index of each test specimen with a standard deviation bar.

Table 4.4. *Average wear index and standard deviation of each test specimen.*

	Number of measurement	Average wear index	Standard deviation
Non-coated	10	23.5	3.37
Coated	10	2.5	2.64
Aluminum 6061-T6	10	7.5	3.54
1020 steel	10	7.0	2.58

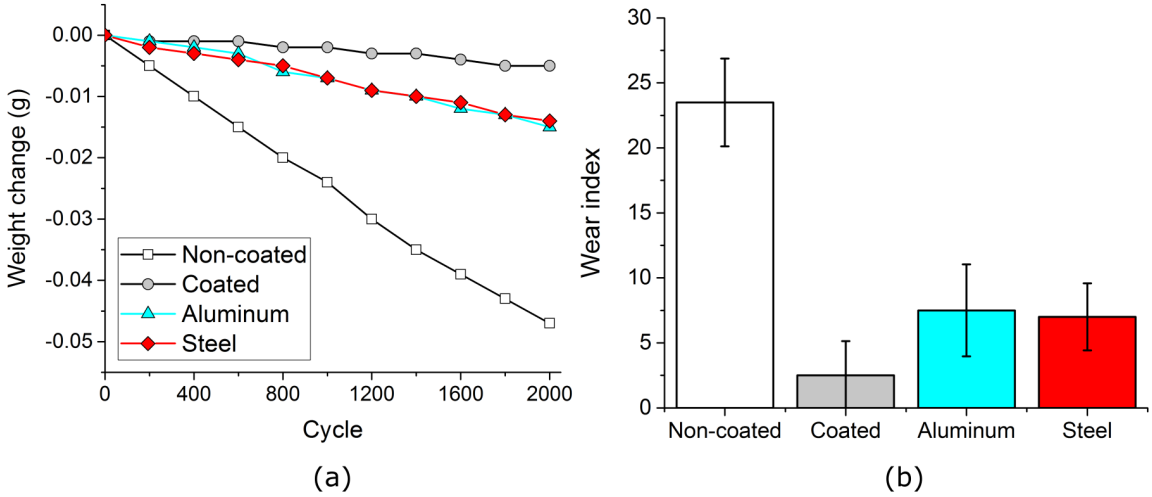

Figure 4.26. (a) The weight change of each test specimen for every 200 abrasion cycles during the abrasion resistance test. (b) The bar graph of the average wear index of each test specimen with a standard deviation bar.

The test results showed that the weight change of all test specimens had a linearly decreasing pattern. The results showed that the average wear index of the coated composite test specimen was 89.36% lower than the non-coated composite test specimen. Also, the average wear index of the coated composite test specimen was even lower than the average wear index of aluminum and steel test specimen. A statistical hypothesis test, two sample t-test, with a 0.05 significance level was performed under the following hypothesis;

$$H_0 : \mu_n = \mu_c \qquad H_a : \mu_n > \mu_c \tag{4.2}$$

where μ_n and μ_c represented the average wear index of the non-coated and coated composite respectively. The two-sample t-test result reported that it rejected its H_0 because the p-value was smaller than the significance level, 0.05 (p-value=$3.68064e^{-12}$). Therefore, the t-test concluded that wear index of the coated test specimen ($M = 2.5$, $SD = 2.64$) was significantly lower than wear index of the non-coated test specimen ($M = 23.5$, $SD = 3.37$); $t(18) = 15.51$, p-value=$3.68064e^{-12}$. A two sample t-test with a significance level of 0.05 was also reported that the wear index of the coated composite test specimen was significantly lower than wear index of the aluminum 6061-T6 test specimen ($M = 7.5$, $SD = 3.54$); $t(18) = 3.59$, p-value=0.00106, and 1020 steel test specimen ($M = 7.0$, $SD = 2.58$); $t(18) = 3.86$, p-value=$5.77294e^{-4}$.

4.5.3 Surface roughness test

The surface roughness test was performed on two of each non-coated and coated composite test specimens. Figure 4.27 showed the non-coated and coated composite surface roughness test specimen. From each test specimen, 20 surface roughness values, arithmetical mean roughness value (R_a), were measured. The roughness tester was set to have a cutoff length of 2.5 mm and an evaluation length of 12.5mm in accordance with ASTM D7127-17 (ASTM International, 2018). Table 4.5 showed average R_a and standard deviation of the non-coated and coated composite test specimen. The roughness test results showed that the coated composite test specimen had a 4.93% higher average R_a than the non-coated composite test specimen. Figure 4.28 showed a bar graph of the average R_a of the non-coated and coated test specimen with a standard deviation bar. A statistical hypothesis test, two sample t-test, with a 0.05 significance level was performed under the following hypothesis;

$$H_0 : \mu_n = \mu_c \qquad H_a : \mu_n > \mu_c \tag{4.3}$$

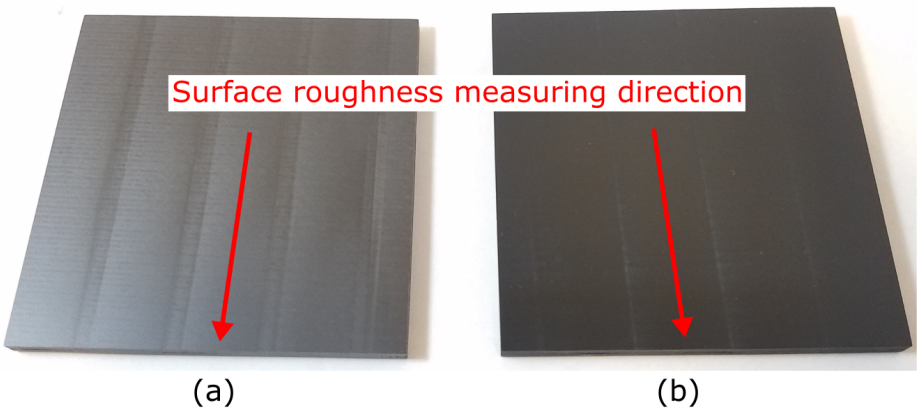

Figure 4.27. (a) Non-coated and (b) coated composite surface roughness test specimen.

Table 4.5. *Average R_a and standard deviation of the non-coated and coated composite test specimen.*

	Number of measurement	Average Ra (μm)	Standard deviation
Non-coated	40	0.90	0.20
Coated	40	0.95	0.11

where μ_n and μ_c were the average surface roughness level of the non-coated and coated composite respectively. The two sample t-test result reported that it failed to reject the H_0 because the p-value was greater than the significance level, 0.05 (p-value=0.89277). Therefore, the t-test concluded that surface roughness (R_a) of the coated test specimen ($M = 0.95$, $SD = 0.11$) was not significantly lower than surface roughness (R_a) of the non-coated test specimen ($M = 0.90$, $SD = 0.20$); $t(78) = -1.25$, p-value=0.89277.

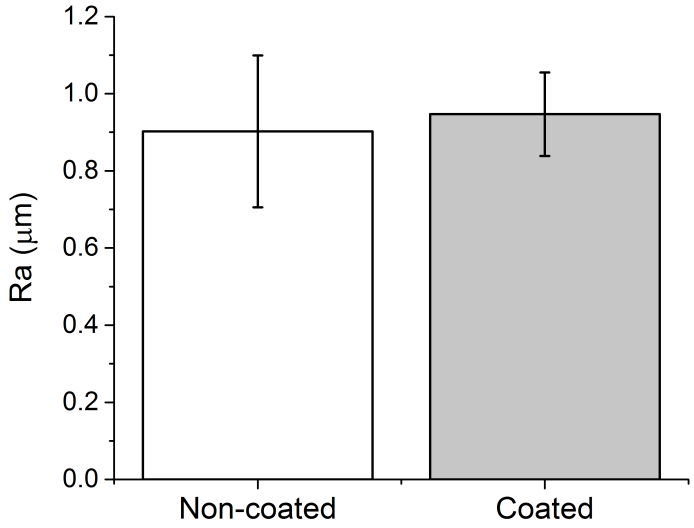

Figure 4.28. Bar graph of the average R_a of the non-coated and coated composite test specimen with a standard deviation bar.

4.5.4 Demolding test

The author prepared one non-coated and one coated demolding test tool. After the coating was applied, the surface of the non-coated tool, coated tool, and the ejector plugs were cleaned and prepared with mold sealer and mold release. Two coats of mold sealer, 15 sealer EZ, and five coats of mold release, Chemlease R&B mold release, were applied in accordance with the instructions from the mold sealer and release manufacturer. The designed plies were cut with an automatic cutting table. In this study, a plain-weave fiberglass reinforced composite prepreg was used as a layup material. Before the first ply was laid up on the tool, a piece of release film was placed on the top of the tool to prevent resin smeared inside of the gap between the tool and the ejector plug as showed in Figure 4.29(a). The ply layup orientation was $[0/90/30/60]_2$ which allowed to cover all surfaces even the designed ply had darts as showed in Figure 4.29(b) and 4.29(c). An additional 8 circular plies were laid up on the top of the tool to reinforce the top part to prevent it from bending while the part was pushed by the ejector pin during the demolding process as showed in Figure 4.29(d).

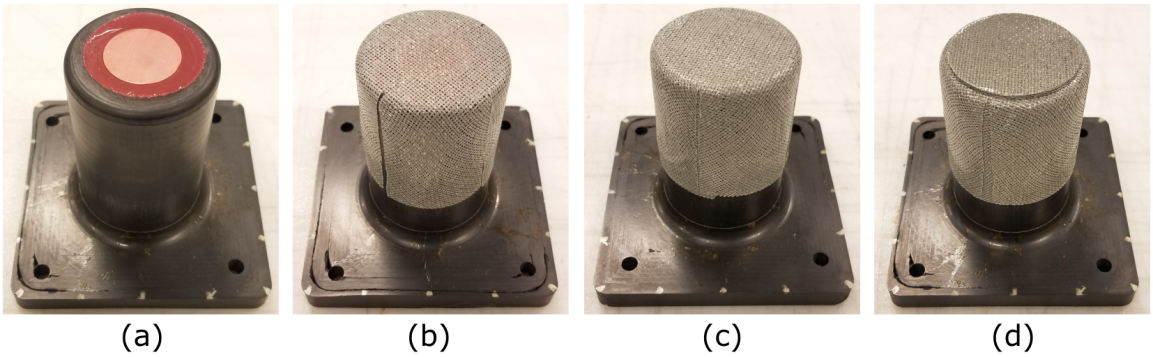

Figure 4.29. The composite prepreg ply layup process for the demolding test. (a) before 1st ply layup, (b) after 1st ply layup, (c) after 8th ply layup, and (d) after additional eight circle plies layup.

After the plies were laid up on the tool, it was bagged and cured using an autoclave using the cure cycle that had a 2-hour soak at 180°C with 586 kPa of pressure as showed in Figure 3.22. After the composite part was cured, the tool was taken out from the vacuum bag and installed in an MTS universal testing system to perform the demolding test. The tool was flipped upside down and placed on the 88.9 mm diameter aluminum support cylindrical tube, and an ejector pin was inserted from the bottom of the tool. Figure 4.30 showed a schematic drawing of the demolding test settings and the demolding test setting in the MTS universal testing system. The MTS testing system was set to compression test with a displacement change of 2 mm/min and 10 displacement and load data were recorded per second. The demolding test was completed and stopped When the composite part was fully demolded from the tool. The load and displacement data were exported and analyzed. The surface of the tool was inspected, and its surface roughness was measured. Two additional coats of mold release, Chemlease R&B mold release, were applied before the next production cycle.

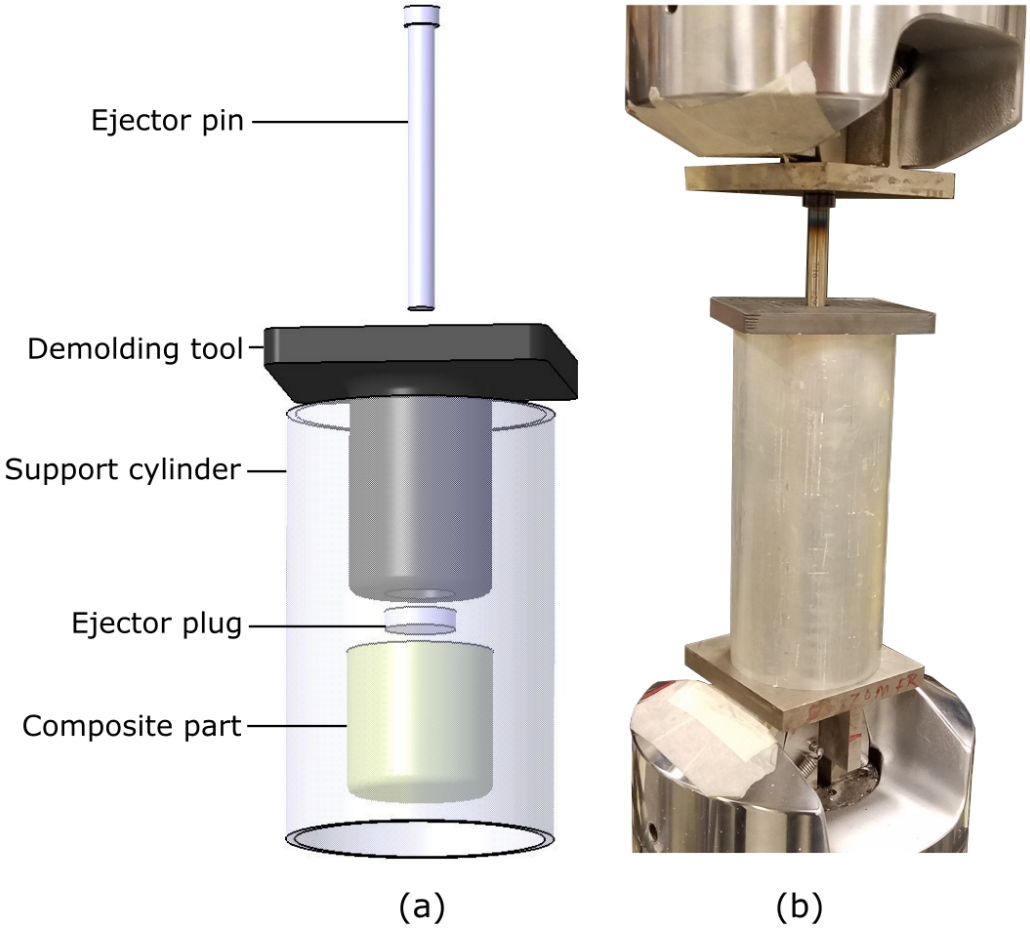

Figure 4.30. (a) Schematic drawing of the demolding test setting and (b) the demolding test setting in the MTS system.

A load versus displacement plot was made for each test and interpreted. The load initially increased linearly until it reached the peak load. Then, the load suddenly dropped to a certain point, and decreased gradually to 0 as showed in Figure 4.31. The load versus displacement data of the demolding test was interpreted and analyzed using the theory of surface friction (Worgull, Heckele, Hétu, & Kabanemi, 2006). Under the theory of surface friction, the plot could be divided into two regions; static region, and kinetic region as showed in Figure 4.32.

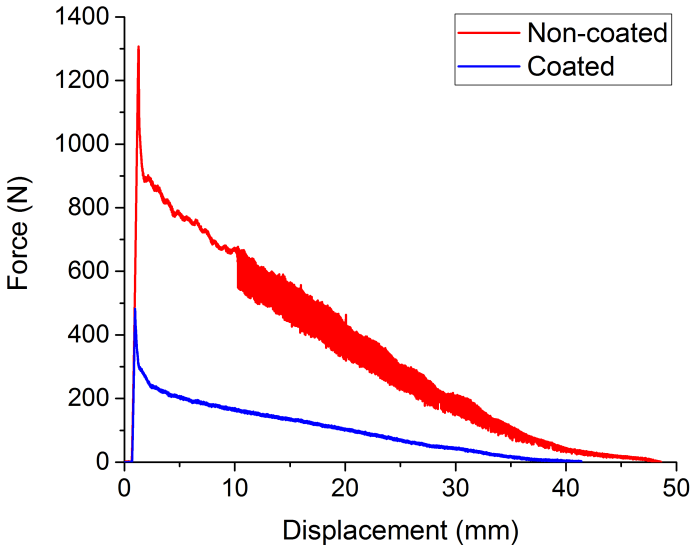

Figure 4.31. Load versus displacement plot of the non-coated and coated tool during the demolding test (cycle 1).

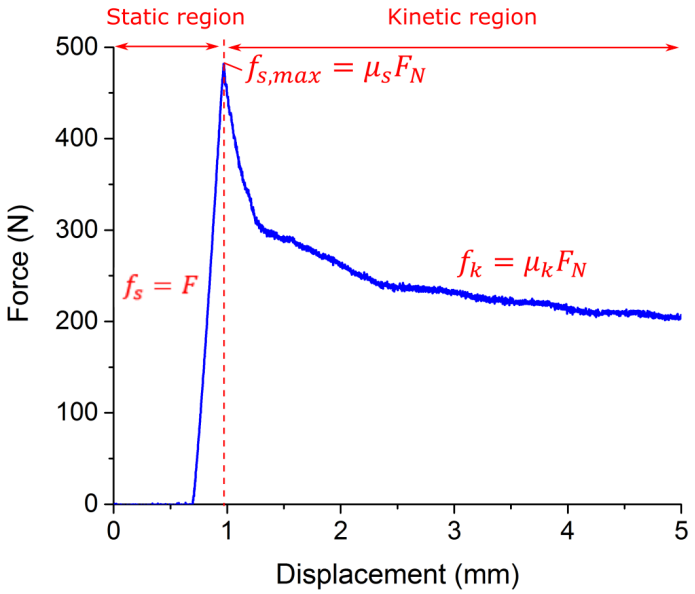

Figure 4.32. Static and kinetic region in the load versus displacement plot of the demolding test data (coated tool, cycle 1).

In the static region, the demolding force was applied to part, but the part did not start to be demolded from the tool yet. Therefore, the friction force in the static region was the same as the force applied to the part.

$$f_s = F \tag{4.4}$$

where f_s was a friction force in the static region and F was the force applied to the part. The force continued increasing until it reached to the maximum static friction force, $f_{s,max}$. The maximum static friction force could be described with the law of friction using the following equation;

$$f_{s,max} = \mu_s F_N \tag{4.5}$$

where μ_s was a static friction coefficient, and F_N was a normal force applied to the part. The normal force resulted from the difference in coefficient of thermal expansion (CTE) between the tool and the part cured on the surface on the tool. In this study, the CTE of the part which made with glass fiber reinforced composite was relatively larger than the CTE of the carbon fiber reinforced PPS composite, thereby giving rise to compressive normal stresses at the surface of the tool when the tool and the part were cooled. In other words, the part was trying to shrink more than the tool upon cooling. After the maximum static friction force was reached, the force-displacement behavior transited from being controlled by the static friction to being controlled by the kinetic friction developed between the tool and the part. The kinetic friction force could be described with the law of friction using the following equation;

$$f_k = \mu_k F_N \tag{4.6}$$

where f_k was a kinetic friction force and μ_k was a kinetic coefficient of friction. The demolding force versus displacement plot showed that the demolding force of the non-coated tool after about 10 mm displacement had a severe load

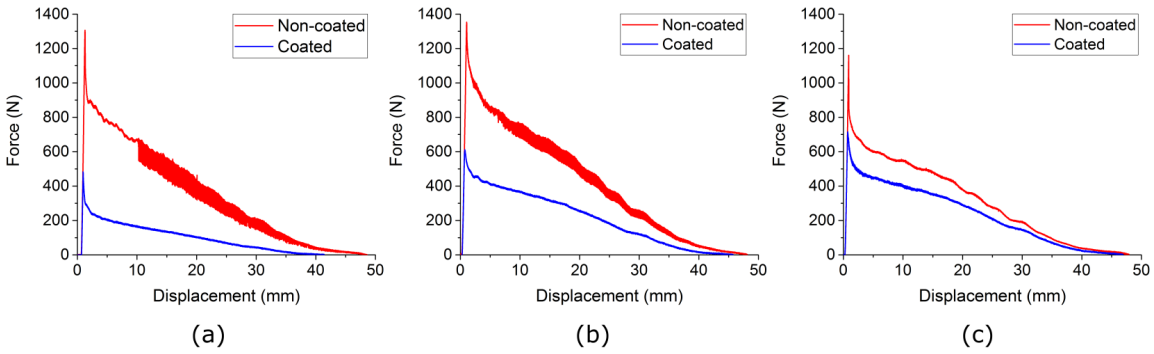

Figure 4.33. Load versus displacement plot of the non-coated and coated tool during (a) 1st, (b) 5th, and (c) 10th demolding test.

fluctuation. The load fluctuation lasted until the part was fully demolded from the tool. The amplification of the load fluctuations got smaller as the displacement increased. Throughout the production cycles, the load fluctuations of the non-coated tool had decreased as showed in Figure 4.33. The load fluctuation observed in this study during the demolding test could be described with the stick-slip phenomenon that described series of jerks motion caused by alternating sticking due to the surface friction and sliding when the applied force overcame the surface friction (Davim, 2012).

$f_{s,max}$ was the maximum static friction force applied to the part during the demolding process. $f_{s,max}$ was important value because high $f_{s,max}$ could lead to damaging either the mold or the part during the part demolding process (Omar et al., 2014). Therefore, $f_{s,max}$ of the non-coated tool ($f_{sn,max}$) and the coated tool ($f_{sc,max}$) was measured during their 10 production cycles. Figure 4.34(a) showed $f_{s,max}$ of the non-coated and coated tool over the number of production cycle. The results showed that $f_{sc,max}$ was lower than $f_{sn,max}$ during all 10 production cycles. Table 4.6 showed average $f_{sn,max}$ and $f_{sc,max}$ for the 10 production cycles and standard deviation. Figure 4.35 showed bar graph of the average of $f_{sn,max}$ and $f_{sc,max}$ during the 10 production cycles with a standard deviation bar.

Table 4.6. *Average $f_{sn,max}$ and $f_{sc,max}$ for the 10 production cycles and standard deviation.*

	Number of measurement	Average $f_{s,max}$ (N)	Standard deviation
Non-coated	10	1311	194
Coated	10	613	123

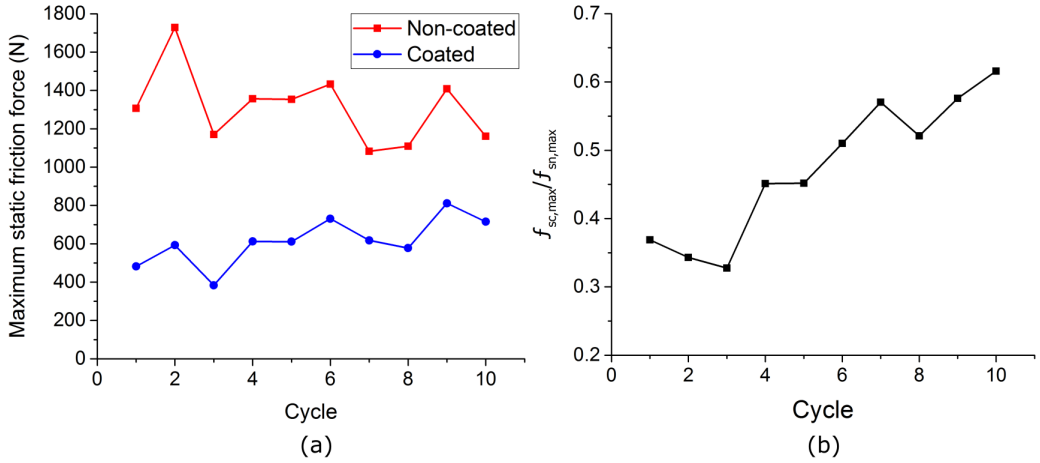

Figure 4.34. (a) Maximum static friction force, $f_{s,max}$, of the non-coated and the coated tool during the 10 cycles of demolding test. (b) Ratio of $f_{sc,max}$ to $f_{sn,max}$ ($f_{sc,max}/f_{sn,max}$) throughout the 10 production cycles.

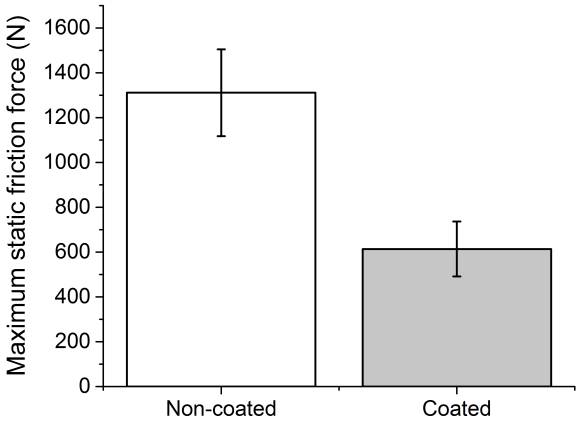

Figure 4.35. Bar graph of the average $f_{sn,max}$ and $f_{sc,max}$ with a standard deviation bar.

The average of $f_{sc,max}$ for the 10 production cycles was approximately 53.21% lower than the average of $f_{sn,max}$ for the 10 production cycles. A statistical hypothesis test, two sample t-test, with a 0.05 significance level was performed under the following hypothesis;

$$H_0 : \mu_n = \mu_c \qquad H_a : \mu_n > \mu_c \tag{4.7}$$

where μ_n and μ_c were the average $f_{sn,max}$ and $f_{sc,max}$ respectively. The two sample t-test result reported that it rejected its H_0 because the p-value was smaller than the significance level, 0.05 (p-value=$8.07298e^{-9}$). Therefore, the t-test concluded that maximum static friction force of the coated tool ($f_{sc,max}$)($M = 613.45$, $SD = 122.61$) was significantly lower than maximum static friction force of the non-coated tool ($f_{sn,max}$)($M = 1311.01$, $SD = 193.75$); $t(18) = 9.62$, p-value=$8.07298e^{-9}$. Also, a Pearson correlation test, with a 0.05 significance level was performed between the $f_{s,max}$ and the number of production cycle for the non-coated and coated tool to investigate how $f_{s,max}$ changed corresponding to the number of the production cycle using the following hypothesis;

$$H_0 : \rho = 0 \qquad H_a : \rho \neq 0 \tag{4.8}$$

where ρ was the population correlation between the $f_{s,max}$ and the number of the production cycles. The Pearson correlation test for the non-coated tool reported that it failed to reject the H_0 because the p-value was greater than the significance level, 0.05 (p-value=0.20786). It concluded that there was not enough evidence at 0.05 significance level to conclude that there was a linear relationship between $f_{sn,max}$ and the number of production cycle. The Pearson correlation test for the coated tool reported that it rejected the H_0 because the p-value was smaller than the significance level, 0.05 (p-value=0.0218). It concluded that there was enough evidence at 0.05 significance level to conclude that there was a linear relationship between $f_{sc,max}$ and the number of production cycle with strong positive correlation

coefficient, $r = 0.70861$. The statistical data analysis results showed that $f_{sc,max}$ had positive relationship with the number of production cycles. Therefore, the difference between $f_{sn,max}$ and $f_{sc,max}$ had decreased over the production cycle, which led the ratio of $f_{sc,max}$ to $f_{sn,max}$ ($f_{sc,max}/f_{sn,max}$) to have an increasing pattern as showed in Figure 4.34(b).

In the demolding test, the shrinkage of the cured composite part on the tool caused the normal force during the demolding process. Therefore, the total normal force applied to the part due to the shrinkage was proportional to the contacting surface area between the tool and the part in the cylindrical section. In the kinetic region of the demolding test, when the part started to be demolded, the contacting surface area between the tool and the part started to decrease which made the total normal force applied to the part towards the tool decreased. Since the displacement linearly changed, 2 mm/min, the contacting surface area also linearly changed. At the same displacement, which assumed that the same normal force was applied, the kinetic friction coefficient of the non-coated and coated tool could be compared by comparing their kinetic friction force using the following equation;

$$\mu_{kc}/\mu_{kn} = f_{kc}/f_{kn} \tag{4.9}$$

where μ_{kn} and f_{kn} were kinetic friction coefficient and kinetic friction force of the non-coated tool, and μ_{kc} and f_{kc} were kinetic friction coefficient and kinetic friction force of the coated tool. However, the data fluctuated due to the stick-slip behavior of the part during the demolding process, the author decided to make a linear fitted line on the data and calculated the slope to compare the kinetic friction coefficient of the non-coated and coated tool. The slope of the fitted line was calculated using the following equation;

$$m = (f_{k2} - f_{k1})/(d_2 - d_1) \tag{4.10}$$

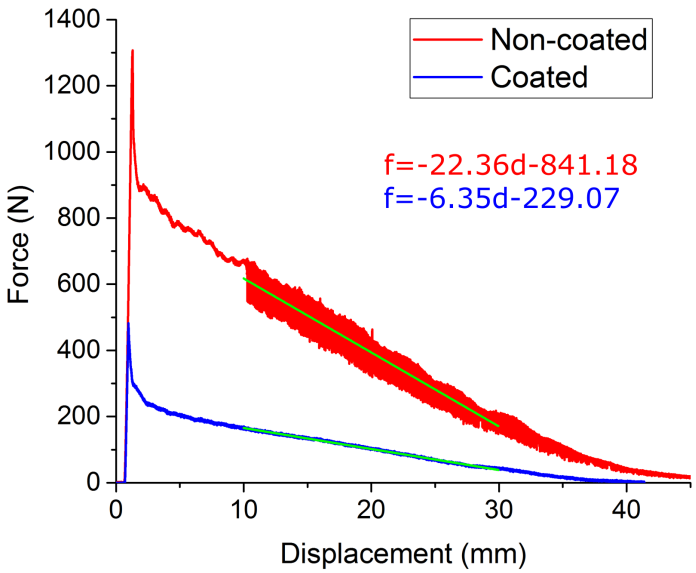

Figure 4.36. Linear fitted line in the kinetic region of the non-coated and coated tool demolding test data (cycle 1).

where m was the slope of the line, and f_{k1} was kinetic friction force at the 1st displacement, d_1, on the fitted line. f_{k2} was kinetic friction force at the 2nd displacement, d_2, on the fitted line. The kinetic friction coefficient ratio between the non-coated and the coated tool could be calculated by finding a slope coefficient ratio between the fitted line for the non-coated tool and the fitted line for the coated tool using the following equation;

$$m_c/m_n = (f_{kc2} - f_{kc1})/(f_{kn2} - f_{kn1}) = \mu_{kc}/\mu_{kn} \tag{4.11}$$

The displacement range which gave a high r-square value for the linear fitted line was found (between 10 mm and 30 mm) and used to calculate the fitted line and its slope as showed in Figure 4.36. Figure 4.37(a) showed the slope coefficient of the linearly fitted line of the non-coated and coated tool test data over 10 production cycles.

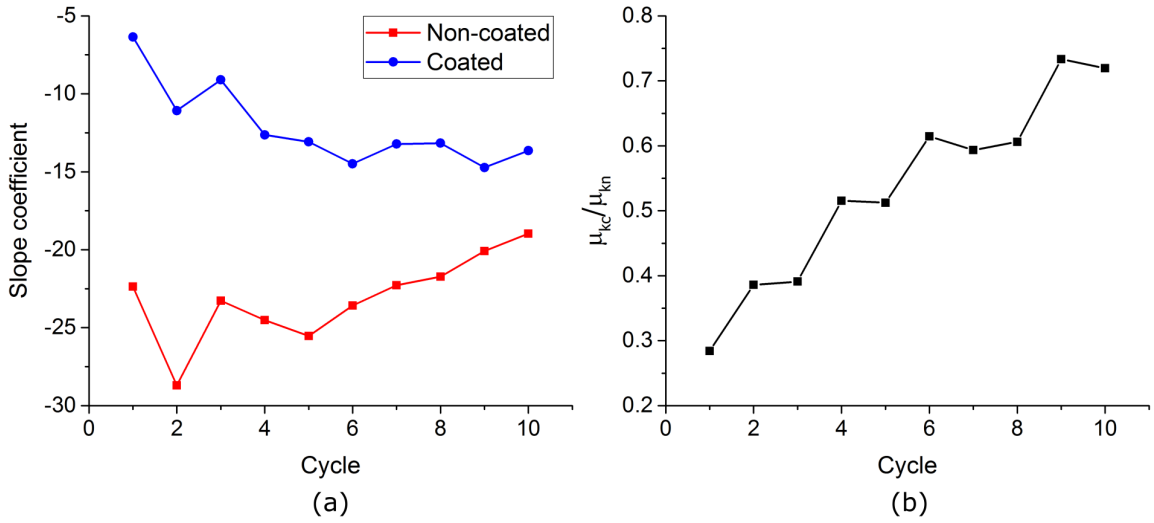

Figure 4.37. (a) The slope coefficient of the fitted line of the non-coated and coated tool test data over 10 production cycles. (b) μ_{kc}/μ_{kn} throughout the 10 production cycles.

Throughout all 10 production cycles, μ_{kc}/μ_{kn} was lower than 1. A statistical hypothesis test, one sample t-test, with a 0.05 significance level was performed to investigate whether μ_{kc}/μ_{kn} was significantly lower than 1, which represented kinetic friction coefficient of the coated tool was significantly lower than the non-coated tool under the following hypothesis;

$$H_0 : \mu = 1 \qquad H_a : \mu < 1 \tag{4.12}$$

where μ was the average μ_{kc}/μ_{kn}. The one-sample t-test result reported that it rejected its H_0 because the p-value was smaller than the significance level, 0.05 (p-value=$1.8153e^{-6}$). Therefore, the t-test concluded that μ_{kc}/μ_{kn} ($M = 0.54$, $SD = 0.15$) was significantly lower than 1; $t(9) = -9.98$, p-value=$1.8153e^{-6}$. Also, a Pearson correlation test, with a 0.05 significance level was performed between the μ_{kc}/μ_{kn} and the number of production cycle to investigate how the μ_{kc}/μ_{kn} changed over the number of production cycle using the following hypothesis;

$$H_0 : \rho = 0 \qquad H_a : \rho \neq 0 \tag{4.13}$$

where ρ was the population correlation between the μ_{kc}/μ_{kn} and the number of production cycle. The Pearson correlation test reported that it rejected the H_0 because the p-value was smaller than the significance level, 0.05 (p-value=$4.60997e^{-6}$). It concluded that there was enough evidence at 0.05 significance level to conclude that there was a linear relationship between μ_{kc}/μ_{kn} and the number of production cycle with the very strong positive correlation coefficient $r = 0.97$. Using Pearson correlation test, it was also able to find that the absolute value of the slope for the non-coated tool was decreasing (p-value=0.02094, $r = -0.71$) and for the coated tool was increasing (p-value=0.00508, $r = 0.80$) over the production cycles. The statistical data analysis results indicated that the kinetic friction coefficient of the coated tool was significantly lower than the non-coated tool. However, over the production cycles, the kinetic friction coefficient of the non-coated tool was decreased and the kinetic friction coefficient of the coated tool was increased which made that the ratio of kinetic friction coefficient of the coated tool to non-coated tool (μ_{kc}/μ_{kn}) increased over the production cycles as showed in Figure 4.37(b).

The surface quality of the non-coated and coated tool during 10 production cycles was investigated by measuring surface roughness of the tool and observing the surface visually and using a stereoscope. The surface roughness was measured in the cylindrical surface of the tool where the major friction between the tool and the part occurred. A surface roughness testing fixture was designed to ensure that the tool stayed flat during the roughness test and stereoscopic image taking process. The fixture was additively manufactured using polylactic acid (PLA). Figure 4.38 showed the roughness testing of the demolding test tool using the customized fixture. The surface roughness, arithmetical mean roughness value (R_a), were measured in 10 different location over the tool surface after every production cycle. The roughness tester was set to have a cutoff length of 2.5 mm and evaluation length of 12.5 mm accordance to ASTM D7127-17 (ASTM International, 2018).

Figure 4.38. Roughness testing of the demolding test tool using the customized fixture.

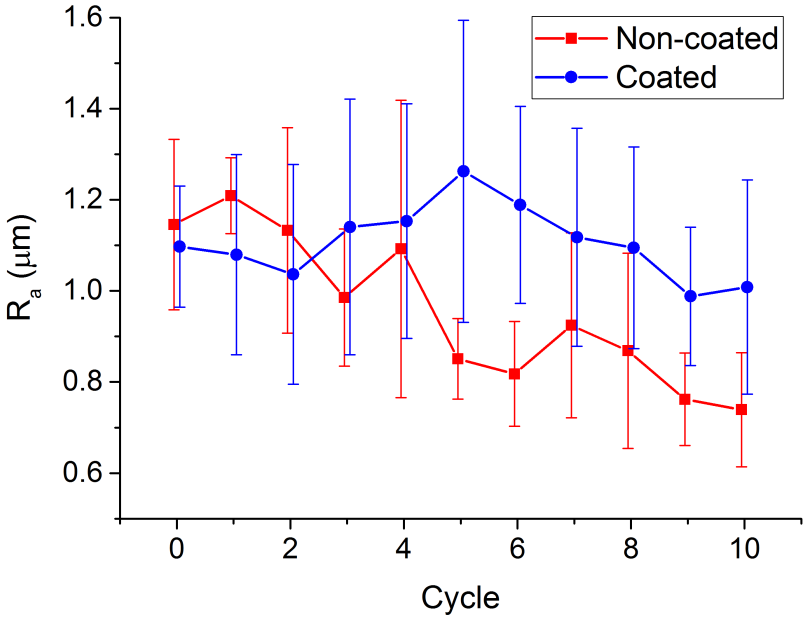

Figure 4.39. Average surface roughness (R_a) of the non-coated and coated demolding test tool with a standard deviation bar over 10 production cycles.

Figure 4.39 showed the average surface roughness (R_a) of the non-coated and the coated tool with a standard deviation bar over 10 production cycles.

A statistical hypothesis test, two sample t-test, with a 0.05 significance level was performed under the following hypothesis;

$$H_0 : \mu_n = \mu_c \qquad H_a : \mu_n \neq \mu_c \tag{4.14}$$

where μ_n and μ_c were the average surface roughness of the non-coated tool and coated tool respectively. In cycle 0 (before the first production cycle), the two sample t-test reported that it failed to reject the H_0 because the p-value was greater than the significance level, 0.05 (p-value=0.51443). It concluded that there was no significantly different surface roughness (R_a) between non-coated ($M = 1.15$, $SD = 0.19$) and coated ($M = 1.10$, $SD = 0.13$) tool; $t(18) = 0.67$, p-value=0.51443 at cycle 0. After 10th cycle, the non-coated tool showed 26.7% lower surface roughness compared to the coated tool, and the two sample t-test reported that it rejected the H_0 because the p-value was smaller than the significance level, 0.05 (p-value=0.00502). It concluded that there was a significantly different surface roughness (R_a) between non-coated ($M = 0.80$, $SD = 0.27$) and coated ($M = 1.01$, $SD = 0.24$) tool after the 10th production cycle. A Pearson correlation test, with a 0.05 significance level was performed between the surface roughness (R_a) of the tool and the number of production cycle using the following hypothesis;

$$H_0 : \rho = 0 \qquad H_a : \rho \neq 0 \tag{4.15}$$

where ρ was the population correlation between the surface roughness (R_a) of the tool and the number of production cycle. The Pearson correlation test between the surface roughness of the non-coated tool and the number of production cycle reported that it rejected the H_0 because the p-value was smaller than the significance level, 0.05 (p-value=$5.43565e^{-13}$). It concluded that there was enough evidence at 0.05 significance level to conclude that there was a linear relationship between the surface roughness of the non-coated tool and the number of production cycle with the moderate negative correlation coefficient $r = -0.62$. The Pearson

correlation test between the surface roughness of the coated tool and the number of production cycle reported that it failed to reject the H_0 because the p-value was greater than the significance level, 0.05 (p-value=0.41472). It concluded that there was not enough evidence at 0.05 significance level to conclude that there was a linear relationship between the surface roughness of the coated tool and the number of production cycle. The statistical data analysis results indicated that the surface roughness of the non-coated tool decreased over the production cycles. Therefore, the surface roughness was not significantly different between non-coated and coated tools before the first production cycle, but the non-coated tool had significantly lower surface roughness than the coated tool after the 10th production cycle.

The visual inspection and stereoscopic images were used to investigate the surface quality of the tool throughout the 10 production cycles. After the machining process, some intra-bead voids, which were located in the interlayer of beads, were visually observed on the surface of the tool. The coated tool surface also showed some voids which could not be covered by the coating. Figure 4.40 showed the surface of the non-coated and the coated tool before the 1st production cycle.

After the 1st production cycle, the surface of the non-coated and coated tool was observed using a stereoscope. The stereoscopic image showed that resin from the prepreg, which was laid up on the tool, filled the voids on the surface of the tool. The non-coated tool surface had many filled voids including not only intra-bead voids, but also inter-bead voids. The stereoscopic image of the coated tool surface showed that the coating covered all small voids on the surface. However, some big voids which could not be covered with coating had filled with resin. Figure 4.41 showed filled voids on the surface of the non-coated and coated tool after the 1st production cycle.

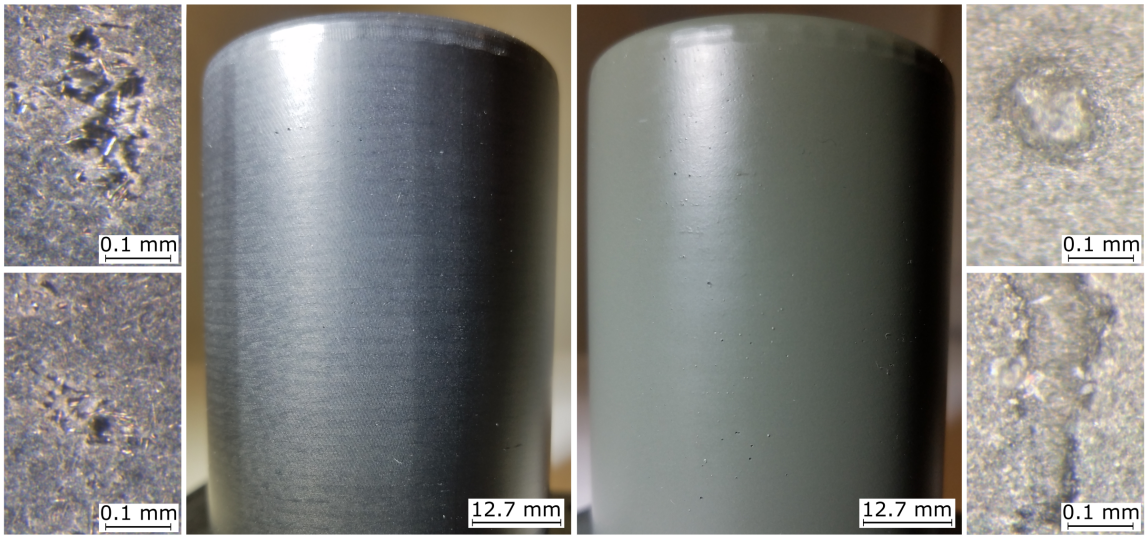

Figure 4.40. The (a) non-coated and (b) coated demolding test tool surface before 1st part production cycle.

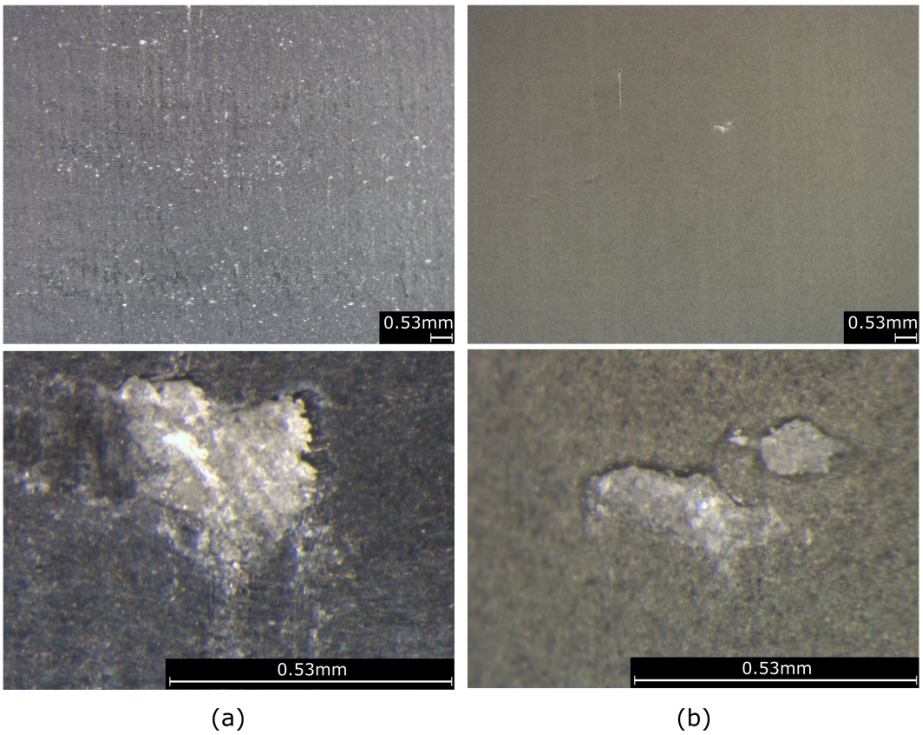

Figure 4.41. Filled voids on the surface of the (a) non-coated and (b) coated tool after 1st production cycle (top: 0.7X magnification, bottom: 9X magnification).

For both tools, it was obvious that the surface of the tool was scratched from the filled voids area towards the demolding direction. After the resin was smeared inside of the void and cured, it either broke away from the part or demolded with the part during the part demolding process. Both cases created a non-smooth surface to the part which caused scratches on the surface of the tool while the part was demolded. Most of the resin that filled the voids on the non-coated tool broke off from the part and stayed inside of the void after the part was demolded. Since the new layer of mold release was applied on the top of the filled resin for the next production cycle, the filled resin became a part of the non-coated tool surface. However, since the resin that filled the voids did not create a perfectly smooth tool surface, scratching still occurred every time the part was demolded from the tool, and the abraded dust from the tool due to the scratches was observed. However, the scratches seemed shallow and did not get much deeper over the 10 production cycles. Figure 4.42(a) showed scratches on the non-coated tool surface after the 10th production cycle and the abraded tool dust on the demolded part. Since the coated tool had less voids on the surface, there were a smaller number of scratches on the surface of the tool. However, the coated tool had not only scratches on the tool surface, but also had chipped coating during the demolding process. In most cases, the resin that filled the voids on the coated tool was demolded with the part. While it was demolded, it chipped the coating on the void area and left a scratch on the tool surface. Figure 4.42(b) showed chipped coating and scratches on the coated tool surface after the 10th production cycle and the resin that filled the voids came out with the demolded part. Also, the size of the chipped coating got increased which created more severe scratches on the tool surface over the production cycle as showed in Figure 4.43. Figure 4.44 showed a schematic drawing of tool surface damaging process in the void area on the non-coated and coated tool surface during the demolding process.

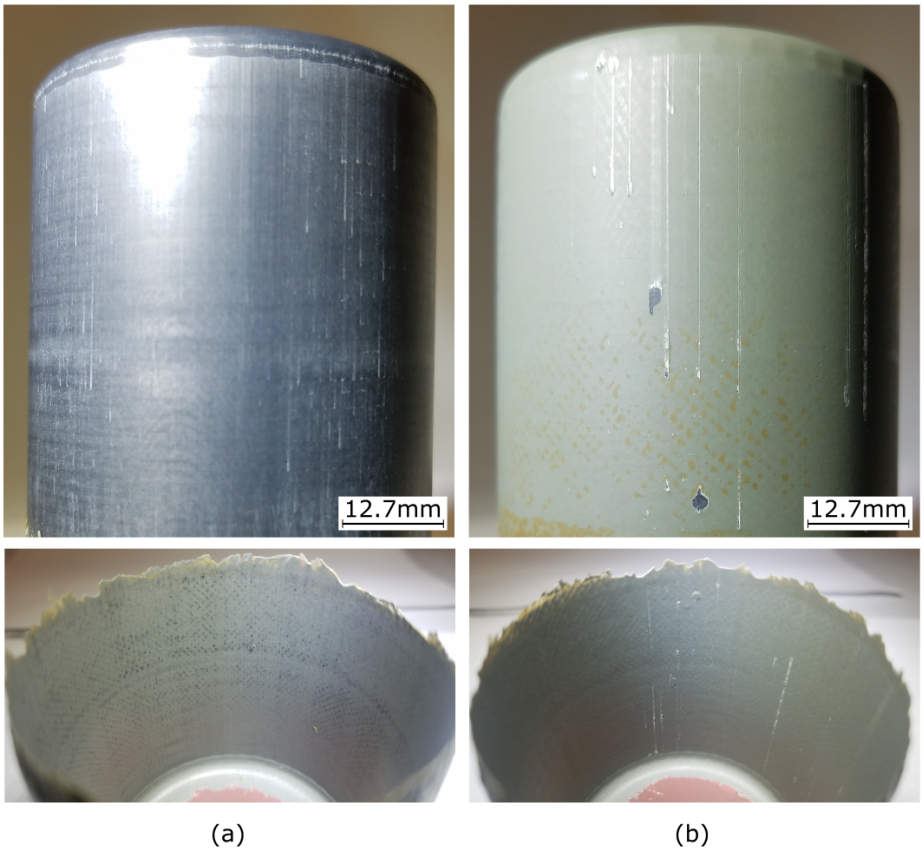

Figure 4.42. The (a) non-coated and (b) coated demolding test tool after the 10th part production cycle and the cured composite laid part from the 10th production cycle.

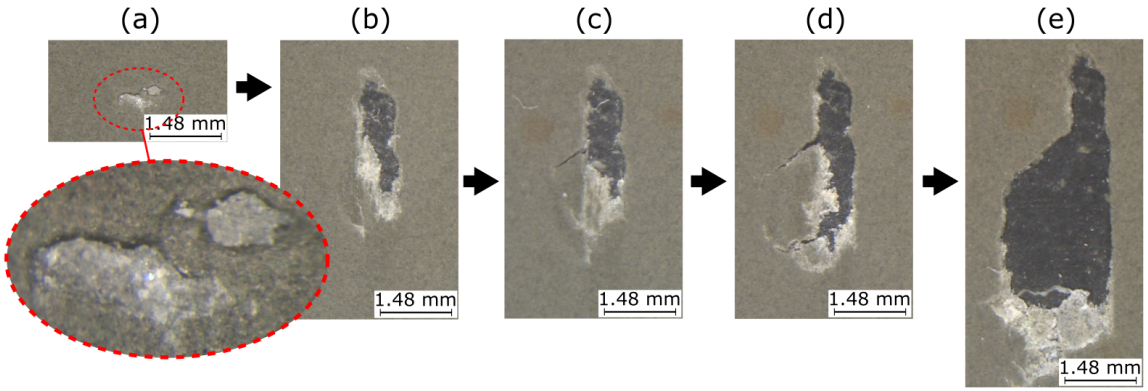

Figure 4.43. Stereoscopic images of the chipped coating after (a) 1st cycle, (b) 2nd cycle, (c) 3rd cycle, (d) 4th cycle, and (e) 9th cycle.

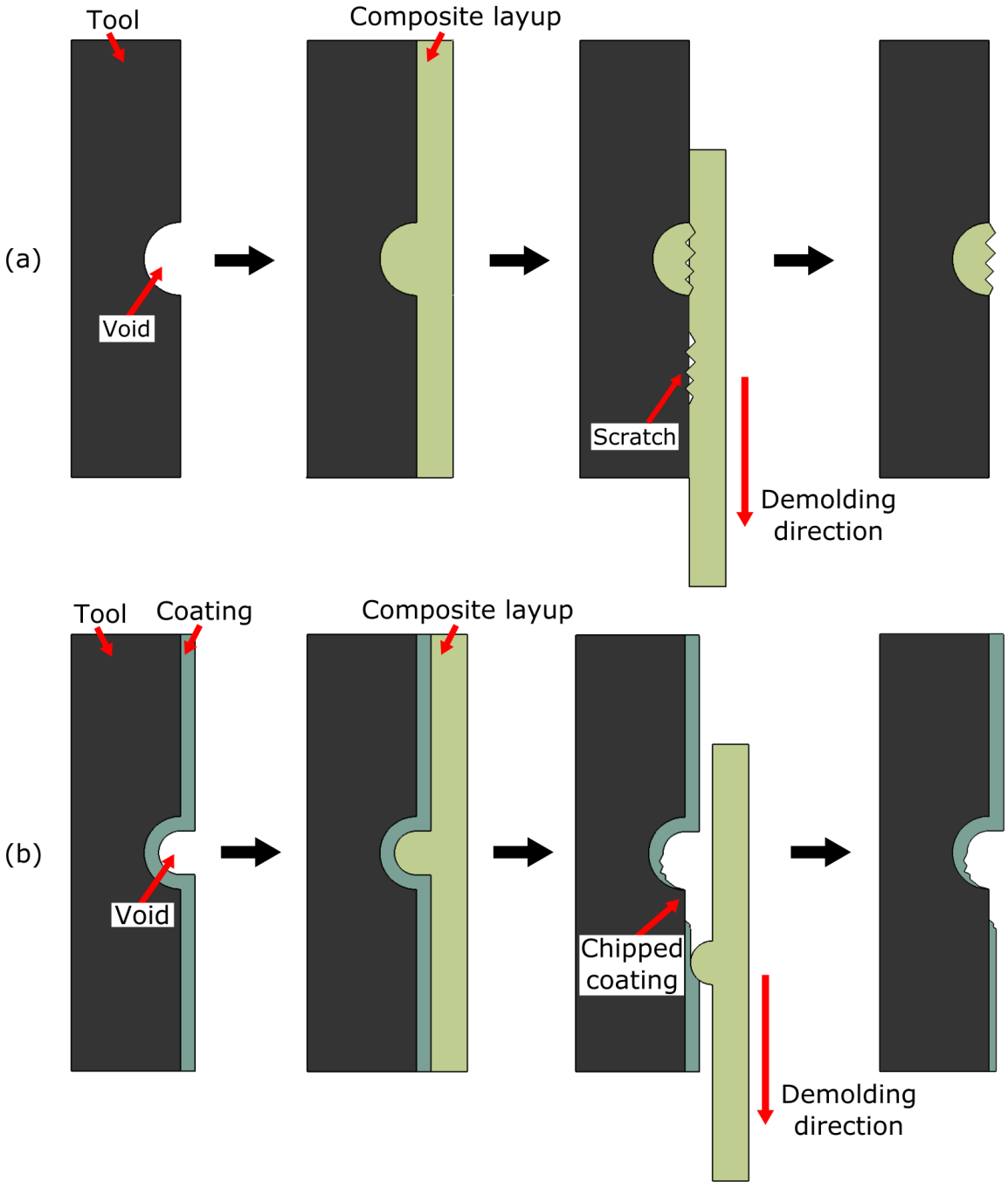

Figure 4.44. Schematic drawing of the tool surface damaging process in the void area on the (a) non-coated and (b) coated tool during the demolding process.

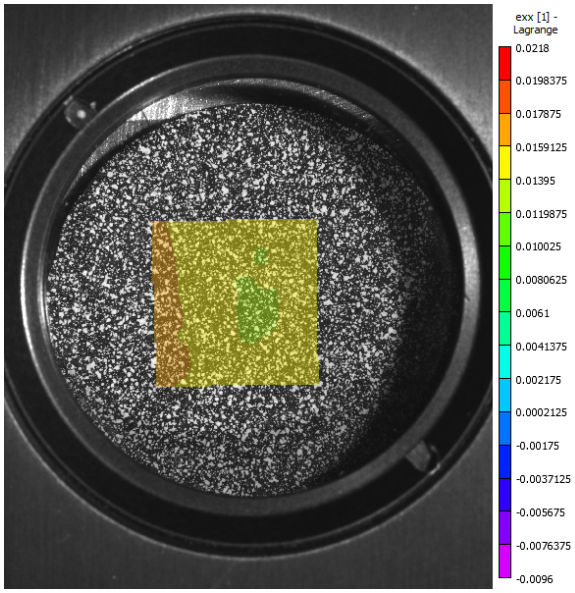

Figure 4.45. Strain change analysis of the speckle pattern during the CTE test.

4.5.5 Coefficient of thermal expansion (CTE) test

The coefficient of thermal expansion (CTE) of the additively manufactured carbon fiber reinforced PPS composite material and the coating material were tested using DIC technology. The images which were taken using DIC camera during the CTE test were exported and analyzed using a DIC software, Vic-2D. Vic-2D analyzed how the speckle pattern on the CTE test specimen moved and calculated strain change of the speckles in x and y direction in the image during the CTE test temperature cycle as showed in Figure 4.45. The calculated strain data was synchronized with the temperature data exported from the hot stage to find the amount of strain change at each temperature. Then, the strain change values only in the temperature soaking period in every 10°C were exported and averaged. Using these averaged strain change values for every 10°C, strain change versus temperature plot was made. Figure 4.46 showed the CTE data analysis process, including synchronizing the temperature and strain change data and sampling and averaging the data.

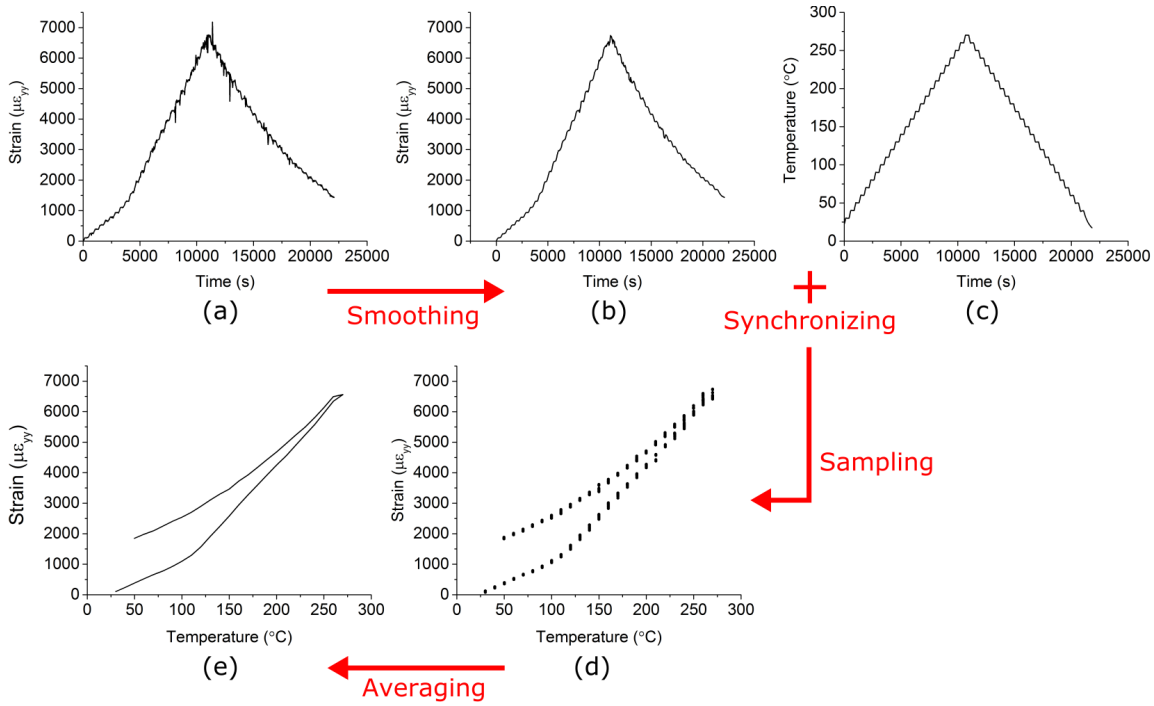

Figure 4.46. CTE test result analysis process map (substrate in 2 direction (in-plane transverse direction)). (a) raw strain versus time, (b) smoothed strain versus time, (c) temperature versus time, (d) sampled strain versus temperature, and (e) averaged sampled strain versus temperature.

After the strain versus temperature plot was attained, CTE was found by calculating the slope of the strain vs temperature data curve. Since the polymer had different CTE below and above T_g, the slope below T_g and above T_g was calculated separately. The T_g of the substrate was estimated to the range between 83.17°C and 95.91°C from the previous DSC and DMA thermal characteristic analysis for the substrate material. However, the T_g of the coating material was not identified yet. Therefore, the thermal analysis of the coating material was conducted using the DSC. DSC was programmed (1) equilibrating at 25°C, (2) ramping at 30°C/min to 200°C, (3) isothermal for 5 minutes, and (4) ramping at 30°C/min to 25°C. Figure 4.47 showed DSC thermal analysis result of the coating material. In the glass transition area, T_{eig}, T_{efg} and T_{mg} were identified in accordance with ASTM D3418 as showed in Figure 4.48 (ASTM International, 2015a). T_{eig}, T_{efg} and T_{mg} were

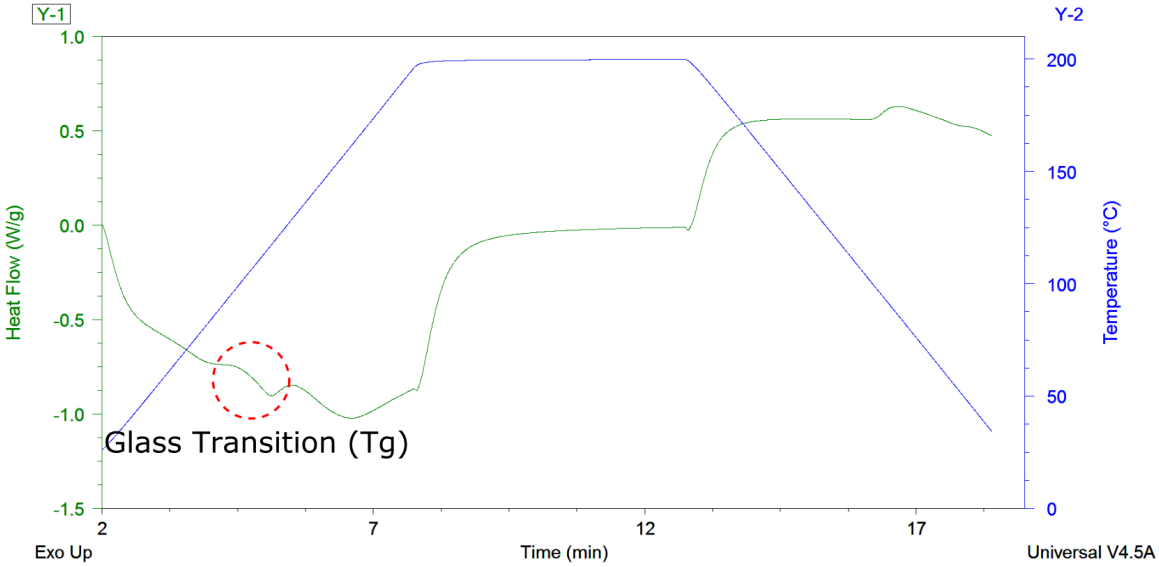

Figure 4.47. DSC thermal analysis result of the coating material with identified glass transition area.

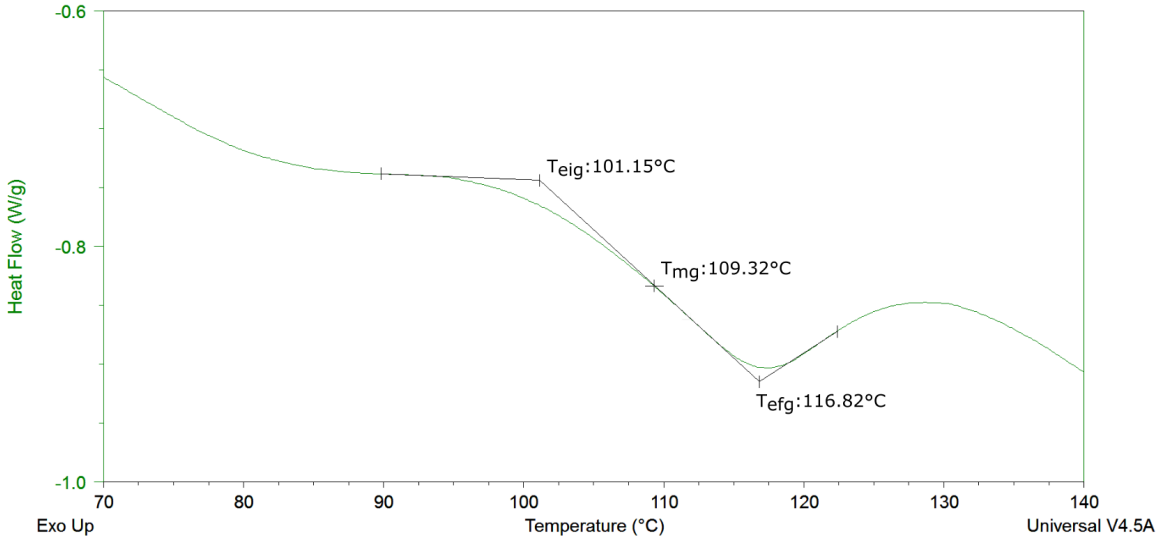

Figure 4.48. Glass transition area in the DSC thermal analysis result of the coating material with identified T_{eig}, T_{efg}, and T_{mg}.

determined to be 101.15°C, 116.82°C, and 109.32°C respectively. T_{mg}, 109.32°C was estimated to the glass transition temperature (T_g) of the coating material.

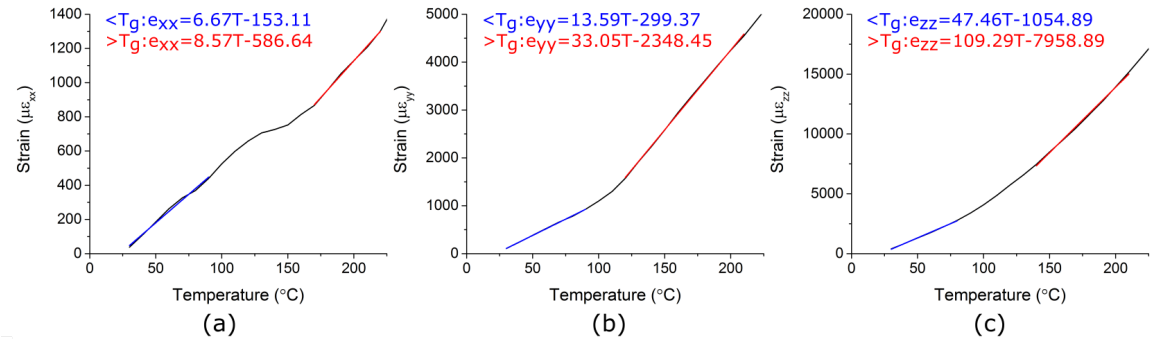

Figure 4.49. Strain change versus temperature plot for the substrate material in (a) 1 direction (printing direction), (b) 2 direction (in-plane transverse direction), and (c) 3 direction (stacking direction).

Since the printed substrate was an anisotropic material which had a different CTE depending on the direction of the measurement, the CTE of the printed substrate was investigated in all 3 directions; 1 direction (printing direction), 2 direction (in-plane transverse direction), and 3 direction (stacking direction). The coating material was an isotropic material, so only one CTE measurement was taken and analyzed. For each strain versus temperature plot, the sections below and above T_g which gave a high r-square value were selected and the linear line was fitted for the sections. The slope of the linear lines was calculated to find the CTE of the material below and above T_g. Figure 4.49 showed a strain versus temperature plot with a calculated slope for the substrate material in 1, 2, and 3 directions. Figure 4.50 showed a strain versus temperature plot with a calculated slope for the coating material.

The CTE test results showed that both substrate (in all 3 directions) and coating material had different CTE below and above its T_g. Also, the substrate material had a different strain versus temperature curve in 1, 2, and 3 directions. The 3 direction (stacking direction) showed the highest CTE, and 1 direction (printing direction) showed the lowest CTE. The CTE of the substrate material in 1 direction below T_g was 6.67 μm/°C and above T_g was 8.57 μm/°C. The CTE of the substrate material in 2 direction below T_g was 13.59 μm/°C and above T_g was 33.05

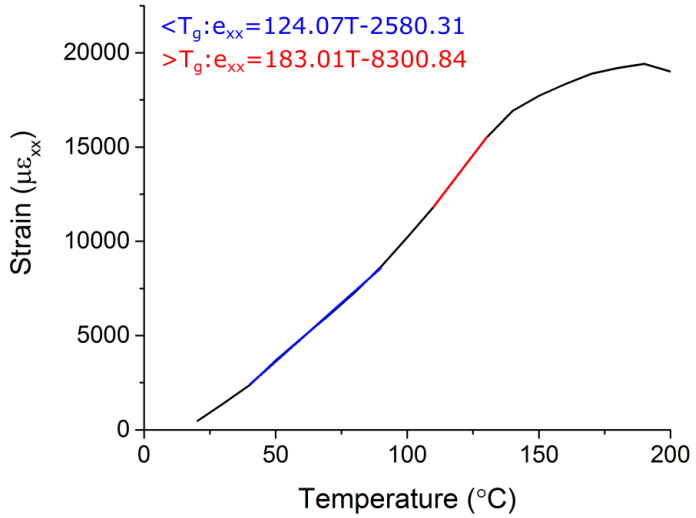

Figure 4.50. Strain change versus temperature plot for the coating material.

Table 4.7. *Coefficient of thermal expansion (CTE) of the substrate and coating.*

CTE of the substrate material (μm/°C)		
Direction	Below T_g	Above T_g
1	6.67	8.57
2	13.59	33.05
3	47.46	109.29

CTE of the coating material (μm/°C)		
Direction	Below T_g	Above T_g
	124.07	183.01

μm/°C. The CTE of the substrate material in 3 direction below T_g was 47.46 μm/°C and above T_g was 109.29 μm/°C. The coating material had a higher CTE than the substrate material. The CTE of the coating material below T_g was 124.07 μm/°C and above T_g was 183.01 μm/°C. The substrate material and coating material had a different CTE which could generate a thermal stress during the composite part curing temperature cycle. The adhesion test was conducted to investigate how this thermal stress affected the adhesion strength of the coating.

4.5.6 Coating adhesion test

The results of the CTE experiment showed the CTE mismatch between the substrate and coating which could cause thermal stress in the bonding area at elevated temperatures. If the thermal stress caused micro-cracks in the bonding area and affected coating adhesion strength, the coating could not be used for a composite part manufacturing process that used an elevated temperature for composite part curing. Therefore, the coating adhesion strength in the repeated temperature cycle was investigated to find how a CTE mismatch between the substrate and coating affected the adhesion strength of the coating. The bonding area of the coated test specimen and the pull-off test dolly were lightly sandblasted and bonded using LORD 7542 urethane adhesive. While the test specimen and the dolly were bonded, the dolly bonding jig was used to align them. After the dolly was bonded, the coating around the dolly was trimmed using a hole saw. Figure 4.51 showed the pull-off coating adhesion test specimen preparation process. The prepared test specimen was tested using MTS universal testing machine with customized pull-off test fixtures. The top test fixture held the dolly and measured the applied load while the bottom test fixture pulled the test specimen. Figure 4.52 showed the coating adhesion pull-off test fixtures and the test specimen during the test. 10 adhesion test specimens for each number of temperature cycle (cycle 0-10), except 10th cycle which had only eight test specimens, were tested (108 test specimen total). The adhesion test data was exported and analyzed. For each number of temperature cycles, the maximum coating pull-off strength of the test specimen was found and averaged. Figure 4.53 showed averaged maximum pull-off strength of the coating for each number of the temperature cycle with a standard deviation bar.

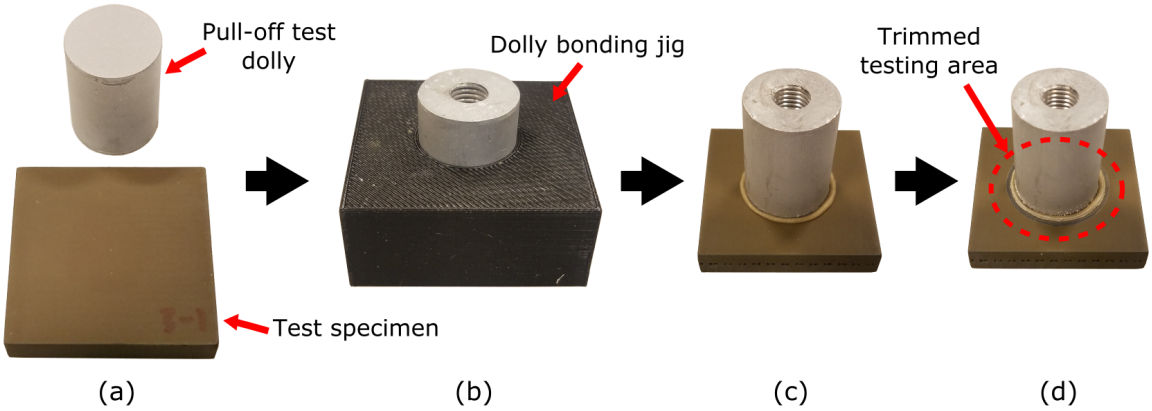

Figure 4.51. Coating adhesion test specimen preparation process; (a) sandblasted test specimen and pull-off test dolly, (b) the test specimen and the dolly were aligned using the dolly bonding jig while they were bonded, (c) the test specimen was bonded with the dolly using a dolly bonding jig, and (d) the coating around the dolly was trimmed using a hole saw.

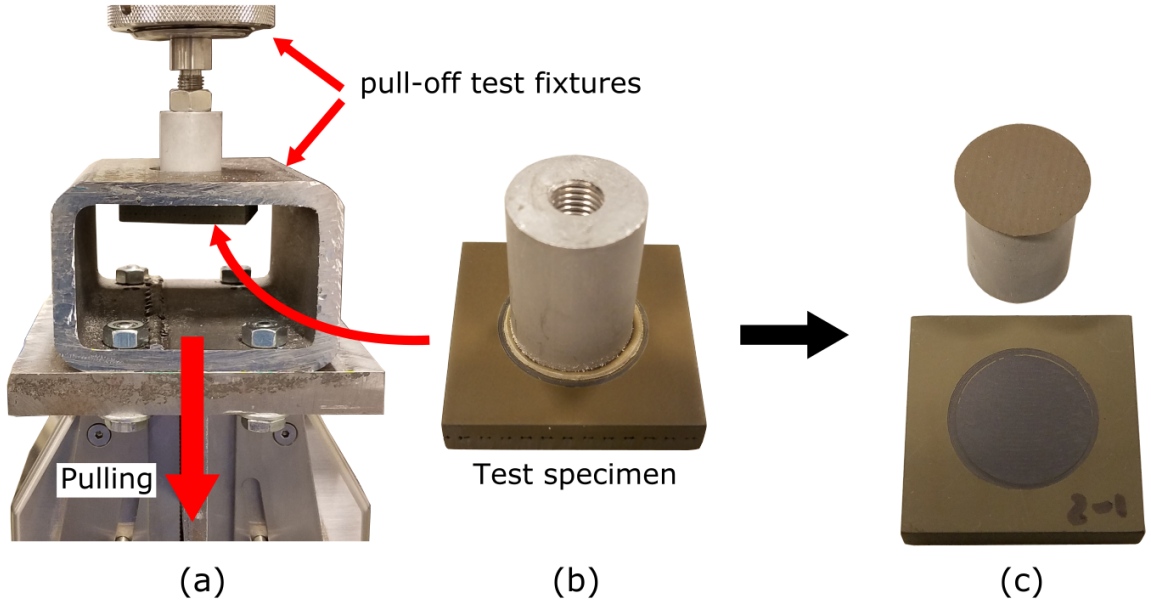

Figure 4.52. Coating adhesion test set up; (a) the pull-off test fixtures, (b) the pull-off test specimen, and (c) the pull off test specimen after the test.

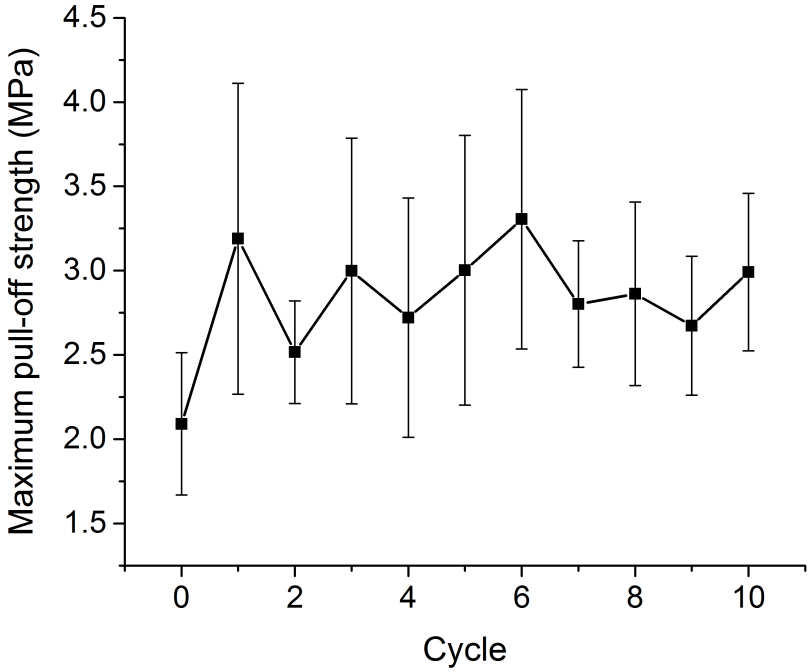

Figure 4.53. Averaged maximum pull-off strength of the coating for each number of the temperature cycle with a standard deviation bar.

To investigate how adhesion strength of the coating changed corresponding to the number of production cycle, a Pearson correlation test, with a 0.05 significance level was performed between the maximum pull-off strength of the coating and the number of production cycle using the following hypothesis;

$$H_0 : \rho = 0 \qquad H_a : \rho \neq 0 \tag{4.16}$$

where ρ was the population correlation between the maximum pull-off strength of the coating and the number of production cycle. The Pearson correlation test reported that it failed rejected the H_0 because the p-value was smaller than the significance level, 0.05 (p-value=0.11167). It concluded that there was not enough evidence at 0.05 significance level to conclude that there was a linear relationship between the maximum pull-off strength of the coating and the number of production cycle. It was found that even there was a CTE mismatch between the

substrate and coating, which could cause thermal stress between them, the coating adhesion strength had no significant relationship with number of the thermal cycles.

4.5.7 Coating sustainability and mold life experiment

To investigate the sustainability of the coating on the composite part manufacturing mold and how it affected the life of the mold, one non-coated and one coated mold life experimental tools were prepared. The surface of both tools was cleaned and treated with a mold sealer and a mold release. Two coats of mold sealer, 15 sealer EZ, and five coats of mold release, Chemlease R&B mold release, were applied in accordance with the application instructions from the mold sealer and release manufacturer. Since a sealant tape for the vacuum bagging process was installed on the top surface of the tool, it was made sure that the mold sealer and release were not applied to the area where the sealant tape was installed. After the designed plies were cut using an automatic cutting table, four plies were laid on the tool with $[0]_4$ orientation. Then, a peel ply, release film, and breather were placed on the top of the ply and a vacuum bag was installed. Figure 4.54 showed composite ply layup and vacuum bagging process for the mold life experiment tool. After the vacuum pressure was applied, the vacuum supply was disconnected and a pressure gauge was installed to the vacuum port. The vacuum pressure was measured for 5 minutes to investigate any air leak of the tool. Once it was verified that the tool had no significant air leak, the tools were placed in an autoclave and the composite parts were cured using a cure cycle that had a 2-hour soak at 180°C with 586 kPa of pressure. After each production cycle, the part was demolded, and the surface of the tool was inspected visually to find any surface defects. Also, the tool shape change in the repeated composite part cure cycles was analyzed by measuring the surface of the tool using a 3D laser scanner, FARO Arm Edge model 14000 for every production run. Then, two additional coats of mold release, Chemlease R&B mold release, were applied to the tool surface for the next cycle.

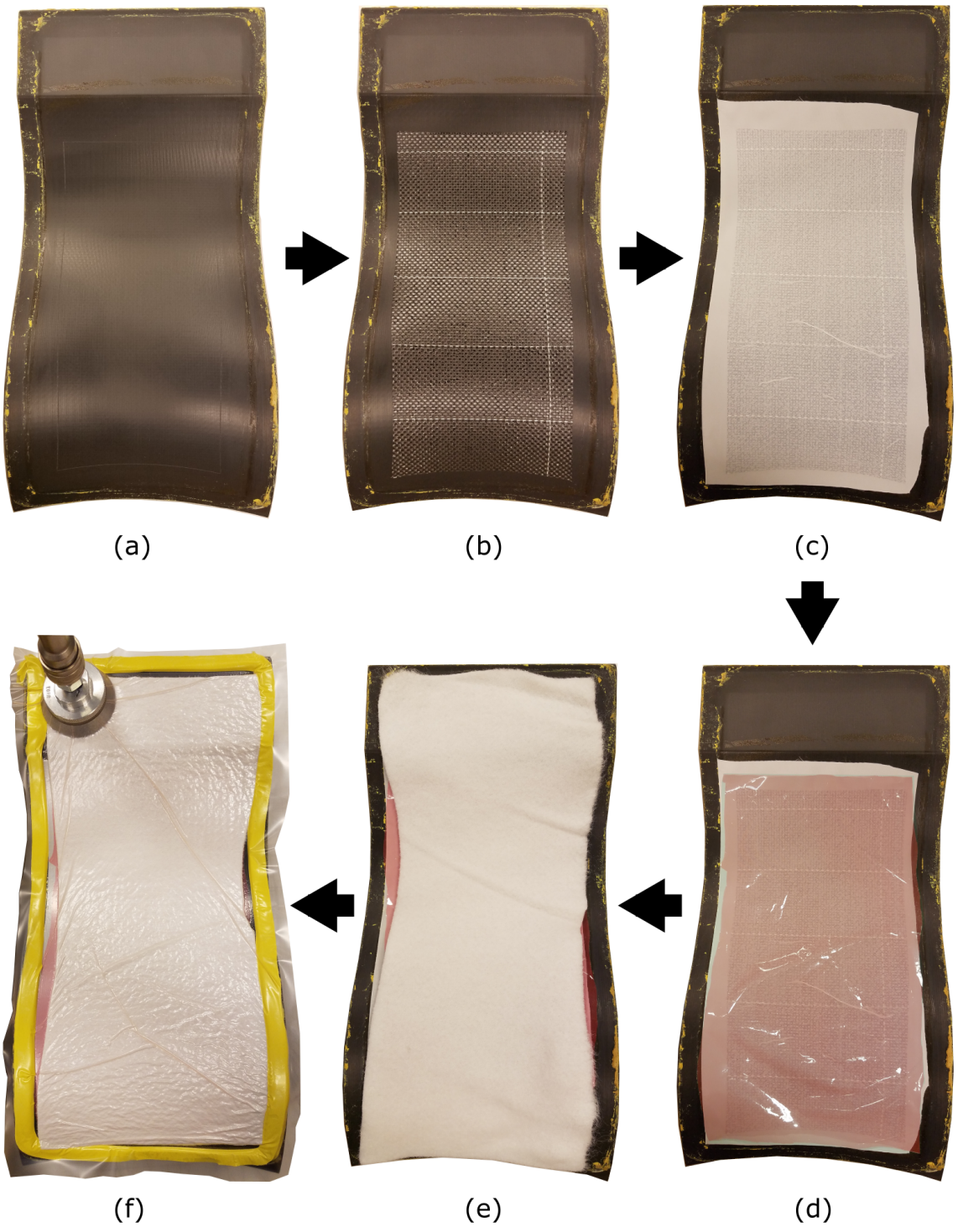

Figure 4.54. Vacuum bagging process of the mold life experiment tool; (a) mold life experiment tool before layup, (b) after layup composite prepreg plies, (c) peel ply, (d) release film, (e) breather cloth, and (f) vacuum bag.

Visual inspection

After the first production cycle, both tools had a light mark on the surface of the tool. Also, excess resin from the prepreg smeared out to where the sealant tape was located and cumulated there. The coated tool had a small amount of coating chipped off at the part trim line and some coating discoloration over the tool surface. Over the repeated part production cycles, the amount of coating that chipped off at the part trim line and discoloration over the coated tool increased. However, besides chipped coating on the part trim line, there was no chipped coating on the part layup surface of the coated tool until the 9th production cycle. After the 9th production cycle, it was found that a small amount of coating chipped off from the composite part layup area (approximately 0.85 mm diameter circle). Figure 4.55 showed the top surface of the coated mold life experiment tool (a) before the 1st production cycle and (b) after the 10th production cycle. The coated tool had only chipped coating on the top surface of the tool, and the part trim line cavity was still coated and the tool was not chipped. However, the non-coated tool showed the actual chipped edge of the tool in the part trim line during the production cycles. Figure 4.56 showed the top surface of the non-coated mold life experiment tool (a) before the 1st production cycle and (b) after the 10th production cycle. The air leak test showed that both tools did not have any critical vacuum leak that was greater than 1.5 kPa for 5 minutes until the 10th production cycle.

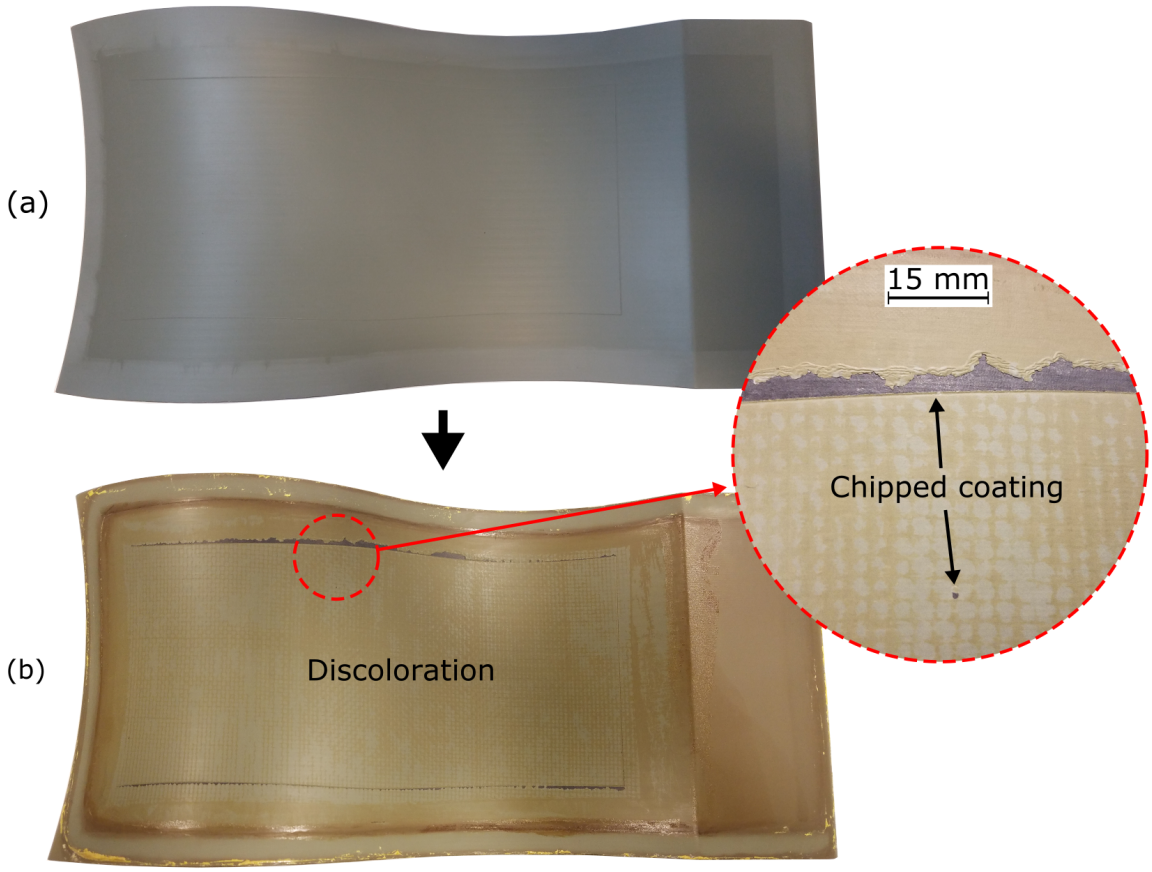

Figure 4.55. Top surface of the coated mold life experiment tool (a) before the 1st production cycle and (b) after the 10th production cycle.

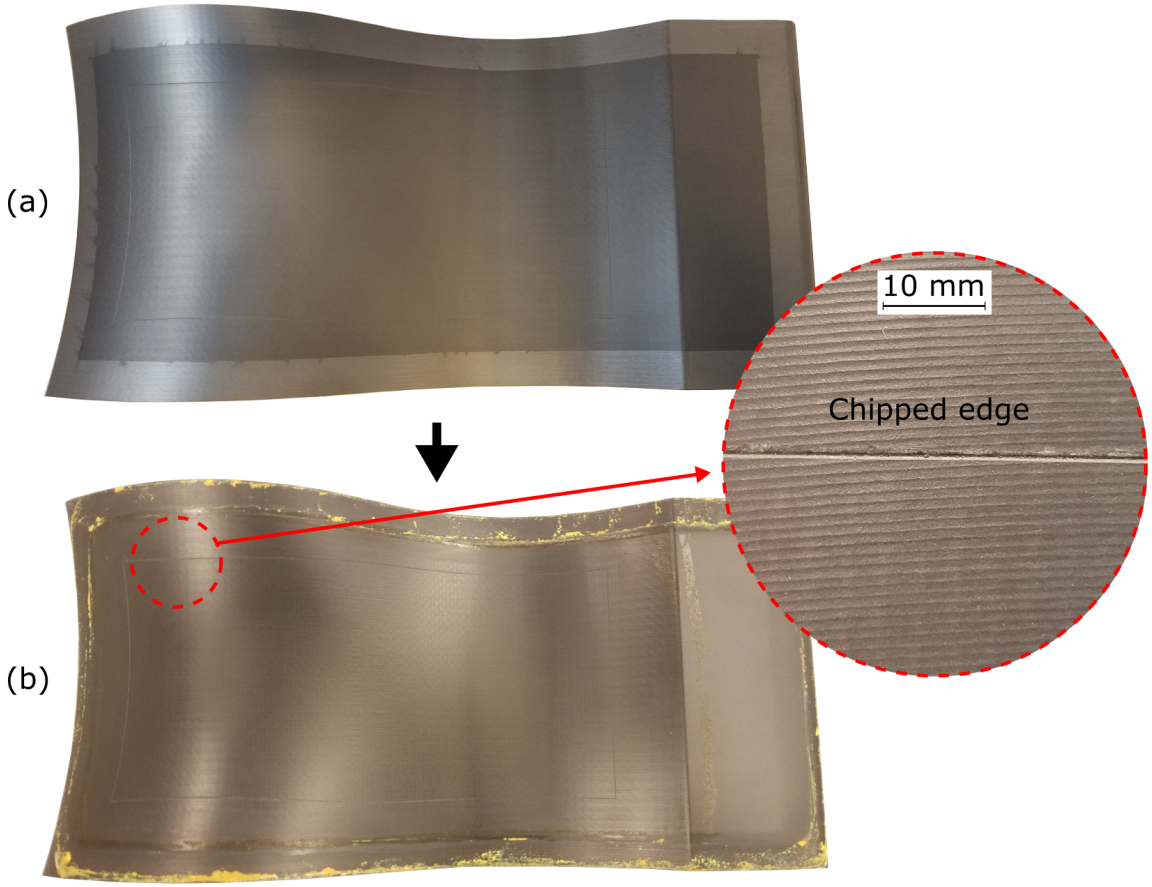

Figure 4.56. Top surface of the non-coated mold life experiment tool (a) before the 1st production cycle and (b) after the 10th production cycle.

Geometrical deviation analysis

The point cloud that was collected from the tool surface using a 3D laser scanner was analyzed to investigate the geometrical deviation of the tool surface during a repeated composite part manufacturing cycle. The collected point clouds were converted to a polygonal mesh and imported into a 3D model post-processing software, Geomagic Wrap, to refine the data. The data was refined by reducing the noise in the data and trimmed to the part trim line because only the inside of the part trim line was used for tool shape deviation analysis in this study. The refined data was used for a deviation analysis of the tool surface after each production cycle. The surface data of each production cycle was aligned to the tool surface data before the first production cycle and a geometrical deviation analysis was performed. The Faro Arm Edge model 14000 had +/- 0.041 mm of tolerance for the volumetric measurement. Therefore, the maximum and minimum nominal values for deviation analysis was set to +/- 0.041 mm. Figure 4.57 showed geometrical deviation analysis of the non-coated and coated tool after the 1st, 5th, and 10th cycle compared to their tool shape data before the 1st cycle.

The tool geometrical deviation analysis result showed that there was no noticeable tool shape change over the 10 production cycles for both the non-coated and coated tool. There was no gradually-changing deviation pattern and the amount of deviation was similar throughout the production cycles. After each production cycle, the tool was scanned three different times, so three different surface measurement were collected. The average deviation amount over the testing surface was calculated for each measurements. The average positive deviation and average negative deviation were calculated separately. Figure 4.58 showed the average positive and negative geometrical deviation amount over the production cycles. To investigate how the geometrical deviation of the tool changed over the production cycle, a Pearson correlation test, with a 0.05 significance level was

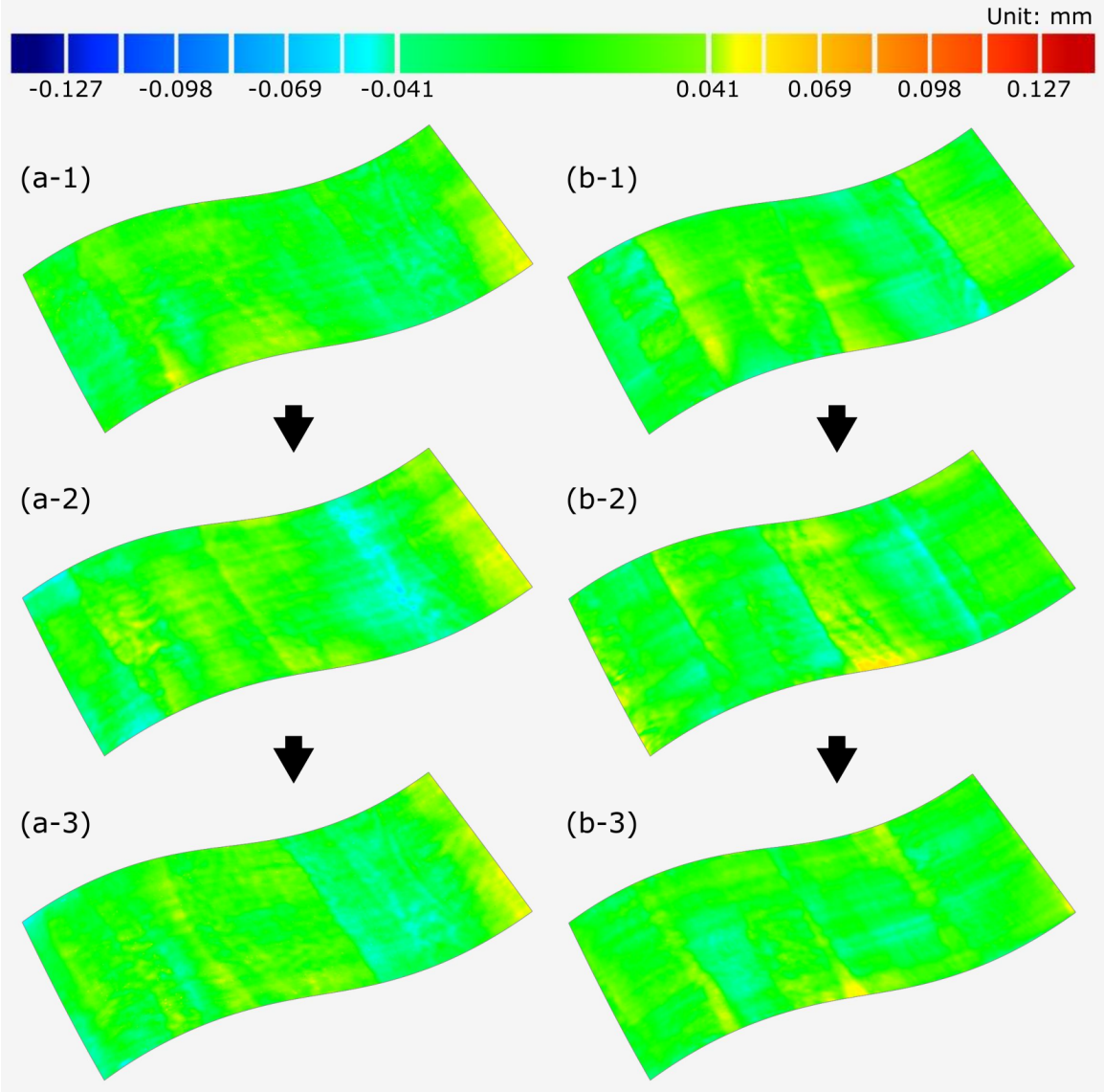

Figure 4.57. The deviation analysis of the non-coated tool after the (a-1) 1st cycle, (a-2) 5th cycle, (a-3) 10th cycle compared to the tool before 1st cycle, and the coated tool after (b-1) 1st cycle, (b-2) 5th cycle, (b-3) 10th cycle compared to the tool before 1st cycle.

performed between the amount of geometrical deviation of the tool and the number of production cycle using the following hypothesis;

$$H_0 : \rho = 0 \qquad H_a : \rho \neq 0 \tag{4.17}$$

where ρ was the population correlation between the amount of geometrical deviation of the tool and the number of production cycle. The Pearson correlation test for both positive and negative geometrical deviation of the non-coated tool reported that it failed to reject the H_0 because the p-value was bigger than the significance level, 0.05 (p-value=0.63341(+), 0.41994(-)). It concluded that there was not enough evidence at 0.05 significance level to conclude that there was a linear relationship between the amount of geometrical deviation of the non-coated tool and the number of production cycle. The Pearson correlation test for both positive and negative geometrical deviation of the coated tool reported that it rejected the H_0 because the p-value was smaller than the significance level, 0.05 (p-value=$8.23731e^{-4}$(+), 0.00109(-)). It concluded that there was enough evidence at 0.05 significance level to conclude that there was a linear relationship between the amount of geometrical deviation of the coated tool and the number of production cycle. The positive deviation had moderate negative correlation coefficient $r = -0.58$, and the negative deviation had moderate positive correlation coefficient $r = 0.57$. The statistical analysis results indicated that the geometrical deviation of the non-coated tool had no relationship with the number of production cycle, and the amount geometrical deviation of the coated tool had decreased over the production cycles. However, the amount of geometrical deviation change over the production cycle was too small. The average geometrical deviation over the coated tool surface after 1st production cycle was 0.01342 mm/-0.01334 mm and after the 10th production cycle was 0.01063 mm/-0.01002 mm. The average geometrical deviation difference between after the 1st and the 10th production cycle was only -0.00279 mm/0.00271 mm (the machine tolerance +/- 0.041 mm). Also, the laser scanning process could be affected by optical property changes of the

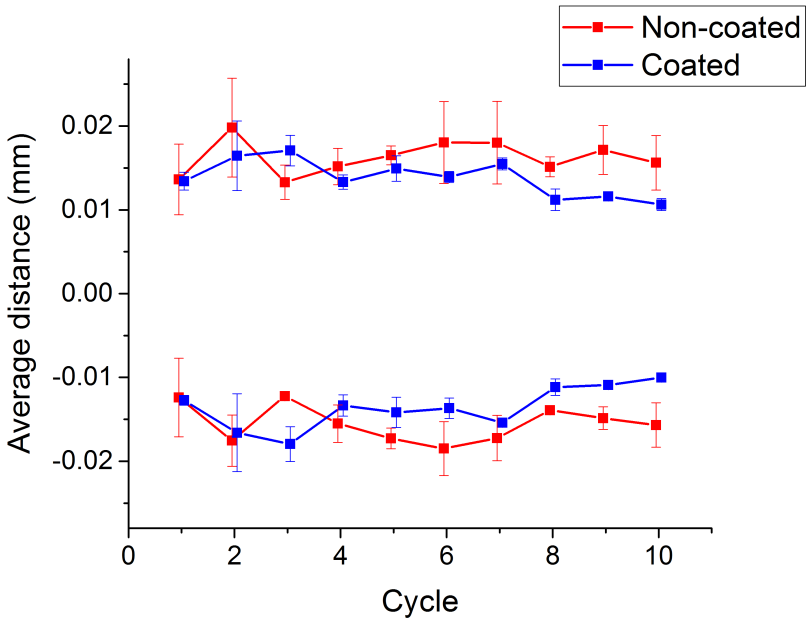

Figure 4.58. Average positive and negative geometrical deviation change of the tool surface over the production cycles.

coating due to its discoloration during the multiple production cycles. Further research is needed to investigate more detail about how the coating affects geometrical deviation change of the tool during repeated composite part cure cycles.

4.6 Summary

This chapter covered the experimental results, analysis, and discussion. It started with the substrate and coating material thermal characterization for testing the coating applicability. Then the coated surface was analyzed using various tests, such as surface hardness, abrasion resistance, roughness, demolding test, CTE, coating adhesion, and mold life test. The next chapter summarized the research, and conclude the research based on the results provided in this chapter.

CHAPTER 5. CONCLUSION

In this study, the effect of additional coating on the performance of the additively manufactured fiber reinforced composite mold for composite part manufacturing was investigated. This study introduced a systematical approach of testing coating for the composite part manufacturing mold which was printed with fiber reinforced thermoplastic composites. To find an applicable coating technique and coating material, the thermal characteristics of the substrate material and the coating material were analyzed. The maximum allowable coating application temperature was determined by finding the glass transition temperature (T_g) of the substrate using DSC and DMA. Also, the thermal degradation of the coating material in the composite part manufacturing temperature cycle was analyzed using TGA to verify that the coating material could be used for a composite part manufacturing mold. Carbon fiber reinforced PPS composite test specimens were additively built, machined, and coated with thermoset liquid coating with ceramic particles using liquid spray coating technique. Various surface property tests were performed to evaluate the performance of the coating.

The surface durability of the test specimen was tested using a surface hardness test and surface abrasion resistance test. The surface hardness test was performed with a Barcol impressor. The hardness test result showed that the coated test specimen had lower (23.38%) Barcol hardness than the non-coated test specimen. However, the surface abrasion resistance test result, which was performed with Taber abraser, reported that the wear index, which represented weight loss per abrasion cycle, of the coated test specimen was significantly lower (89.36%) than the non-coated test specimen. The coated test specimen even had a lower wear index than traditional metals, aluminum 6061 T-6, and 1020 steel test specimens.

The surface performance of the coating was tested using a surface roughness test and the demolding test. The surface roughness of the coated test specimen was not significantly improved compared to the non-coated test specimen. The demolding test was performed using a customized demolding test tool. The composite material was laid on the tool and cured. The demolding force while the cured composite part was demolded from the tool was recorded and analyzed. The coated tool showed significantly decreased (53.21%) maximum static friction force compared to the non-coated tool. Also, the kinetic surface friction coefficient of the coated tool was significantly lower (46.44%) than the non-coated tool. The visual inspection result of the coating on the demolding test tool showed that the coating helped to cover the voids on the tool surface. However, the uncovered voids on the tool surface caused chipped coating, and once the coating chipping occurred, it became larger after every production cycle.

The sustainability of the coating was tested using a coefficient of thermal expansion (CTE) test, coating adhesion test, and mold life experiment. The CTE of the additively manufactured carbon fiber reinforced PPS composite and the coating material was measured to investigate CTE mismatch between the substrate and coating. The CTE test result showed there was a CTE mismatch between the two materials which could cause thermal stress during the composite part manufacturing cycle. However, the coating adhesion test result showed that there was no significant relationship between the adhesion strength of the coating and the number of composite part curing temperature cycles. In the mold life experiment, the sustainability of the coating on the tool during the repeated composite part manufacturing processes was investigated. The mold life experiment result showed that the coating was easily chipped on the part trim line of the tool surface and the chipped coating propagated over the production cycles. There was no significantly noticeable geometrical deviation change of the tool and vacuum leak for both non-coated and coated tools.

Overall, the additional thermoset polymer coating with ceramic particles provided some beneficial surface properties, which were necessary for the composite part manufacturing mold made from additively manufactured carbon fiber reinforced PPS composite. The surface abrasion resistance was improved and the coefficient of surface friction and required demolding force were decreased with the coating. However, the surface roughness was not improved, and the surface hardness of the coated surface was even lower than the non-coated surface. Also, the sustainability of the coating on the additively manufactured carbon fiber reinforced composite mold still had the chipped coating issue. Therefore, the coating material with the coating application process utilized in this study could not be an ultimate solution for the additively manufactured fiber reinforced composite mold for the composite part manufacturing process. Further research is necessary to study different coating materials for the application, or any additional steps during the coating application process to compensate for the issues faced in this study.

REFERENCES

Addou, F., Duguet, T., Bosso, P., Zhang, A., Amin-Chalhoub, E., Fanelli, F., & Vahlas, C. (2016). Metallization of carbon fiber reinforced polymers: Chemical kinetics, adhesion, and properties. *Surface and Coatings Technology*, *308*, 62–69.

Ahmad, M., Abdullah, A. S., & Abd Kadir, A. S. (2015). Effect of the gel coat composition on the tensile strength for glass fibre reinforced polyester composites. *Advanced Materials Research*, *1125*, 79–83.

Alhulaifi, A. S., Buck, G. A., & Arbegast, W. J. (2012). Numerical and experimental investigation of cold spray gas dynamic effects for polymer coating. *Journal of Thermal Spray Technology*, *21*(5), 852–862.

Amin, S., & Panchal, H. (2016). A review on thermal spray coating processes. *Transfer*, *2*(4).

Armstrong, K., Cole, W., & Bevan, G. (2005). *Care and repair of advanced composites*. SAE.

Assadi, H., Kreye, H., Gärtner, F., & Klassen, T. (2016). Cold spraying–a materials perspective. *Acta Materialia*, *116*, 382–407.

Asthana, R., Kumar, A., & Dahotre, N. B. (2006). *Materials processing and manufacturing science*. Elsevier.

ASTM International. (2010). *Astm f2792-10: Standard terminology for additive manufacturing technologies* (Tech. Rep.). ASTM.

ASTM International. (2013). *Astm d2583-13a: Standard test method for indentation hardness of rigid plastics by means of a barcol impressor* (Tech. Rep.). ASTM.

ASTM International. (2014). *Astm d4060-14: Standard test method for abrasion resistance of organic coatings by the taber abraser* (Tech. Rep.). ASTM.

ASTM International. (2015a). *Astm d3418-15: Transition temperature and enthalpies of fusion and crystallization of polymers by differential scanning calorimetry* (Tech. Rep.). ASTM.

ASTM International. (2015b). *Astm d5687-95: Standard guide for preparation of flat composite panels with processing guidelines for specimen preparation* (Tech. Rep.). ASTM.

ASTM International. (2015c). *Astm d7028-07: Standard test method for glass transition temperature (dma tg) of polymer matrix composites by dynamic mechanical analysis (dma)* (Tech. Rep.). ASTM.

ASTM International. (2017). *Astm d4541-17: Standard test method for pull-off strength of coatings using portable adhesion testers* (Tech. Rep.). ASTM.

ASTM International. (2018). *Astm d7127-17: Standard test method for measurement of surface roughness of abrasive blast cleaned metal surfaces using a portable stylus instrument* (Tech. Rep.). ASTM.

Bach, F.-W., Laarmann, A., Wenz, T., & Nakhosteen, C. B. (2006). *Modern surface technology*. Wiley Online Library.

Baranek, S. (2012). Tool steel and aluminum staying strong (mold materials). *MoldMaking Technology*, *15*(7), 32.

Barocio, E. (2020). *Fusion bonding of fiber reinforced semi-crystalline polymers in extrusion deposition additive manufacturing*. Unpublished doctoral dissertation, Purdue University Graduate School.

Barocio, E., Brenken, B., Favaloro, A., & Pipes, R. (2017). Extrusion deposition additive manufacturing of composite molds for high-temperature applications. In *International sampe technical conference* (pp. 1512–1523). Soc. for the Advancement of Material and Process Engineering.

Barsoum, R. G. S. (2015). *Elastomeric polymers with high rate sensitivity: Applications in blast, shockwave, and penetration mechanics*. William Andrew.

Basgul, C., Yu, T., MacDonald, D. W., Siskey, R., Marcolongo, M., & Kurtz, S. M. (2020). Does annealing improve the interlayer adhesion and structural integrity of fff 3d printed peek lumbar spinal cages? *Journal of the mechanical behavior of biomedical materials*, *102*, 103455.

Baur, E., Ruhrberg, K., & Woishnis, W. (2016). *Chemical resistance of engineering thermoplastics*. William Andrew.

Bhatnagar, A. (2016). *Lightweight ballistic composites: military and law-enforcement applications*. Woodhead Publishing.

Bossi, R. H. (2006). Nde developments for composite structures. In *Aip conference proceedings* (Vol. 820, pp. 965–971). American Institute of Physics.

Brenken, B., Barocio, E., Favaloro, A., Kunc, V., & Pipes, R. B. (2019). Development and validation of extrusion deposition additive manufacturing process simulations. *Additive Manufacturing*, *25*, 218–226.

Buckley, D. H. (1978). Tribological properties of surfaces. *Thin Solid Films*, *53*(3), 271–283.

Buschow, K. J., Cahn, R. W., Flemings, M. C., Ilschner, B., Kramer, E. J., & Mahajan, S. (2001). *Encyclopedia of materials : science and technology*. Elsevier.

Campbell Jr, F. C. (2003). *Manufacturing processes for advanced composites*. Elsevier.

Centea, T., Grunenfelder, L. K., & Nutt, S. R. (2015). A review of out-of-autoclave prepregs–material properties, process phenomena, and manufacturing considerations. *Composites Part A: Applied Science and Manufacturing*, *70*, 132–154.

Cha, S. C., & Erdemir, A. (2015). *Coating technology for vehicle applications*. Springer.

Chardon, G., Chanal, H., Duc, E., & Garnier, T. (2017). Study of surface finish of fiber-reinforced composite molds. *Proceedings of the Institution of Mechanical Engineers, Part B: Journal of Engineering Manufacture*, *231*(4), 576–587.

Chawla, K. K. (1987). *Composite materials science and engineering*. Springer.

Che, H., Chu, X., Vo, P., & Yue, S. (2017). Cold spray of mixed metal powders on carbon fibre reinforced polymers. *Surface and Coatings Technology*, *329*, 232–243.

Che, H., Vo, P., & Yue, S. (2017). Metallization of carbon fibre reinforced polymers by cold spray. *Surface and Coatings Technology*, *313*, 236–247.

Chun, H., Kim, Y.-J., Tak, S.-Y., Park, S.-Y., Park, S.-J., & Oh, C. H. (2018). Preparation of ultra-low cte epoxy composite using the new alkoxysilyl-functionalized bisphenol a epoxy resin. *Polymer*, *135*, 241–250.

Crawford, C. B. (2017). *Microplastic pollutants*. Elsevier.

Davim, J. P. (2012). *Materials and surface engineering: Research and development*. Elsevier.

Deo, R., Starnes Jr, J., & Holzwarth, R. (2003). Low-cost composite materials and structures for aircraft applications. *STAR*, *41*(22).

Dong, C., & Davies, I. J. (2013). Flexural properties of glass and carbon fiber reinforced epoxy hybrid composites. *Proceedings of the Institution of Mechanical Engineers, Part L: Journal of Materials: Design and Applications*, *227*(4), 308–317.

Dutton, S., Kelly, D., & Baker, A. (2004). *Composite materials for aircraft structures*. American Institute of Aeronautics and Astronautics.

Duty, C. E., & Springfield, R. M. (2015). *Evaluation of additive manufacturing for composite part molds* (Tech. Rep.). Oak Ridge National Lab.(ORNL), Oak Ridge, TN.

Faure-Geors, A. (1994). *Structural characterization and thermal cycling behaviour of eb-pvd thermal barrier coating systems.* Unpublished doctoral dissertation, University of Toronto.

Friz, M., & Waibel, F. (2003). Coating materials. In *Optical interference coatings* (pp. 105–130). Springer.

Gadelmawla, E., Koura, M., Maksoud, T., Elewa, I., & Soliman, H. (2002). Roughness parameters. *Journal of Materials Processing Technology*, *123*(1), 133–145.

Golzar, M., & Poorzeinolabedin, M. (2010). Prototype fabrication of a composite automobile body based on integrated structure. *The International Journal of Advanced Manufacturing Technology*, *49*(9-12), 1037–1045.

Gombos, Z. J., & Summerscales, J. (2016). In-mould gel-coating for polymer composites. *Composites Part A: Applied Science and Manufacturing*, *91*, 203–210.

Graves, B. (2002). Tooling up a tough thin film. *Products Finishing*, *66*(12), 68.

Griffiths, C., Rees, A., Kerton, R., & Fonseca, O. (2016). Temperature effects on dlc coated micro moulds. *Surface and Coatings Technology*, *307*, 28–37.

Grigoriev, S., Okunkova, A., Sova, A., Bertrand, P., & Smurov, I. (2015). Cold spraying: From process fundamentals towards advanced applications. *Surface and Coatings Technology*, *268*, 77–84.

Grill, A. (1999). Diamond-like carbon: state of the art. *Diamond and Related Materials*, *8*(2-5), 428–434.

Groenewoud, W. M. (2001). *Characterisation of polymers by thermal analysis*. Elsevier.

Guo, N., & Leu, M. C. (2013). Additive manufacturing: technology, applications and research needs. *Frontiers of Mechanical Engineering*, *8*(3), 215–243.

Hashmi, S. (2016). *Comprehensive materials finishing*. Elsevier.

Hassen, A. A., Lindahl, J., Chen, X., Post, B., Love, L., & Kunc, V. (2016). Additive manufacturing of composite tooling using high temperature thermoplastic materials. In *International sampe technical conference* (pp. 23–26). Soc. for the Advancement of Material and Process Engineering.

Hassen, A. A., Springfield, R., Lindahl, J., Post, B., Love, L., Duty, C., ... Kunc, V. (2016). The durability of large-scale additive manufacturing composite molds. In *CAMX 2016* (pp. 26–29). The Composites and Advanced Materials Expo (CAMX).

He, B. (2011). Reseach on the failure and material selection of plastic mold. *Procedia Engineering*, *23*, 46–52.

Hollaway, L. (1994). *Handbook of polymer composites for engineers*. Elsevier.

Hornbaker, M., Keene, L., Krawiec, R., & Wilken, T. (2013). The basic of liquid and powder coatings. *The Fabricator*, *NOVEMBER 2013*.

Humfeld Jr, G. R. (1997). *Mechanical behavior of adhesive joints subjected to thermal cycling*. Unpublished doctoral dissertation, Virginia Tech.

Innocenzi, P. (2019). *The sol-to-gel transition* (2nd ed. ed.). SpringerBriefs in Materials.

Ivkovic, B., Djurdjanovic, M., & Stamenkovic, D. (2000). The influence of the contact surface roughness on the static friction coefficient. *Tribology in Industry*, *22*, 41–44.

Izdebska, J. (2016). *Printing on polymers*. William Andrew.

Izdebska, J., & Thomas, S. (2015). *Printing on polymers: fundamentals and applications*. William Andrew.

Jhavar, S., Paul, C., & Jain, N. (2013). Causes of failure and repairing options for dies and molds: A review. *Engineering Failure Analysis*, *34*, 519–535.

Jiang, Z., Hornsby, P., McCool, R., & Murphy, A. (2012). Mechanical and thermal properties of polyphenylene sulfide/multiwalled carbon nanotube composites. *Journal of Applied Polymer Science*, *123*(5), 2676–2683.

Kim, G., Sterkenburg, R., & Tsutsui, W. (2018). Investigating the effects of fluid intrusion on nomex® honeycomb sandwich structures with carbon fiber facesheets. *Composite Structures*, *206*, 535–549.

King, D., & Bell, J. (1988). Thermal shock failure in thick epoxy coatings. *The Journal of Adhesion*, *26*(1), 37–58.

Knotek, O., Löffler, F., & Bosserhoff, B. (1993). Pvd coatings for diecasting moulds. *Surface and Coatings Technology*, *62*(1-3), 630–634.

Koepfer, C. (1996). Cutting tool considerations for high speed machining. *Modern Machine Shop*, *68*(8), 56.

Kunc, V., Lindahl, J., Dinwiddie, R., Post, B., Love, L., Matlack, M., ... Hassen, A. (2016). Investigation of in-autoclave additive manufacturing composite tooling. In *CAMX 2016.* The Composites and Advanced Materials Expo (CAMX).

Lupoi, R., & O'Neill, W. (2010). Deposition of metallic coatings on polymer surfaces using cold spray. *Surface and Coatings Technology*, *205*(7), 2167–2173.

Mahltig, B., & Kyosev, Y. (2018). *Inorganic and composite fibers: Production, properties, and applications*. Woodhead Publishing.

Mallick, P. K. (2007). *Fiber-reinforced composites: materials, manufacturing, and design*. CRC press.

Martínez-Mateo, I., Carrión-Vilches, F., Sanes, J., & Bermúdez, M. (2011). Surface damage of mold steel and its influence on surface roughness of injection molded plastic parts. *Wear*, *271*(9-10), 2512–2516.

Mehdikhani, M., Gorbatikh, L., Verpoest, I., & Lomov, S. V. (2019). Voids in fiber-reinforced polymer composites: A review on their formation, characteristics, and effects on mechanical performance. *Journal of Composite Materials*, *53*(12), 1579–1669.

Mellouli, D., Haddar, N., Köster, A., & Ayedi, H. F. (2014). Hardness effect on thermal fatigue damage of hot-working tool steel. *Engineering Failure Analysis*, *45*, 85–95.

Mercer, J. (2012). Diamond-like carbon mold coatings for increased durability. *Moldmaking Technology Magazine*, *15*(5), 45–48.

Mohammadi, M. S., Ghani, M., Komeili, M., Crawford, B., & Milani, A. (2017). The effect of manufacturing parameters on the surface roughness of glass fibre reinforced polymer moulds. *Composites Part B: Engineering*, *125*, 39–48.

Muthu, S. S., & Savalani, M. M. (2016). *Handbook of sustainability in additive manufacturing* (Vol. 1). Springer.

Neale, M. J. (2001). *Lubrication and reliability handbook*. Newnes.

Nunes, V., Silva, F., Andrade, M., Alexandre, R., & Baptista, A. (2017). Increasing the lifespan of high-pressure die cast molds subjected to severe wear. *Surface and Coatings Technology*, *332*, 319–331.

Omar, F., Brousseau, E., Elkaseer, A., Kolew, A., Prokopovich, P., & Dimov, S. (2014). Development and experimental validation of an analytical model to predict the demoulding force in hot embossing. *Journal of Micromechanics and Microengineering*, *24*(5), 055007.

Parandoush, P., & Lin, D. (2017). A review on additive manufacturing of polymer-fiber composites. *Composite Structures*, *182*, 36–53.

Paris, H., Mandil, G., et al. (2017). Environmental impact assessment of an innovative strategy based on an additive and subtractive manufacturing combination. *Journal of Cleaner Production*, *164*, 508–523.

Peters, S. T. (2013). *Handbook of composites*. Springer Science & Business Media.

Powers, J. M., Sakaguchi, R. L., Craig, R. G., et al. (2012). *Craig's restorative dental materials*. Elsevier.

Raoelison, R., Verdy, C., & Liao, H. (2017). Cold gas dynamic spray additive manufacturing today: Deposit possibilities, technological solutions and viable applications. *Materials & Design*, *133*, 266–287.

Raoelison, R., Xie, Y., Sapanathan, T., Planche, M. P., Kromer, R., Costil, S., & Langlade, C. (2018). Cold gas dynamic spray technology: A comprehensive review of processing conditions for various technological developments till to date. *Additive Manufacturing*, *19*, 134–159.

Rezzoug, A., Abdi, S., Kaci, A., & Yandouzi, M. (2018). Thermal spray metallisation of carbon fibre reinforced polymer composites: Effect of top surface modification on coating adhesion and mechanical properties. *Surface and Coatings Technology*, *333*, 13–23.

Sauerbier, P., Anderson, J., & Gardner, D. (2018). Surface preparation and treatment for large-scale 3d-printed composite tooling coating adhesion. *Coatings*, *8*(12), 457.

Sheikh-Ahmad, J. Y. (2009). *Machining of polymer composites*. Springer.

Siddique, R., & Cachim, P. (2018). *Waste and supplementary cementitious materials in concrete: Characterisation, properties and applications*. Woodhead Publishing.

Silicon Semiconductor Magazine. (2019, April 4). Comparing ptfe and pfa fluoropolymers as wetted parts in advanced semiconductor manufacturing. Retrieved from https://siliconsemiconductor.net/article/106829/Comparing_PTFE_And_PFA_Fluoropolymers_As_Wetted_Parts_In_Advanced_Semiconductor_Manufacturing/feature

Silva, F. J., Martinho, R., Alexandre, R., & Baptista, A. (2011). Increasing the wear resistance of molds for injection of glass fiber reinforced plastics. *Wear*, *271*(9-10), 2494–2499.

Sterkenburg, R., & Wang, P. (2014). *Structural composites: Advanced composites in aviation.* Avotek Information Resources.

Stewart, R. (2009). Moldmaking for composite materials: Part quality starts with attention to detail in tooling. *Plastics Engineering*, *65*(3), 16–24.

Sturgeon, A., Dunn, B., Celotto, S., & O'Neill, W. (2006). Cold sprayed coatings for polymer composite substrate. *ESA SP*, *616*(1), 1–5.

Sudbury, T. Z., Springfield, R., Kunc, V., & Duty, C. (2017). An assessment of additive manufactured molds for hand-laid fiber reinforced composites. *The International Journal of Advanced Manufacturing Technology*, *90*(5-8), 1659–1664.

Suzuki, E., Kikuchi, T., Takai, Y., Goto, A., & Hamada, H. (2015). An investigation on skillful gel-coat techniques and its application to beginner's application. In *International conference on digital human modeling and applications in health, safety, ergonomics and risk management* (pp. 182–191). Springer.

Tabor, D. (1970). The hardness of solids. *Review of Physics in Technology*, *1*(3), 145.

Tabor, D. (2000). *The hardness of metals.* Oxford university press.

Thomas, S., & Visakh, P. (2011). *Handbook of engineering and specialty thermoplastics, volume 3: Polyethers and polyesters* (Vol. 63). John Wiley & Sons.

Tsai, J.-T., Bahr, D., Akin, S., Zhou, F., Jun, M. B.-G., & Park, M. (2020). Simulation and characterization of cold spray deposition of metal powders on polymer substrate electrically conductive application. In *Proceedings of the asme 2020 15th international manufacturing science and engineering conference.*

Vangerko, H. (1988). Composite tooling for composite components. *Composites*, *19*(6), 481–484.

Wang, B., Eberhardt, W., Tian, S., & Kück, H. (2006). Metallization of a liquid crystal polymer by pvd using a nickel interlayer. *Journal of Adhesion Science and Technology*, *20*(2-3), 175–182.

Watson, J., & Taminger, K. (2018). A decision-support model for selecting additive manufacturing versus subtractive manufacturing based on energy consumption. *Journal of Cleaner Production*, *176*, 1316–1322.

Wen, S., Hu, H., Zhou, Y., Chen, Z., Wei, Q., & Shi, Y. (2018). Enhanced hardness and wear property of s136 mould steel with nano-tib2 composites fabricated by selective laser melting method. *Applied Surface Science*, *457*, 11–20.

Worgull, M., Heckele, M. P., Hétu, J. F., & Kabanemi, K. (2006). Modeling and optimization of the hot embossing process for micro-and nanocomponent fabrication. *Journal of Micro/Nanolithography, MEMS, and MOEMS*, *5*(1), 011005.

Yan, X., Cai, Y., Lu, R., & Miyakoshi, T. (2017). Development and characterization of new coating material of blended epoxy-lacquer with aluminum. *International Journal of Polymer Science*, *2017*.

Yin, S., Cavaliere, P., Aldwell, B., Jenkins, R., Liao, H., Li, W., & Lupoi, R. (2018). Cold spray additive manufacturing and repair: Fundamentals and applications. *Additive Manufacturing*, *21*, 628–650.

Zhang, H., Ong, N., & Lam, Y. (2007). Effects of surface roughness on microinjection molding. *Polymer Engineering & Science*, *47*(12), 2012–2019.

Zhou, X., Chen, A., Liu, J., Wu, X., & Zhang, J. (2011). Preparation of metallic coatings on polymer matrix composites by cold spray. *Surface and Coatings Technology*, *206*(1), 132–136.

Zhou, Y., Zhu, H., Zhang, W., Zuo, X., Li, Y., & Yang, J. (2015). Influence of surface roughness on the friction property of textured surface. *Advances in Mechanical Engineering*, *7*(2), 1687814014568500.